Dynamics of polymer thin films and surfaces

by

Zahra Fakhraai

A thesis
presented to the University of Waterloo
in fulfilment of the
thesis requirement for the degree of
Doctor of Philosophy
in
Physics

Waterloo, Ontario, Canada, 2007

AUTHOR'S DECLARATION FOR ELECTRONIC SUBMISSION OF A THESIS

I hereby declare that I am the sole author of this thesis. This is a true copy of the thesis, including any required final revisions, as accepted by my examiners.

I understand that my thesis may be made electronically available to the public.

Abstract

The dynamics of thin polymer films display many differences from the bulk dynamics. Different modes of motions in polymers are affected by confinement in different ways. The enhancement in the dynamics of some modes of motion can cause anomalies in the glass transition temperature (T_g) of thin films, while other modes of motion such as diffusion can be substantially slowed down due to the confinement effects.

In this thesis, different modes of dynamics are probed using different techniques. The interface healing of two identical polymer surfaces is used as a probe of segmental motion in the direction normal to the plane of the films and it is shown that this mode of motion is slowed down at temperatures above bulk glass transition, while the glass transition itself is decreased indicating that the type of motion responsible for the glass transition is enhanced. The glass transition measurements at different cooling rates indicate that this enhancement only happens at temperatures close to or below bulk glass transition temperature and it is not expected to be detected at higher temperatures where the system is in the melt state. It is shown that the sample preparation technique is not a factor in observing this enhanced dynamics, while the existence of the free surface can be important in observed reductions in the glass transition temperature.

The dynamics near the free surface is further studied using a novel nano-deformation technique, and it is shown that the dynamics near the free surface is in fact enhanced compared to the bulk dynamics and this enhancement is increased as the temperature is decreased further below T_g. It is also shown that this mode of relaxation is much different from the bulk modes of relaxations, and a direct relationship between this enhanced motion and T_g reduction in thin films can be established. The results presented in this thesis can lead to a possible universal picture that can resolve the behavior of different modes of motions in thin polymer films.

Acknowledgements

This thesis has been written with the help, advice and moral support of many people to whom I am greatly in debt and who I can never thank adequately. I would like to thank my supervisor James A. Forrest for his help and support during my PhD, his trust in giving me the freedom to try my own ideas and for his exuberance throughout my degree. I'd like to acknowledge Kari Daknoli-Veress for his guidance and for his letting us use his lab when our instrument was broken. I would also like to thank the members of my committee, Stefan Idziak, Tong Leung, Bernie Nickel and the reader of my thesis Robert Hill for their useful comments and suggestions. My sincere gratitude goes to John M. Torkelson for our many useful discussions, for reading my thesis and most of all for his kindness. I would also like to thank my previous supervisor H. Arfaei for his moral support during our difficult move to Canada and for helping me choose my next graduate school. I also acknowledge the help of co-authors James S. Sharp and Sina Valadkhan for their constructive collaboration.

My friends have made my life happy and helped me to succeed during the difficult periods. I would like to express my appreciation towards my friends in the lab, James Chan, James Benson, Jonathan Teichroeb, Gianfranco Mazzanti, James Sharp, Dongping Qi, Maria Khomenko, Patrick McVeigh, Jane Robinson, Sara Guthrie, Shahla Aliakbari, Valentina Ngai, Gaven MacDonald, Raeshri Bhookmohan, Iouri Khramtsov, Chris Collins and Kanwarjeet Kaur, who made it exciting to go to work every day. I really enjoyed our many coffee breaks, lunches and talks during the day. They helped me adjust to my new life here and made my Canadian experience a great one. I would also like to thank many other friends who have made a difference in my life. I wish to thank Michael Massa, Andrew B. Croll, Marie-Jose Colbert in Kari's lab for their friendship during the time I spent in their lab and my friends Ghazal Geshnizjani, Sima Ghasemi, Fatemeh Jafargholi, Hanif Bayat-Movahed, Nasimeh Asgarian, Mohamadreza Salavatipoor, Weihong Huang, Mohadeseh Azimlu, Faranak Zamani, Behnaz Bozorgi, Mania Maleki, Houshin Nejati, Nina Azadian, Nima Hamedani-Raja, Maryam Jafaraghdami, Kaveh Khojasteh, Arnavaz Danesh, Maryam Beygmohamadi, Azadeh Farahzadi, Fatemeh Azimlu, Farhang Habibi, Akbar Jafari, Sattar Taheri-Araghi, Ali Tabei, Ronak Mosavi-

This thesis is dedicated to the memories of my father.

Contents

List of Figures

Chapter 1

Introduction

The behavior of glassy materials in confined systems can be different from their bulk behavior due to the effects induced by the boundaries of the system. Polymer thin films have been used to study the effect of confinement on the dynamics of glassy materials in a quest to understand the glass transition phenomena either in general or in the specific case of polymeric materials. Since polymers are large molecules with several different characteristic length scales, anomalies due to chain confinement effects can also be observed in thin polymer films. To understand the dynamics of polymer thin films, one needs to study different modes of motion and understand the effect of confinement on each of these modes of motions, as each can be affected by the confinement in a different way.

In this thesis, different methods are used to study and compare different modes of dynamics, the results of which can help build a universal picture of dynamics in thin films and can be potentially used as a base for more theoretical work in explaining the dynamics of polymers in confinement. The structure of this thesis is as follows. In the rest of chapter one a brief introduction is given about the structure and dynamics of polymers followed by a general introduction of glass transition phenomena and theories of the glass transition. In chapter two the effect of confinement on the behavior of glassy polymers is discussed. In chapter three sample preparation and experimental tools used in this thesis will be explained. Chapter four provides a summary of the attached papers, along with concluding
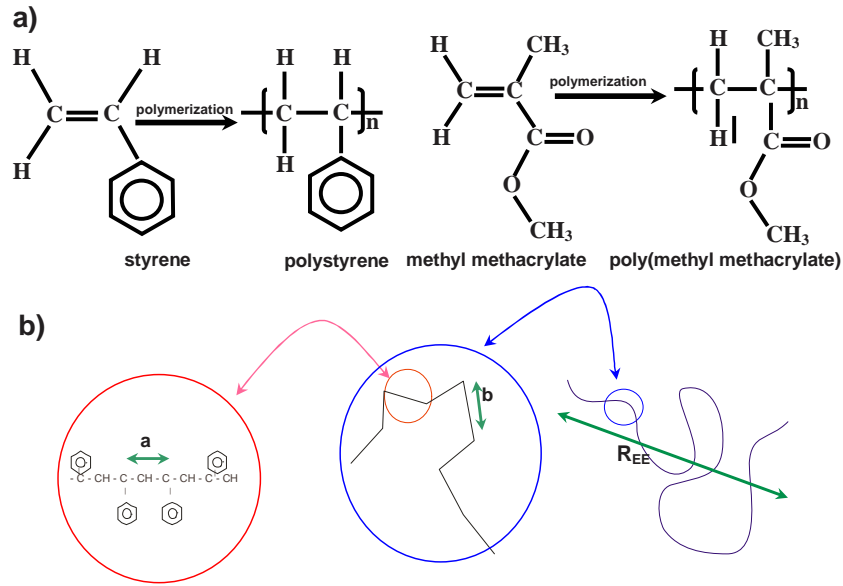
Figure 1.1: a)Polymerization of polystyrene and poly(methyl methacrylate). b)Schematic picture of a polymer chain at different length scales.

remarks.

1.1 Introduction to polymers

1.1.1 The structure of polymers

Polymers are large molecules made of repeated elementary units called monomers by a polymerization process. Figure 1.1(a) shows an example of polymerization of polystyrene (PS) and poly(methyl methacrylate) (PMMA) from styrene and methyl methacrylate monomers, respectively. The degree of polymerization is the number of monomers N in a polymer chain. The molecular weight of a polymer is usually used as a measure of the polymer size. In the melt the number average molecular weight M_N is defined as

$$M_N = \int \rho(M) M dM \tag{1.1}$$

where $M = N \times M_{mon}$ is the molecular weight of the polymer and $\rho(M)dM$ is the fraction of molecules with mass in the range of M and $M + dM$. The weight average molecular weight is defined as

$$M_w = \frac{\int \rho(M)M.MdM}{\int \rho(M)MdM} \tag{1.2}$$

The ratio of these two values (M_w/M_N) can be used as a measure of the width of the distribution of polymer sizes and is known as polydispersity coefficient. If this factor is equal to one, then the polymer is mono-disperse and all chains have the same length. The deviation of this factor from one, shows how poly-disperse the chains are.

Since polymers are large particles made of semi-independent units, they can occupy a huge number of translational and rotational states in configurational space. In the melt or solution, polymer chains have a chance to move from one state to the other state following Boltzmann statistics. The shape of chains and the amount of chain stretching depends on the interaction of the monomers with each other and with the solvent molecules. Figure 1.1(b) shows different important length scales of a polymer chain. Each two neighboring monomers are separated by a distance a which is the monomer size and depends on the chemical structure of the polymer. This is the shortest important length scale in the polymer dynamics. In larger length scales the chain properties depend on the chemical structure of the monomer, its size and the angle between two neighboring monomers, which also depends on the chemical structure of the polymer. The persistence length b is the length scale at which the monomers motion becomes uncorrelated. Two monomers that are farther away from each other than this persistence length can move independent of each other, so at length scales larger than this length scale, the chain appears flexible. This size of persistence length depends on the chain stiffness and will be discussed in more details later. R_{EE} the end to end distance of the polymer, is the average distance between the two ends of the polymer chain, and is a measure of the size that the polymer chain occupies in the space.
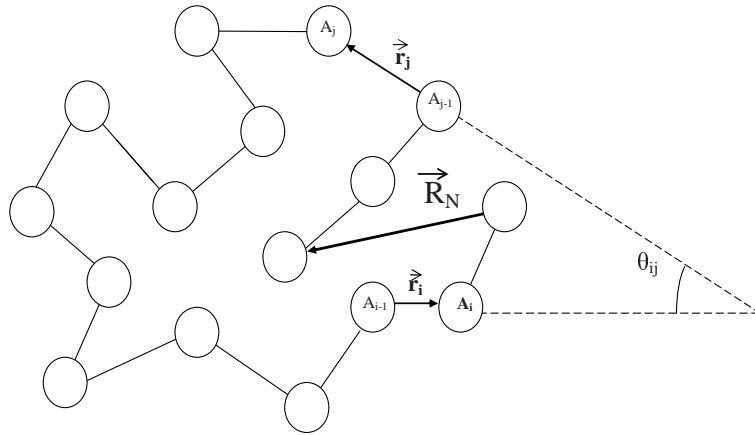
Figure 1.2: Schematic picture of a polymer chain.

Ideal chains

Imagine a situation in which each monomer can move freely without feeling the existence of neighboring monomers. If $\vec{r}_i$ is defined as the translation vector from monomer $i-1$ to i with the size $|\vec{r}_i| = a$, then the end to end vector is $\vec{R}_N = \sum_{i=1}^{N} \vec{r}_i$ for a chain of size N as schematically shown in figure 1.2. Since the monomers are moving randomly, the position of the monomer number i is similar to the ith step taken in a random walk. A one to one correspondence between the random walk path and the configuration of the polymer in a time frame can be built. The shape taken by the polymer chain is then similar to the Brownian motion path, and its shape in the space is given by the Gaussian distribution. Then it is easy to show that

$$\left\langle \vec{R}_N \right\rangle = 0 \tag{1.3}$$

where $\langle \, \rangle$ is the average over a large number of steps in the random walk or a large number of monomers in the polymer chain respectively. The average mean square end to end distance of a chain is then given by

$$R_{EE}^2 = \left\langle R_N^2 \right\rangle = N a^2 \tag{1.4}$$

where N is the chain length and a is the monomer length. The radius of gyration can also be calculated [2]:

$$R_g^2 = \frac{1}{N^2} \sum_{i=1}^{N} \sum_{j-1}^{N} (\vec{R}_i^2 - \vec{R}_i \vec{R}_j) = \frac{\langle R_{EE}^2 \rangle}{6} \tag{1.5}$$

In a real chain, two neighboring monomers can not move independent of each other, the chemical structure of the chain imposes an angle θ between them (schematically shown in figure 1.2) so $\vec{r}_i.\vec{r}_j = a^2 \cos \theta_{ij}$, For two monomers that are sufficiently far from each other, the average value of this angle falls to zero:

$$\lim_{|i-j| \to \infty} \langle \cos \theta_{ij} \rangle = 0 \tag{1.6}$$

So the sum of these angles will be a finite number and one can show that [2]

$$\langle R_{EE}^2 \rangle = a^2 \sum_{i=1}^{N} \sum_{j=1}^{N} \langle \cos \theta_{ij} \rangle = CNa^2 \tag{1.7}$$

where C is an scaling factor, which depend on the chain stiffness. The behavior of the chain is thus similar to an ideal chain with an enlarged monomer size $b = \sqrt{C}a$. b is known as persistence length and is the length at which the monomers can move without feeling the existence of each other. At length scales shorter than b the chain appears more stiff and the angle between the monomers defines the position of monomers in respect to each other. Depending on the stiffness of polymer chain the size of b can be between one monomer length to several tens of monomer lengths.

Real Chains

The interaction of a monomer with its neighbors is not the only interaction that can affect the chain structure. For example, in a good solvent the chains can be more stretched because of the favorable interaction of monomers with solvent molecules [1, 2]. Ideal chains are only found in melts and theta solvents. A theta solvent is a solvent-temperature condition in which the excluded volume of other monomers becomes zero and the monomers do not feel the existence of other particles in the solvent. The excluded volume is defined as followed. If $U(r)$ is the interaction
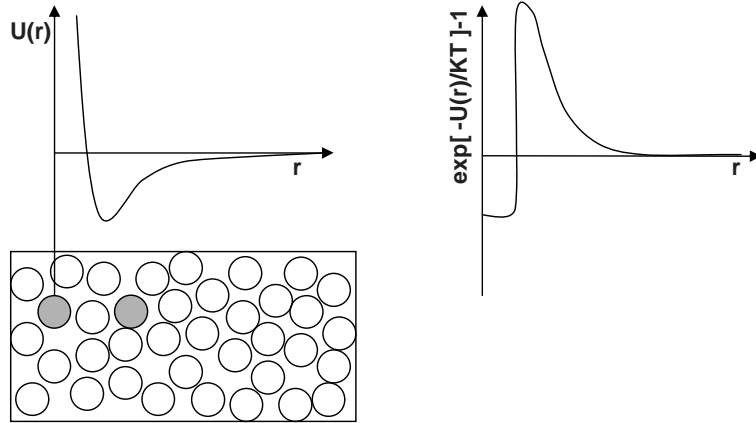
Figure 1.3: Schematic form of the potential U(r) (left) in a liquid and the function $\exp[(-U(r)/kT)] - 1$ (right). Reproduced from ref. [2]

potential between two monomers, then the probability of finding another monomer at a distance r from a monomer is equal to $\exp(-U(r)/kT)$ and the excluded volume can be defined as

$$V = -\int [1 - \exp(-U(r)/kT)]d^3r \tag{1.8}$$

Figure 1.3 shows the schematic shape of $U(r)$ and $1 - \exp(-U(r)/kT)$. The excluded volume V is the area under this second graph.

Based on the excluded volume, different solvent conditions can be defined as:

- **Athermal Solvent**:In the high temperature limit the excluded volume becomes independent of temperature and is equal to the size of the particles, $b^2 d$ for a monomer of persistence length b, and the smaller diameter d.In this situation the only interaction in the system is the hard core repulsion of the monomers.

- **Good Solvent**:In good solvents the favorable attraction between the monomer and the solvent particle creates an excluded volume that is smaller than the athermal value $0 < V < b^2 d$.

- **Theta Solvent**:At some temperature θ the excluded volume becomes zero, and the chain behavior becomes ideal motion.

- **Poor Solvent**: At temperatures below θ, $-b^2d < V < 0$ and the attraction between the chain monomers, makes a more packed structure, which becomes almost spherical shape in the case of non-solvents $V = -b^2d$.

As mentioned before, in good solvents the interaction between the solvent particles and monomers can result in a more stretched shape. The Flory theory shows that the behavior of the chain can be modeled as a self avoiding random walk rather than the ideal random walk, so the chain size dependance to the chain length becomes

$$R \sim N^{3/5} \tag{1.9}$$

In general the Flory theory leads to a universal power-law dependance of the polymer size to the number of monomer units

$$R \sim N^{\nu} \tag{1.10}$$

The quality of the solvent changes with the excluded volume V, but for any $V > 0$ the exponent ν remains unchanged. Compared to the ideal chain with $\nu = 1/2$ the chains occupies a larger space and has a smaller fractal dimension. More details about the Flory theory can be found in references $[1, 2]$.

1.1.2 The dynamics of polymer chains

Rouse model

The Rouse model is a model that describes the internal modes of motion of short polymer chains or polymer monomers below the entanglement length scale and time constant. In the Rouse model it is assumed that the polymer chains are made of small massless beads connected to each other by massless springs with the same spring constants.

The diffusion coefficient D of a particle moving in a liquid is proportional to its mean square displacement after a time t

$$\left\langle [\vec{r}(t) - \vec{r}(0)]^2 \right\rangle = 6Dt \tag{1.11}$$

The friction coefficient ζ is defined as the coefficient relating the velocity of the particle $\vec{v}$ to the frictional force $\vec{f}$.

$$\vec{f} = \zeta\vec{v} \tag{1.12}$$

The diffusion coefficient and the friction coefficient are related by the Einstein relation

$$D = \frac{kT}{\zeta} \tag{1.13}$$

For a spherical particle $\zeta = 6\pi\eta R$, where η is the viscosity and R is the radius of the particle. Combining equations 1.11 and 1.13 the characteristic time τ required for a particle to move a distance of the order of its own size R is equal to

$$\tau \approx \frac{R^2}{D} \approx \frac{R^2\zeta}{kT} \tag{1.14}$$

In a Rouse chain the beads are connected with springs of length b. Each bead is dragged in the melt or solution with a friction coefficient ζ, so the total friction coefficient for a chain of size N is equal to, $\zeta_N = N\zeta$. The relaxation time for a chain with the end to end distance of R is then

$$\tau_R \approx \frac{R^2}{D_R} = \frac{\zeta}{kT}NR^2 \tag{1.15}$$

This relaxation time is known as the Rouse relaxation time. Combining with equation 1.10, one has

$$\tau_R \approx \tau_0 N^{1+2\nu} \tag{1.16}$$

where $\tau_0 \approx \frac{\zeta b^2}{kT}$ is the time scale of the motion of individual beads.

The Rouse model can be solved exactly and modes of harmonic motion of the beads can be calculated. In the melt where the chains behave like ideal chains the exact solution of the Rouse model leads to [1]

$$\tau_R = \tau_0 N^2 = \frac{\zeta b^2}{3\pi^2 kT}N^2 \tag{1.17}$$

This is the longest Rouse relaxation time. Other relaxation times are similarly given by

$$\tau_m = \tau_0 m^2 = \frac{\zeta b^2}{3\pi^2 kT}m^2, 1 < m < N \tag{1.18}$$
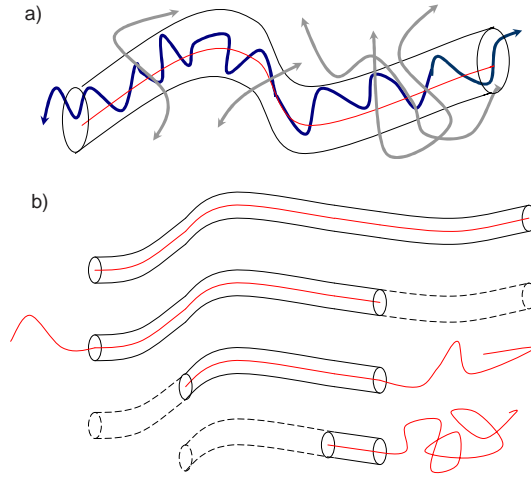
Figure 1.4: a)Schematic illustration of an entanglement tube. The red line indicates the primary path of the chain. b)The decomposition of a tube as a result of reptative motion of the primitive path. Modified from ref. [1]

The Rouse model can be used to calculate the stress relaxation in a system made of Rouse chains and it can be shown that the shear stress relaxation modulus has the following time dependance [1][1]

$$G(t) \sim t^{-1/2} \tag{1.19}$$

and the viscosity of the system is equal to $\eta \sim N$. This behavior has been confirmed in experiments on polymers with short chains or measurements of short time relaxations in entangled systems. For example the experiment of Pearson *et al.* shows the validity of Rouse model for short chain polyethylene [3]

Chain entanglement and reptation

Polymer chains with sufficient length in the melt or concentrated solution are interpenetrated and the degree of this interpenetration increases with the molecular weight. At high molecular weights the polymer molecules become so entangled that

---

[1]The definition of shear modulus is given in the following section where the macroscopic dynamics of polymers are discussed.

the molecules can not move freely, and their motion as a whole becomes dependent to the motion of surrounding chains. Doi and Edwards [4] proposed the reptation model to explain the dynamics of entangled polymers. In this model it is assumed that the motion of a chain is confined in tubes that are made by adjacent molecules. Figure 1.4 (a) shows how the lateral constraints on the chain motion imposed by surrounding chains produces an entanglement tube. The line along the tube center of this entanglement tube is called the primitive path. The motion of the chain is composed of fast relaxation of the monomers inside the tube which is driven by Rouse mode relaxations and the time dependent evolution of the primitive path which leads to disentangling of the chains and eventual diffusion of the chain. Figure 1.4(b) shows the reptative motion of the primary path. Both the actual chains and the primitive paths represent random coils, and both have the same end to end distance

$$R^2 = Na^2 = l_{pr}a_{pr} \tag{1.20}$$

where l_{pr} is the length of the primitive path and a_{pr} is a parameter which defines the stiffness of the entanglement tube. The friction coefficient of the chain is equal to $\zeta_N = N\zeta$, so from Einstein relation the diffusion of the motion of primitive path is given by

$$D = \frac{kT}{\zeta_N} = \frac{kT}{N\zeta} \tag{1.21}$$

The time needed for the chain to diffuse over a length comparative to the length of primitive path is of the order of

$$\tau_d \sim \frac{l_{pr}^2}{D} \tag{1.22}$$

Combining equations 1.20 1.21 and 1.22 the time constant of reptation can be obtained.

$$\tau_d \sim \zeta N^3 \sim M^3 \tag{1.23}$$

This result can be compared to the experimental results of creep measurements in an entangled system. The reptation model predicts a relaxation time $\tau_d \sim M^\nu$ where $\nu = 3$ while the experimental results show $\nu \approx 3.2 - 3.6$. Although this agreement is not perfect, the simple scaling approach of the reptation model can reasonably explain the characteristic behavior of entangled polymeric systems.
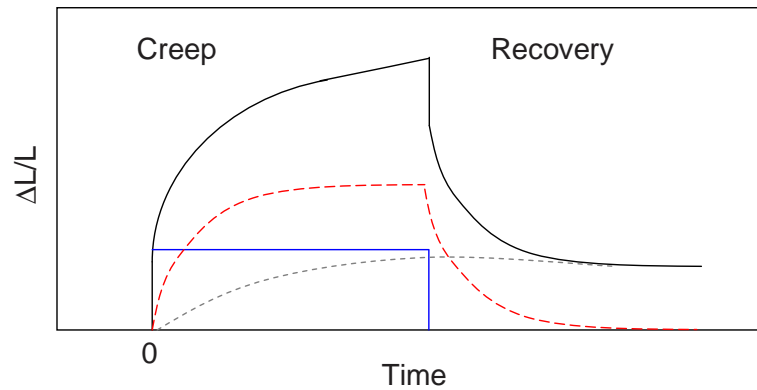
Figure 1.5: Schematic creep and recovery of a polymeric system under a constant stress at time zero.

1.1.3 Macroscopic dynamics of polymers

If a small mechanical or electric field is applied to a polymeric system, the response of the system which is a mechanical deformation or change in polarization respectively, can be described by linear equations. In this section linear viscoelasticity and linear dielectric response of polymers are discussed.

Linear viscoelasticity

In a simple creep experiment where a constant load is applied to the system the response of the system is made of three components schematically shown in figure 1.5

- An elastic instantaneous response (blue line)

- A retarded anelastic deformation, which is a function of time (red dashed curve)

- viscous flow (grey dotted curve)

Figure 1.5 shows the response of the system to a creep and the recovery of the system after the load is removed. After removing the load, an instantaneous elastic

recovery is followed by a slower time dependent recovery, but the viscous flow part of the motion is irreversible. The tensile creep compliance is defined as

$$D(t) = \frac{e_{zz}(t)}{\sigma_{zz}^0} \tag{1.24}$$

where $e_{zz}(t) = \frac{\Delta L_z}{L_z}$ is the time dependent longitudinal strain, L_z is the initial length of the sample and σ_{zz}^0 is the constant tensile stress applied to the sample at $t = 0$. A second type of mechanical experiment is the stress relaxation experiment where a constant deformation is applied at time $t = 0$ and the stress relaxation is monitored. The time dependent tensile modulus is defined as

$$E(t) = \frac{\sigma_{zz}(t)}{e_{zz}^0} \tag{1.25}$$

The third method that can be used is the oscillatory creep experiment. Here a periodically varying stress field is induced on the sample

$$\sigma_{zz}(t) = \sigma_{zz}^0 \exp(i\omega t) \tag{1.26}$$

The resulting strain varies with the same frequency but usually has a phase lag

$$e_{zz}(t) = e_{zz}^0 \exp(-i\phi) \exp(i\omega t) \tag{1.27}$$

The complex dynamic tensile compliance D^* is defined as

$$D^*(\omega) = \frac{e_{zz}(t)}{\sigma_{zz}(t)} = D' - iD'' \tag{1.28}$$

Similarly the dynamic tensile modulus can be defined

$$E^*(\omega) = \frac{\sigma_{zz}(t)}{e_{zz}(t)} = \frac{1}{D^*(\omega)} = E' + iE'' \tag{1.29}$$

Similar to tensile experiments, shear response experiments can also define the viscoelastic properties of polymeric materials. shear modulus and compliance in constant stress or strain experiments, or in dynamic experiments can be defined as the linear response constants in such experiments,

- Shear compliance $J(t) = \frac{e_{zx}(t)}{\sigma_{zx}^0}$

- time dependent shear modulus $G(t) = \frac{\sigma_{zx}(t)}{e_{zx}^0}$

- dynamics shear compliance $J^*(\omega) = \frac{e_{zx}^0}{\sigma_{zx}^0} \exp(-i\phi)$

- dynamics shear modulus $G^*(\omega) = \frac{\sigma_{zx}^0}{e_{zx}^0} \exp(i\phi)$

So far only the responses to a step function and an oscillatory force have been discussed, in order to find the general response of a system, one needs to find the primary response function, which is the response of the system to an infinitely short pulse. Assume the general force function [1]

$$\psi(t) = \psi_0 \delta(t) \tag{1.30}$$

The primary response function $\mu(t)$ describes the time dependent displacement $x(t)$ caused by this short pulse force as [1]

$$x(t) = \psi_0 \mu(t) \tag{1.31}$$

An arbitrary force function can be divided into a sequence of short pulses. If the force is small enough that the response of the system remains linear, then the Boltzmann superposition principle implies that the response of the system can be described as the sum over all responses [5]. The displacement of the system $x(t)$ as a result of a general shaped force $\psi(t')$ is then equal to

$$x(t) = \int_{-\infty}^{t} \mu(t - t')\psi(t')dt' \tag{1.32}$$

Single relaxation time process

The viscoelastic properties of materials reflect the underlying microscopic dynamics of the system. The most simple case is when the system has a single relaxation process, with a single relaxation time τ. For a creep experiment under a constant shear stress, the equation governing the response of such a system is

$$\frac{de_{zx}}{dt} = -\frac{1}{\tau}(e_{zx}(t) - \Delta J \sigma_{zx}^0) \tag{1.33}$$

where τ is the relaxation time of the system, and $\Delta J = J_r - J_u$ is the difference between the non-elastic and elastic part of the shear compliance of the system, and σ_{zx}^0 is the applied stress. The solution to this equation is

$$e_{zx}(t) = \Delta J \sigma_{zx}^0 \left(1 - \exp(-\frac{t}{\tau})\right) \tag{1.34}$$

Similarly if an oscillatory shear stress $\sigma_{zx}(t) = \sigma_{zx}^0 exp(i\omega t)$ is applied to the system, it can be shown that the oscillatory shear strain has the following form

$$e_{zx}(t) = \sigma_{zx}^0 J^*(\omega) \exp(i\omega t) \tag{1.35}$$

where $J^*(\omega)$ the dynamic compliance of the system can be described as

$$J^*(\omega) = \frac{\Delta J}{1 + i\omega\tau} = \frac{\Delta J}{1 + \omega^2\tau^2} - i\frac{\Delta J\omega\tau}{1 + \omega^2\tau^2} \tag{1.36}$$

Once the single relaxation time behavior is established, one can use the fact that the response of the system is linear to find the response of the system in the general situation where the system has two or more relaxation processes.

$$J^*(\omega) = J_u + \sum_l \frac{\Delta J_l}{1 + i\omega\tau_l} \tag{1.37}$$

Glass-rubber transition

Figure 1.6 shows the creep compliance of a polymer schematically. The response of the system consists of three different behaviors. The short time response of the system is a solid like compliance of the order of $10^{-9}N/m^2$. A transition from the glassy behavior to rubber behavior happens at longer times (or higher temperatures) and the compliance gradually increases to about $10^{-5}N/m^2$, this transition is called the glass-rubber transition. For a certain time the creep value stays at the rubbery plateau before eventually changing to the viscous flow regime where the compliance increases linearly with time.

The glass-rubber transition also known as the α-relaxation process, is not a real phase transition like the melting transition. This transition is of pure kinetic origin and whether or not a system behaves like a glass or rubber only depends on the
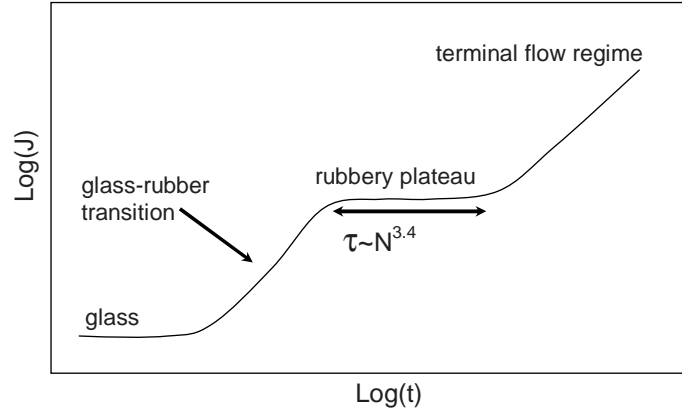
Figure 1.6: Schematic shape of the complete creep curve of a polymer

time scale of the experiment. The α relaxation will be discussed in more detail in the next section.

The existence and the width of the rubbery plateau, however depends on the molecular weight of the polymer and is an indication of the existence of chain entanglement which starts at a critical molecular weight M_c, the critical molecular weight of entanglement. The measurements at high temperatures(long times) indicate a viscous flow with a constant creep rate

$$\frac{dJ}{dt} \sim \frac{1}{\eta} \tag{1.38}$$

where η is the viscosity, which is related to the complete diffusion of the chains. The viscosity of the polymer is molecular weight dependent

$$\eta \sim M^{\nu} \tag{1.39}$$

The exponent ν has different values below and above the critical molecular weight M_c. Below M_c where the rubbery plateau doesn't exist, $\nu = 1$, as predicted by the Rouse model. Above M_c a $\nu \sim 3.2 - 3.6$ is observed, which is an indication of chain entanglement and reptative motion, which predicts a $\nu = 3$.

Dielectric relaxation

Dielectric relaxation of a polymer system can also be described by linear response theory. When an electric field E is applied to a polymeric system, the polarization induced by the electric field is given by

$$P = \epsilon_0(\epsilon - 1)E \tag{1.40}$$

where ϵ_0 and ϵ are the permittivity of vacuum and the permittivity of the dielectric substance respectively. The dielectric displacement vector D is equal to

$$D = \epsilon_0 E + P = \epsilon_0 \epsilon E \tag{1.41}$$

If at time zero a constant electric field is applied to the system, the polarization vector will have an instantaneous response followed by a slower time dependent response

$$P(t) = P_u + P_{or}(t) = \epsilon_0(\epsilon_u - 1)E_0 + \epsilon_0 \Delta\epsilon(t)E_0 \tag{1.42}$$

Respectively the response to an oscillating electric field $E(t) = E_0 \exp(i\omega t)$ is

$$P(t) = P_0 \exp(-i\phi) \exp(i\omega t) \tag{1.43}$$

The complex dielectric function $\epsilon^*(\omega)$ is thus given by

$$\epsilon^*(\omega) = \frac{D(t)}{E(t)} = \epsilon_0 + \frac{P_0}{E_0} \exp(-i\phi) \tag{1.44}$$

Similar to mechanical response measurements, dielectric measurements can also be used to define the characteristic relaxation times of the system, corresponding to different dipole relaxations of the system. In polymeric system which have strong susceptibility, dielectric measurements are ideal measurements to find different relaxation modes of the system such as α-relaxation. Dielectric measurements are usually carried out in the oscillatory modes.

1.2 Introduction to the glass transition

The glass transition has been called "The deepest and most interesting unsolved problem in solid state theory." [6] Despite years of experimental and theoretical
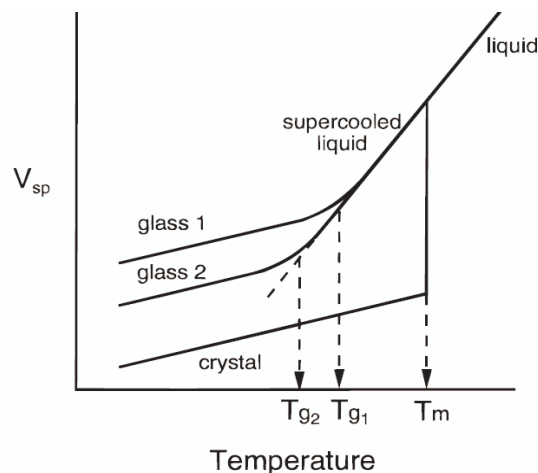
Figure 1.7: Schematic representation of the specific volume as a function of temperature for a liquid which can both crystallize or form a glass. Adapted from ref. [8]

studies, the nature of the glass transition remains unknown and there is no universal theory that can explain all aspects of this phenomena. In order to describe the glass transition an ideal theory should be able to explain all aspects of experimental data. On the other hand experiments should be developed to confirm different predictions of this theory, and ideally a self consistent picture should emerge. In The current theories, each grasp some aspects of the glass transition phenomena observed in the experiments, but usually fall short of explaining the others. In this section, some important aspects of the glass transition phenomena are discussed along with some of the major theories of the glass transition.

1.2.1 Phenomenology

If a liquid is cooled down fast enough, the molecules won't have enough time to sample the configurational space and crystallization can be avoided. As the temperature is decreased below the crystalization point, the motion of liquid molecules becomes slower and eventually it will take a molecule a long time to diffuse a distance of the order of its size and the system appears to be frozen in the experimental

time scale. This statically disordered frozen state of the system is called the glass. Figure 1.7 shows the changes of the volume of a glass forming material as a function of temperature. A system that is cooled below its crystallization temperature is called a supercooled liquid. As the material is supercooled, at some point the system falls out of equilibrium and forms a glass. The glass transition is defined by extrapolating the specific volume in the glassy state back to the specific volume in the supercooled state. The point that these two lines coincide is defined as the glass transition temperature T_g. If the liquid is cooled more slowly the particles will have more time to rearrange and hence falling out of equilibrium happens at a lower temperature and a lower T_g is obtained. As an example, glass 2 in figure 1.7 was formed with a slower cooling rate than glass 1, and thus has a lower T_g. The transition from a liquid to a glass is not a real phase transition, it does not include any discontinuities in the physical parameters and does not happen at a constant temperature. The glass transition is often called a dynamical transition rather than a thermodynamic transition because the only real difference between the glass and liquid phase is the dynamical slow down in the glass compared to a liquid. [7, 8]

The reason that the glass transition temperature depends on the cooling rate of the system is that once the relaxation time of the system becomes larger than the time scale of the measurement, a complete relaxation can not be seen in the experiment and the system appears frozen. Measurement at different cooling rates, are probes of different relaxation times. A cooling rate of 10K/min in a typical differential scanning calorimetry (DSC) measurement is approximately a probe of a relaxation time of 100 seconds and the cooling rate is inversely proportional to the relaxation time [9]. So the glass transition temperature T_g of small molecule liquids can also be defined as the temperature at which the relaxation time of the system becomes larger than 100 seconds or similarly the shear viscosity of the supercooled liquid becomes larger than 10^{12}Pa.S.

As the temperature of the system is decreased towards T_g the viscosity increases very rapidly. For some glasses such as silica the behavior of viscosity can be described by Arrhenius relation $\eta = A \exp(E/k_B T)$, where A and E are constants related to the material properties and k_B is the Boltzmann's constant. These
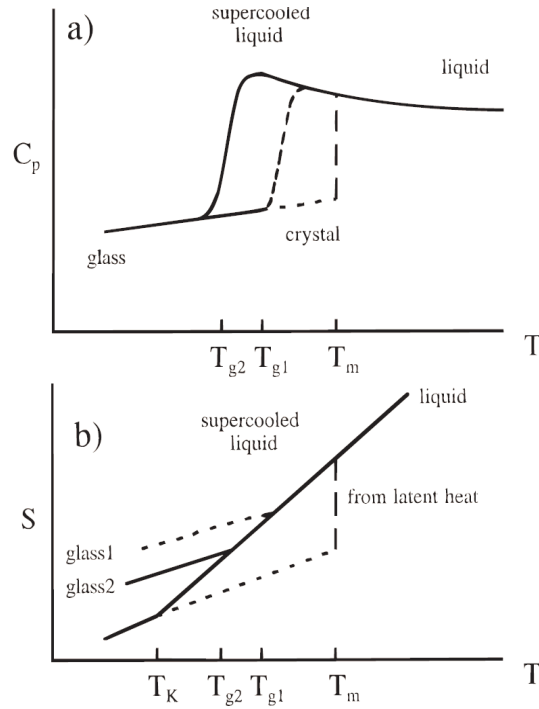
Figure 1.8: A schematic diagram of the temperature dependence of (a) the specific heat, c_p, and (b) the specific entropy, s, of a crystal, liquid, supercooled liquid, and glass. Adapted from ref. [8]

glasses are called strong glasses. For most other glasses, the change in the viscosity and relaxation time is more pronounced and the viscosity appears to be diverging if the behavior is extrapolated to a temperature about 50 degrees below the glass transition temperature. The behavior of the viscosity can usually be described by an empirical relation called Vogel-Fulcher-Tammann (VFT) equation [7,8].

$$\eta = A \exp[B/(T - T_0)] \tag{1.45}$$

Where A and B are material related constants and T_0 is the temperature at which the system dynamics appears to be diverging. The origin of this dramatic slowing down of the dynamics and whether not it continues below T_g is one of the main questions in the physics of glass transition. Glassy materials that exhibit VFT behavior are called fragile glasses [10].

The entropy crisis

Figure 1.8 shows the schematic behavior of the heat capacity and entropy of a supercooled liquid. In an ideal crystal the configurational entropy is equal to zero and as the temperature goes toward zero, the vibrational entropy also goes to zero. The configurational entropy of a liquid can be defined by Boltzmann entropy

$$S(N, V, E) = k_B \ln \Omega \qquad (1.46)$$

where Ω is the number of configurational states available for N particles with a total energy of E at a constant volume of V. As the liquid is cooled towards crystallization Ω becomes one and the configurational energy becomes zero. In a liquid above the melting point the number of states available to the system is always higher than one. In a supercooled liquid the difference between the entropy of the liquid and that of the crystal decreases rapidly, so that at some non-zero temperature it is expected to vanish. In reality the glass transition always intervenes to avoid this entropy crisis. In figure 1.8 glass 2 is obtained using a slower cooling rate, and thus its entropy becomes closer to the crystal entropy before it freezes. It has been suggested by some theories that although the glass transition is a dynamical transition and it is not a real phase transition, there probably exists a real second order phase transition behind it which happens at the Kauzmann temperature T_K at which the system has a unique configuration. To reach this point however, one needs to choose the limit of zero cooling rate. This means that the entropy crises is practically always avoided. The Kauzmann temperature is estimated to be about 50 degrees below T_g by the extrapolation of the slope of the entropy in the liquid state into the slope in the crystalline state. Some models suggest that this temperature is the same temperature as T_0 in which the dynamics of the system appear to diverge. Although many glass transition theories are based on the existence of this phase transition, there is not enough experimental evidence that directly confirms this fact and there are other theories that explain glass transition phenomena without having to introduce this diverging point [11].
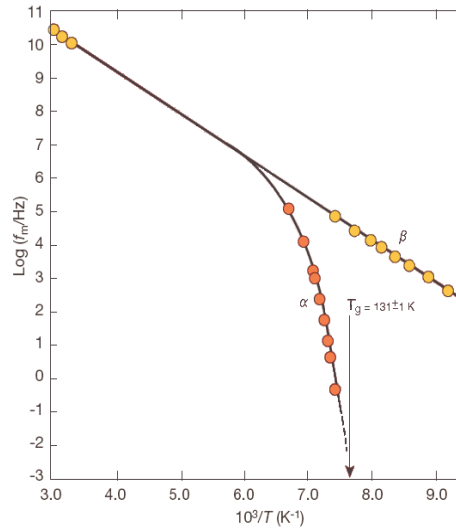
Figure 1.9: Temperature dependence of the peak dielectric relaxation frequency of chlorobenzene/cis-decalin. Adapted from ref. [7]

α and β relaxations

In a glass forming material well above its glass transition temperature the dielectric relaxation time has an Arrhenius dependence to the temperature, and only one relaxation peak is seen in the system. As the temperature is decreased, most materials show two distinct relaxation processes [12]. The slow relaxation time is called α-relaxation and is believed to be from collective motion of particles. This relaxation time increases rapidly near T_g, such that for every 3-5 degrees decrease in temperature the relaxation time increases approximately one decade. The fast relaxation process which remains Arrhenius is called β-relaxation, and is believed to be from local vibration of the molecules. The temperature at which the splitting between the two relaxation functions happens is known as the $\alpha - \beta$ splitting temperature $T_{\alpha\beta}$. Figure 1.9 shows an example of $\alpha - \beta$ splitting in a glass forming material. It can be seen that at high temperatures there is a single relaxation mechanism. In the moderately supercooled regime the peak splits into α (slow) and β (fast) relaxations, of which α-processes exhibit non-Arrhenius temperature dependence and diverges at T_0.

Nonlinear response functions

At temperatures below $T_{\alpha\beta}$, the response functions of the system, such as creep compliance and dielectric relaxations deviate from a single exponential relaxation to a behavior that can be roughly described by a stretched exponential function known as Kohlrausch-Williams-Watts (KWW) function.

$$\phi(t) = \exp\left[-(t/\tau)^\beta\right] \tag{1.47}$$

where $\beta < 1$. In this equation τ is the characteristic relaxation time(α relaxation), the temperature dependence of which can usually be described by VFT equation. For fragile glasses the β value is about 0.5 and generally systems that show more deviation from Arrhenius relation also have lower β values and deviate more from single relaxation behavior. There are some theories that suggest that there is a coupling between the stretched exponential exponent β and the degree of the deviation of the relaxation time from Arrhenius behavior [13].

The break down of symmetry

When the temperature of a liquid is decreased towards T_g, the symmetry between translational and rotational diffusion or viscosity breaks down and the translational diffusion is not proportional to the rotational diffusion or viscosity anymore [8]. At high enough temperatures, both translational and rotational diffusions are proportional to the inverse of viscosity. When the temperature is decreased below about $1.2 \times T_g$, which is approximately the same temperature as $T_{\alpha\beta}$, the translational diffusion becomes faster and the Stokes-Einstein relation becomes invalid. The symmetry between rotational diffusion and viscosity however remains unaffected [14, 15]. It is seen that as the temperature is lowered the difference between the two diffusions becomes more enhanced. There seems to be a correlation between this break down of symmetry and the exponent of the stretched exponential β. Systems with lower β values show more pronounced break down of this symmetry and the difference between the translational and rotational diffusion becomes larger.

Cooperative motion and Dynamical heterogeneity

One of the important issues in understanding the glass transition phenomena is the dramatic slow down of the dynamics. For example the viscosity of the liquid can change by about 12 orders of magnitude as the temperature is decreased from about $1.2 \times T_g$ to T_g. This slowing down happens without any apparent phase transition, or structural change in the liquid as the temperature approaches T_g from above. For strong glass formers such as SiO_2, the dynamics are Arrhenius, and a simple activated process with a single activation energy can explain the slow dynamics. In fragile glasses however the VFT slowing down is much more dramatic, and the activation energy near the glass transition can be of the order of 500KJ/mol which is higher than the strength of interaction of chemical bonds in organic liquids. This activation energy is thus unlikely to be associated to the motion of one particle in the field of fixed neighbors. Some theories such as the Adam-Gibbs theory [16] explain the existence of this activation energy by introducing a relaxation process based on the cooperative motion of neighboring molecules.

As the temperature is decreased towards T_g, the individual particles do not have enough energy or volume available to rearrange separately. Figure 1.10(a) shows three possible ways that the particles can rearrange. In all of these three situations the average particle moves about 20% of its diameter. In each frame the original position of the particle is shown with pale red and the final position is shown in red. Individual particles can move to fill out the local voids that are produced by the rearrangement of other particles (A), or they can collectively move as a small group (B) or all particles can move together (C). Each of these motion requires a correlation between the motion of different particles. It is expected that the size of this cooperatively rearranging region (CRR) increases as the temperature is decreased. This cooperatively rearranging region has not been directly observed in experiments of glass formers, and experiments that provide an estimation of the size of this region near T_g are based on some initial assumptions about the existence and the shape of this region. Experiments on colloidal glass formers, in which the concentration is changed instead of the temperature, show that this cooperative motion exists in the suspension but only in subset of fast particles, and the rearrangement in those glasses is more similar to case (C) in figure 1.10. This
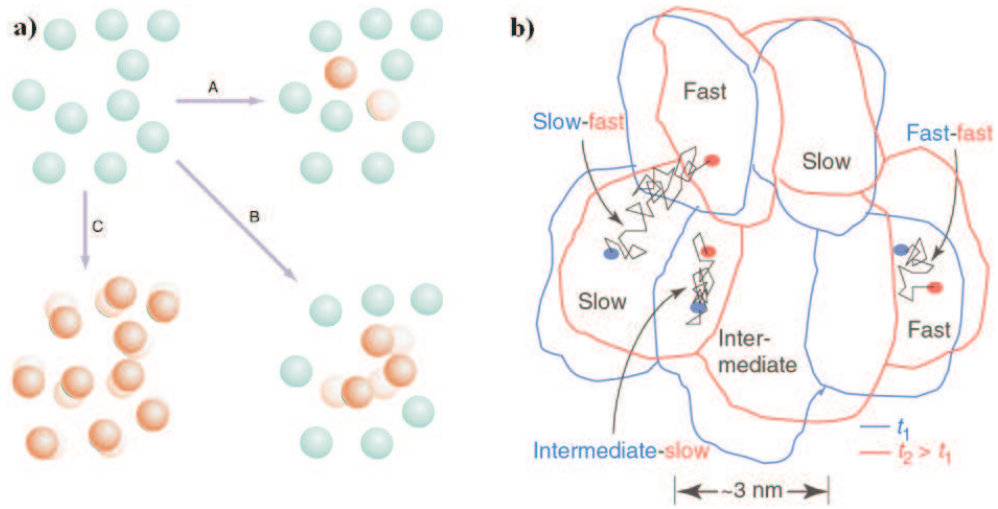
Figure 1.10: a) Different possibilities for the motion of particles near T_g. Adapted from ref. [18]. b)Regions of different dynamics at two different times t_1 and t_2, showing possible trajectories of individual molecules in such a heterogeneous environment. Adapted from ref. [19]

motion however is not enough to explain the complex behavior seen in molecular glass formers, and theories that only use cooperative motion, can not cover all other aspects of the dynamics such as the break down of symmetry in these systems.

Measurements of colloidal glasses also show heterogeneity in the dynamics. Regions that are only a few nanometers apart can have dynamics that are orders of magnitude different in the time scale where the average particle has moved only about 20% of its size [17]. Figure 1.10 (b) shows a schematic picture of the dynamical heterogeneity. The cooperatively rearranging clusters are usually located in the fast relaxing regions. Some observed phenomena such as non exponential relaxation processes and the break down of the symmetry between translational and rotational diffusion can be explained by the concept of dynamical heterogeneity. One can explain the non exponential dynamics in two different ways, schematically shown in figure 1.11. In this figure each graph represents the relaxation function at a different location in the sample. One possibility is that all molecules in the supercooled liquid are moving homogenously and the relaxation of each of them
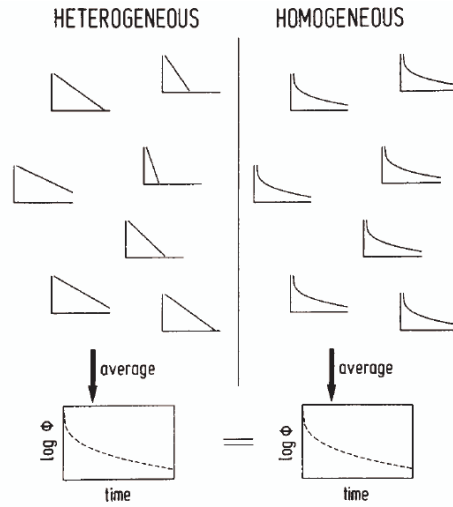
Figure 1.11: Schematic illustration of heterogeneous and homogeneous explanations for a non-exponential relaxation function. Adapted from ref. [8].

is stretched due to cooperative motion of particles (right). In this case a lower β value is associated to increased cooperativity. The other explanation could be that the relaxation of individual particles remain exponential (left), but different regions in the system have different relaxation times and the average relaxation time over different domains produces the stretched shape of the relaxation function. Lower β in this scenario corresponds to the increased heterogeneity in the system. The relaxation function $\phi(t)$ of a system is the Laplace transform of the density auto-correlation function

$$\phi(t) = \int_0^\infty G(\tau)e^{-t/\tau}d\tau \qquad (1.48)$$

In the heterogenous explanation $G(\tau)$ represents the spatial distribution of the relaxation times, while in the cooperativity view point this function doesn't have any direct physical meaning. Recent experiments support the heterogenous view point, which is also backed by simulations [20, 21]. This view point can also explain the break down of symmetry in between rotational and translational diffusion. Dynamical heterogeneity is based on the assumption that domains that are only a couple of nanometers apart can have relaxation times that differ from each other by orders of

magnitude (figure 1.10 b). This can explain the existence of fast moving domains, that translate through the liquid, and can enhance the translational diffusion by orders of magnitudes, without having to move all liquid molecules around to do so [14].

1.2.2 Theories of the glass transition

Any theory that deals with explaining the glass transition, should be able to explain all different aspects of the complex behavior seen in glass formers. The existing theories of glass transition often can explain some of the aspects depending on the type of the theory, but fall short in explaining the others, or predicting the new phenomena that emerge from the experiments everyday. The behavior of a supercooled liquid near T_g is often described by VFT equation or a power law equation such as [22]

$$\tau = \tau_0 [T - T_0/T_0]^{-B} \tag{1.49}$$

All these types of equations have a singularity at some temperature T_0 which is about 50 degrees below T_g. In reality, the relaxation time becomes so long that no experiment can actually measure a relaxation time near that temperature. So the question of whether or not an actual phase transition exists at that temperature and whether the dynamics diverges as a result of this phase transition cannot be directly answered in experiments.

There are three different classes of glass theories. The first class of theories predict that a real phase transition exists below T_g and the dynamics are described based on the fact that near this temperature the relaxation time diverges. The second class of theories predict a transition at a temperature much above the glass transition temperature, where the dynamics starts deviating from simple liquid dynamics. As the temperature is decreased, the system passes close to a critical point at a temperature close to $T_{\alpha\beta}$, and narrowly avoiding this critical point is what causes dramatic slow down of the liquid dynamics. In the third class there is no real phase transition, and the slow dynamics are of a purely kinetic origin. In the rest of this chapter some of these models are briefly introduced.

Free volume theory

Free volume theory is one of the first theories that could successfully explain some aspects of glass formation such as dramatic slow down of the dynamics near the glass transition [23, 24]. This theory is also attractive because it provides an intuitive picture of glass transition that can be really useful in understanding different phenomena. The idea behind the theory is that molecular transport happens by the motion of particles into the voids formed by redistribution of the free volume of the system, that are larger than a critical size. The slowing down of the dynamics is attributed to the reduction of this free volume. The average free volume per molecule is equal to $\overline{v}_f = V/N - v_0$, where v_0 is the volume occupied by the molecule itself and N and V are the number of particles in the system and the volume of the system respectively. If the thermal expansion is assumed to be constant, then the dependance of the average free volume to temperature can be described as

$$\overline{v}_f(T) = \alpha(T - T_0) \tag{1.50}$$

where T_0 is the temperature at which the free volume becomes zero. The probability density that a particle has an available free volume v_f is assumed to be

$$\rho(v_f) = (1/\overline{v}_f) \exp(-v_f/\overline{v}_f) \tag{1.51}$$

The rate of transport(the relaxation time of the system), is proportional to the probability of finding a free volume which is larger than a critical value v_c.

$$1/\tau = \rho(v_c) = A \exp(-\frac{V_c}{\alpha(T - T_0)}) \tag{1.52}$$

Although the free volume theory can be used to reconstruct the VFT behavior, it has some fundamental problems. This theory does not yield to any predictions about the stretching of the response functions, or dynamical heterogeneity. The other main problem with this theory is that if the reduction of the free volume was the main cause of the slow dynamics, then decreasing the temperature at a constant volume instead of constant pressure would result in the disappearance of the glass transition, while there are experiments that show that the glass transition happens even at a constant volume [25].

Adam-Gibbs theory

Adam-Gibbs Theory [16,24] is based on the existence of a cooperatively rearranging region (CRR) in supercooled liquids. This theory is very similar to the free-volume theory, but it uses an entropy approach to describe the slow dynamics, instead of making assumptions about the volume of the system.

The behavior of a supercooled liquid is sometimes described by the Williams-Landel-Ferry (WLF) equation which is mathematically equivalent to the VTF equation.

$$-\log a_T = C_1(T - T_s)/[C_2 + (T - T_s)] \tag{1.53}$$

In this equation $a_T = \tau(T)/\tau(T_s)$ is the ratio of relaxation times at temperature T to the relaxation time at a reference temperature T_s. The reference temperature T_s is usually about 50 degrees below T_g. In this theory it is assumed that there exists a real second order phase transition at a temperature T_2 at which the configurational entropy becomes zero. At higher temperatures cooperatively rearranging domains exit with domain sizes that diverge at T_2. Assuming that a subsystem z of the particles, interact weakly with the rest of the system, and only interact with each other. These particles are in mechanical and thermal contact with each other. An isobaric isothermal ensemble of N subsystems, each composed of z molecules, which are indistinguishable and independent of each other is assumed. The particles inside a number n of these subsystems are allowed to cooperatively rearrange, while the other $N - n$ subsystems are not allowed a relaxation and appear to be frozen. The Gibbs free energy of the whole system is defined as $G = -kT \ln \Delta$, where Δ is the partition function

$$\Delta(z, P, T) = \sum_{E,V} \omega(z, E, V) \exp(-E/kT) \exp(-PV/kT) \tag{1.54}$$

If the sum is imposed only over the subsystems that are allowed to rearrange, then the partition function Δ' gives the Gibbs free energy for the rearrangeable subsystem, $G' = -kT \ln \Delta'$. Thus $n/N = \Delta'/\Delta = \exp[-(G' - G)/kT]$, and the cooperative transition probability is defined by

$$W(T) = A \exp(-z\delta\mu/kT) \tag{1.55}$$

where $z\delta\mu = z(\mu' - \mu) = G' - G$. The average transition probability is the sum over all possible subsystem sizes z that can cooperatively rearrange. In a supercooled liquid there is a critical minimum size for a cooperatively rearranging domain z^*, below which the subsystem can not rearrange. One can show that the average transition probability is approximately equal to

$$\overline{W} = \overline{A}\exp(-z^*\delta\mu/kT) \tag{1.56}$$

Since these subsystems are independent of each other the configurational entropy is the sum of entropies of the subsystems. Since $\delta\mu$ is almost constant $S_c = Ns_c$, where s_c is the entropy of each region and thus $z^* = Ns_c^*/S_c$. This leads to

$$\overline{W} = \overline{A}\exp(-\Delta\mu s_c^*/kTS_c) = \overline{A}\exp(C/TS_c) \tag{1.57}$$

where C is a constant. The WLF equation can now be reconstructed.

$$\log a_T = \log[W(T_s)/W(T)] \tag{1.58}$$

with some rearrangements and assuming that $S_c(T_2) = 0$, $S_c(T_s) = \Delta C_p \ln(T_s/T_2)$ this leads to

$$C_1 = 2.3\Delta\mu s_c^*/K\Delta C_p T_s \ln(T_s/T_2) \tag{1.59}$$

$$C_2 = \frac{T_s \ln(T_s/T_2)}{1 + \ln(T_s/T_2)} \tag{1.60}$$

The existence of the phase transition in this theory explains how the entropy crisis, also known as the Kauzmann paradox can be avoided. The theory predicts that the system reaches a unique configuration at temperature T_2 which is the same temperature as the Kauzmann temperature $T_2 = T_K$. Calorimetric measurements of the Kauzmann temperature show that this temperature is also close to the VFT diverging temperature T_0 which is an important success for this theory. DiMarzio and Yang used a modified form of the Adam and Gibbs theory [26], in which the system does not need to reach a unique configuration. Instead the phase transition happens when the structural arrest reaches the percolation point, and the configurational entropy reaches a small non-zero amount $S_c(T_2, P_2) \rightarrow S_{c,0}$. Small regions in the system can still rearrange, even below the glass transition temperature, and

there is no sudden break in the viscosity. Instead the viscosity behavior changes from VFT to Arrhenius. The viscosity of the system is equal to

$$\log \eta = B - AF_c/kT \tag{1.61}$$

where F_c is the configurational Helmholtz free energy, $F_c = -kT \ln Q$. Close to T_g, the heat capacity behaves like $C_{p,c} = \alpha/T$ so $S_c = \alpha(1/T_2 - 1/T)$, and since $S_c = \partial F_c/\partial T$, this leads to

$$F_c = -C \quad -\alpha(T/T_2 - 1) + \alpha \ln(T/T_2) \quad T \geq T_2 \tag{1.62}$$

$$F_c = -C \qquad\qquad\qquad\qquad\qquad T < T_2 \tag{1.63}$$

where the constant C is part of the activation energy. This Arrhenius behavior of the viscosity below the glass transition has been observed in aging experiments of glass formers such as polycarbonate [27].

Edwards model

In the Edwards model the glass transition is studied in a system of rigid rods. The fact that the properties of a glassy material does not depend on the shape of its particles, is used to extrapolate the results into a universal behavior of the glassy materials [28]. This model is also useful in the studies of glass transition in systems made of liquid crystals or polymers, which have cylindrical molecules or segments respectively. In this model the diffusion constant of a solution of rod like molecules is calculated, by considering that the particle motions are delayed by closing and opening of random gates produced by the motion of neighboring molecules. The first order term is calculated by assuming that other particles of the liquid are moving freely. Then a self consistency argument is used to add the effect of theses delays to the random motion of the neighbors as well. The calculated diffusion constant is equal to

$$D = D_0[1 - C(cdL^2)^{3/2}] \tag{1.64}$$

where c is the concentration, L and d are the rod length an diameter and C is a number of the order of one. If the concentration is increased (the temperature is

decreased), at some concentration the diffusion becomes zero and the solution of rod like particles freezes $(T = T_g)$

$$D = D_0(\frac{T}{T_g} - 1) \tag{1.65}$$

This is a mean field solution that only considers the motion of single particles, the cooperative motion of particles can be added as higher order terms [29]. These higher order terms are calculated based on the motion of rods following each other in lines or loops. Using these terms one can reconstruct the VFT equation

$$D = D_0 \exp[-\frac{(\Delta T_g)^2}{4T_0(T - T_0)}] \tag{1.66}$$

where the constants $A = -\frac{(\Delta T_g)^2}{4T_0}$ and T_0 are obtained experimentally.

The Edwards model is also insightful in modeling the glass transition of polymeric systems. For example the dependance of T_g on molecular weight can be calculated by assuming that the glass transition is caused by the blockage at the end of chains and entanglement points [30]. The total number of problem points would be of the order of $L/a - 1$, where a is the monomer size. If $T_g(\infty)$ is the T_g at the limit of $L \to \infty$, then

$$T_g = T_g(\infty)[1 - \gamma\frac{a}{L}] = T_g(\infty)[1 - \gamma\frac{M_e}{M}] \tag{1.67}$$

Which is in well agreement with the experimental data. Other properties of glass transition in polymers can be similarly obtained using this model.

Similar to the free volume theory this model suffers from the fact that even at constant volume, the glass transition must happen, but there are some important aspects to this model which should be considered carefully. This model suggests that in order to have a cooperatively rearranging region, it is not necessary to have a three dimensional region, the molecules can follow each other in string-like paths, and the CRR could be a one dimensional region.

The results of measurements in colloidal glasses [31] and simulations also confirm this point [21]. It is seen in the simulations that the heterogeneous domains are composed of particles that follow each other in string like motions. As the
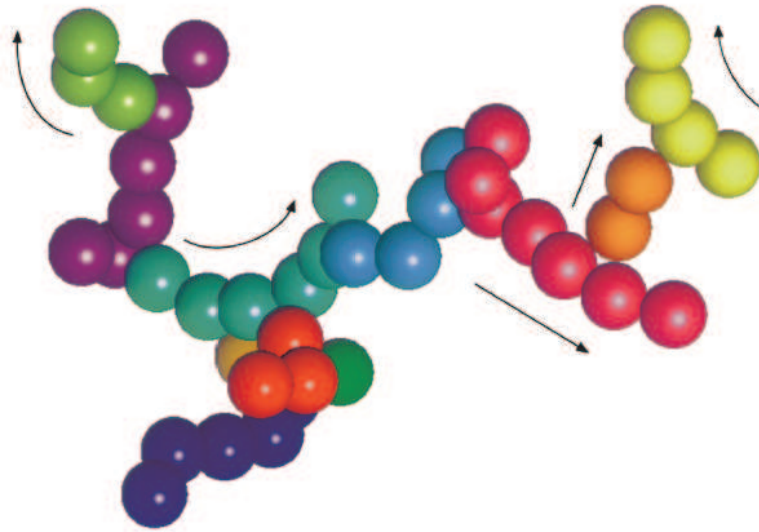
Figure 1.12: Schematic picture demonstrating how a typical cluster of mobile particles is composed of smaller, quasi-one-dimensional strings of particles which move collectively as a single unit. Adapted from ref. [21].

temperature of the system is decreased towards the freezing point the average size of these heterogenous domains increases rapidly with a power-law dependence to the temperature and appears to be diverging, while the size of the cooperatively moving domains, which are inside these heterogeneous domains, increases towards a constant size L. The probability distribution of these domain sizes decreases with the size of the domain with an exponent which is almost equal to one (as opposed to the probability distribution of the heterogenous domains which makes an exponent equal to $\nu = -1.9$ with the size of the clusters) showing the one dimensional nature of these cooperatively rearranging regions. Figure 1.12 shows the simulation results [21] showing a typical heterogenous domain made of the top %5 of fast moving particles inside which particles are following each other on string like motions indicated by different colors. The arrows show the direction of motion of these particles.
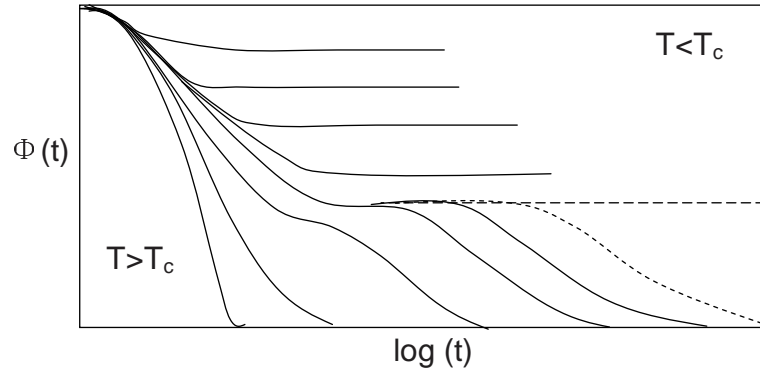
Figure 1.13: Schematic behavior of the density auto-correlation function

Mode coupling theory (MCT)

The mode coupling theory [24] is based on the assumption that the response of the density-density correlation function

$$\phi(t) = \frac{< \rho(o)\rho(t) >}{< |\rho|^2 >}$$

(1.68)

is a non-linear response with a memory effect [24]

$$\frac{d\phi(t)}{dt} = i\Omega_0\phi(t) - \int_0^t \gamma(t')\phi(t - t')dt' + R(t)$$

(1.69)

where ρ_Q is the Fourier component of the spatial density correlation function. The time evolution of $\phi(t)$ depends on the dynamic variable $\phi(t)$ itself a random force $R(t)$ and the memory effect introduced by the coupling variable $\gamma(t)$ which is a function of $\phi(t)$ itself. In the classic mode coupling theory the coupling parameter can be symbolically shown as [10, 32]

$$\gamma[\phi] = c_1\phi + c_2\phi^2$$

(1.70)

Assuming that c_1 and c_2 are functions of temperature and larger than zero, there is a critical temperature below which the autocorrelation function will not decay to zero. Figure 1.13 shows a schematic behavior of the density correlation function.

The critical temperature T_c predicted in mode coupling theory is higher than T_g, and it is rather close to $T_{\alpha\beta}$. Some revisions of the ideal mode coupling theory

indicate that the reason that no divergence is seen at T_c in the experiments is that higher order couplings become more important at lower temperatures which allow activated processes to happen below this critical point. One of main successes of the mode coupling theory is its prediction of a relaxation function consisting of several different distinct regimes. As shown in figure 1.13 the density autocorrelation function first decays via fast microscopic process which follows a power-law relation $\phi(t) \approx f + A_1 t^{-a}$. At longer times the decay crosses over to another power-law $\phi(t) \approx f - A_2 t^b$, and finally at very long times the decay appears to be similar to the α relaxation process, $\phi(t) \approx \exp[-(t/\tau)^\beta]$. This sequence of relaxation times has been verified experimentally in colloidal systems and in computer simulations.

Although mode coupling theory is successful in explaining different phases of slowing down of the dynamics it has several problems. For example mode coupling theory is not directly connected to the molecular motion of the particles. Extra modeling is needed to establish this connection. Dynamics heterogeneity is not predicted by this model directly. Extra assumptions are necessary to relate the two pictures.

Avoided singularity

Kivelson and coworkers have a theory which is similar to MCT in that it is based on an avoided transition [11, 25, 33], but unlike MCT this model is directly based on heterogenous dynamics.

In this model a critical temperature T^* exists above the crystallization temperature T_m. Where it is possible, the system would prefer to crystalize into a locally preferred structure, but it is prevented to do so, by the fact that this structure will not tile a three dimensional space, so the system is geometrically frustrated, and freezes into domains, with locally relaxed structure. At $T > T^*$ the system is disordered, at $T < T^*$ the system is ordered if the frustration parameter K is zero. $T = T^*, K = 0$ is a critical point, but in reality K is a small non zero parameter and the system narrowly avoids this critical point. The system has two characteristic length scales. a critical correlation length ξ with $\xi/a_0 = [T^* - T/T^*]^{2\nu} = \epsilon^{2\nu}$, which governs the dynamics in the absence of frustration, and R_D the length scale

at which otherwise ordered structure is broken up into frustration limited domains. as $K \to 0$, R_D diverges. Therefore for $T < T^*$, $R_D \ll \xi$ and the frustration doesn't have an effect on short length scale dynamics. Based on this theory a universal equation is obtained for the dynamics

$$T[\ln(\tau/\tau_0)] \propto (R_d/\xi)^2 T^* = BT^* \epsilon^{4\nu} \tag{1.71}$$

where $4\nu = \frac{3}{8}$ is a universal exponent. In the neighborhood of T^* the $R_D \ll \xi$ is violated and this equation governs the dynamics.

The frustration limited domain theory seems to be very successful in explaining the relaxation behavior of different glass formers over wide range of time scales without having to use different functional forms at different time scales and without introducing a stretched exponential parameter, β [34]. The fact that this model is directly based on heterogenous dynamics makes this model even more interesting.

The energy landscape

The energy landscape model provides a convenient framework to conceptually explain the complex behavior of the glassy systems [7]. The potential energy of a system is defined as $\phi(r_1, ...r_N)$, where r_i accounts for position, orientation, velocity and other relevant parameters of the system particles. This function is a multi dimensional surface with a non-trivial form which depends on all interactions in the liquid or glass. Figure 1.14 shows a schematic illustration of this landscape. The number of potential energy minima, their depth, and the nature of saddle points separating energy minima defines the properties of the system. In a system with fixed volume V the landscape is fixed. The way that a system samples the landscape as a function of temperature defines the dynamics of the system. At high temperatures the system has enough time or energy to sample all possible configurations of the system. As the temperature is decreased, there is not enough kinetic energy for the system to sample all energy minima, and it becomes trapped in deeper minima. When this happens the kinetics change from single exponential relaxations to stretched exponential relaxations. At a low enough temperature, the system is stuck in a single minimum, the depth of which increases with decreasing cooling rate, and the glass transition happens. Excluding the crystallization
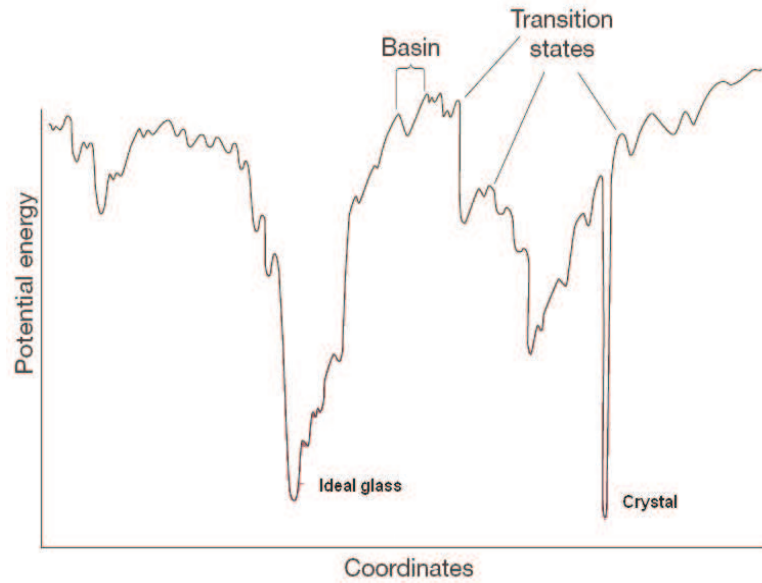
Figure 1.14: Schematic illustration of the energy landscape. The X axis represents all degrees of freedom. Adapted from ref. [7]

minimum, which is very narrow, the other deepest minimum represents the ideal glass. The landscape picture, provides a natural separation between molecular motion into sampling the potential minima and vibrational motion within a certain minimum. It also provides a picture to explain the difference between fragile and strong glasses. The energy landscape of a strong glass former is made of a main mega-basin with no major energy barriers, while the energy landscape of a fragile glass is made of several mega-basins, separated by high energy barriers. The cooperative rearrangement of the particles, enables transitions between these basins. At low temperatures these rearrangements are rare, and the system remains trapped in one of these basins. The diversity and pathways between these basins, defines the stretched exponential shape of the relaxation time, as opposed to single relaxation times seen in strong glass formers, that show relaxations within a single mega-basin. Depending on how fast the glass is cooled, the system falls into one of these local minima. It also explains dynamical heterogeneity based on the number of minimums accessible at each energy level. The only disadvantage of this picture is that it is nearly impossible to define the landscape of a real system with huge degrees

of freedom, so applying this picture to a real world glass transition problem, and finding quantitative results using the energy landscape model becomes impractical.

More details about glass transition phenomena and different theories can be found in references [7, 8, 10, 22, 25].

Chapter 2

Dynamics of polymers in confinement

Theories of the glass transition are based on the existence of one or two important length scales. Observing these length scales in the real world has been a challenging task for experimentalists. There are very few measurements that are able to measure such length scales. But usually these measurements have to rely on some initial assumptions about the existence of such length scales to be able to relate the experimental data to a length scale. There is no consensus about the size, dimension or whether or not these length scales diverge in the vicinity of glass transition. One way to study these length scales is to use confined systems, and study their behavior as the glass transition in approached. When the size of the experimental system becomes comparable to a characteristic length scale of the system, one may expect to see some anomalies in the dynamics as a result of the interaction of the system with its boundaries or other finite size effects. A traditional way to measure the confinement effect on the dynamics of glassy materials was to measure the behavior of supercooled liquids and glasses in porous media. Jackson and McKenna [35] measured the glass transition of O-terphenyl and benzyl alcohol confined in small glass pores using differential scanning calorimetry (DSC) and saw a reduction in glass transition temperature as the pore size was decreased. For the smallest size pores (4 nm in diameter) the glass transition of O-terphenyl
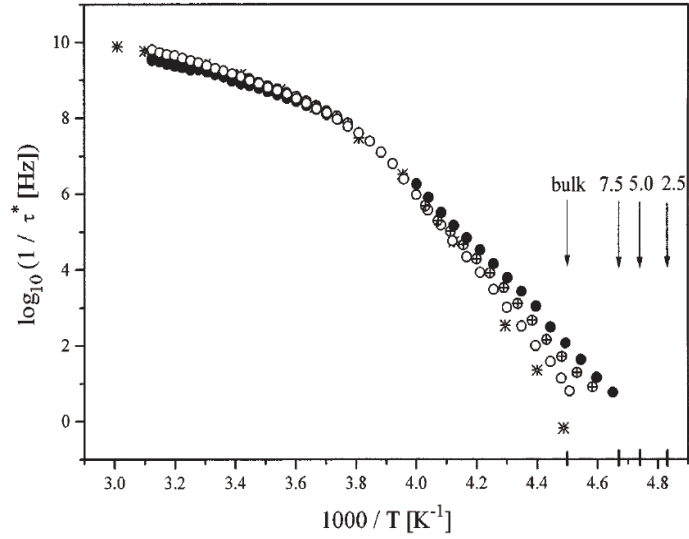
Figure 2.1: Activation plot for salol confined in coated pores; 7.5 nm, 5.0 nm, 2.5 nm, and bulk salol. The arrows indicate the calorimetric glass transition temperatures. Adapted from ref. [40]

$(T_g(bulk) = 248K)$ was observed to be 18 degrees lower than its bulk value. Later studies showed that T_g can be either higher or lower than bulk T_g depending on the type of interaction between the pore surface and the glass forming material [36–39]. Arndt *et al.* [40] showed that when interaction of the pore and the material is not strong, an enhancement of the dynamics can be seen in dielectric relaxation (Figure 2.2). The deviation from the bulk dynamics starts at a temperature above bulk T_g, and increases as the temperature is decreased towards T_g. It was shown that this effect can be modeled by assuming that there is a layer near the pore surface with a thickness of 0.38 nm that has enhanced dynamics compared to the bulk dynamics. A reduction in the T_g values measured by DSC was also seen which was consistent with the observed enhanced dynamics. Later studies showed that similar behavior is also seen in polymeric glass formers [41, 42] Sasaki *et al.* [43] measured the T_g of polystyrene spheres with diameter $d = 40 - 500$ nm in aqueous suspensions using DSC and observed a reduction and broadening in the ΔC_p value, without any reduction in the T_g itself. A model based on the existence of a more mobile layer near

the interface was used to explain the reduction in the ΔC_p value. It was assumed that the relaxation of this layer is so fast that it does not contribute in the glass transition. Based on this model the size of this layer was estimated to be about 4 nm. Simulations of dynamics of particles confined in hard wall pores at temperatures above the freezing point, also showed slow down of relaxation time and broader relaxation compared to bulk. The relaxation as a function of the distance from the wall showed a gradual change from very slow to bulk like behavior which could explain the broadening of the dynamics [44]. Wang *et al.* obtained similar results for propylene glycol using fluorescent intensity technique [45].

The results of these experiments indicates that the glass transition is sensitive to the boundaries of the system when the system is in a confined geometry, but they are unable to provide more details on the nature of these effects. The interaction of the glass former with the walls can not be eliminated and hence the exact origin of observed enhancement of the dynamics can not be explained. It is also not clear whether or not other parameters are affecting the enhanced dynamics, such as a reduction of density during the injection of the material into the pores. It is thus important to find a system that provides more degrees of freedom in terms of sample properties and the ways the sample can be studied. Polymer thin films are systems that can be easily made and studied using many different techniques. This enables us to better understand the confinement effects on the dynamics of glassy materials.

Polymer thin films and surface are also widely used in different systems and applications such as packaging, barriers, membranes and catalysts [46], sensors [47], medical implants [48], adhesives [49] and lithography [50]. So it is crucial to understand the effect of confinement to their dynamics in order to better quantify their properties in such systems.

2.1 Glass transition in thin polymer films

Perhaps the easiest way to study the dynamics of thin polymer films is to measure their glass transition temperature and compare it to the bulk glass transition. There

are many different experiments and simulations concerning the T_g measurements of thin films. In this sections a review of these experiments and some related theories is provided.

2.1.1 T_g measurements in thin polymer films

T_g studies of thin supported films

The first class of experiments discussed in this section are studies of T_g reduction in thin polymer films supported on a substrate. These films are usually produced by spin-coating a solution of polymer onto a substrate. The first experiment of this kind was the experiment of Keddie, Jones and Cory [51], where ellipsometry was used to measure the glass transition temperature of polystyrene thin films with different thicknesses and molecular weights ($12 \times 10^4 < M_w < 29 \times 10^5$). Measurements were done upon heating of 2K/min, after the samples were cooled from a temperature above T_g with a cooling rate of 0.5K/min. It was observed that the T_g of all films with thicknesses less than 50 nm was decreased below its bulk value. The results were independent of the molecular weight of the polymer used and could be fitted to the following empirical equation

$$T_g(d) = T_g(\infty) \left[1 - \left(\frac{A}{d} \right)^{\delta} \right]$$ (2.1)

where $T_g(\infty) = 373.8$K is equal to the bulk T_g of polystyrene, $A = (3.2 \pm 0.6)$ nm and $\delta = 1.8 \pm 0.2$. The authors used a model based on the existence of a more mobile layer near the free surface with the thickness ξ that increases as the temperature is increased towards bulk T_g

$$\xi(T) = A \left(1 - \frac{T}{T_g(\infty)} \right)^{-1/\delta}$$ (2.2)

which has a reduced T_g compared to the bulk T_g. Using this model it was shown that the equation 2.1 can be reconstructed and the size of this layer, ξ is equal to 8-13Å at $T = T_g$. It was also observed that the expansivity in the glassy region and as a result, the contrast of the transition is decreased as the film thickness is
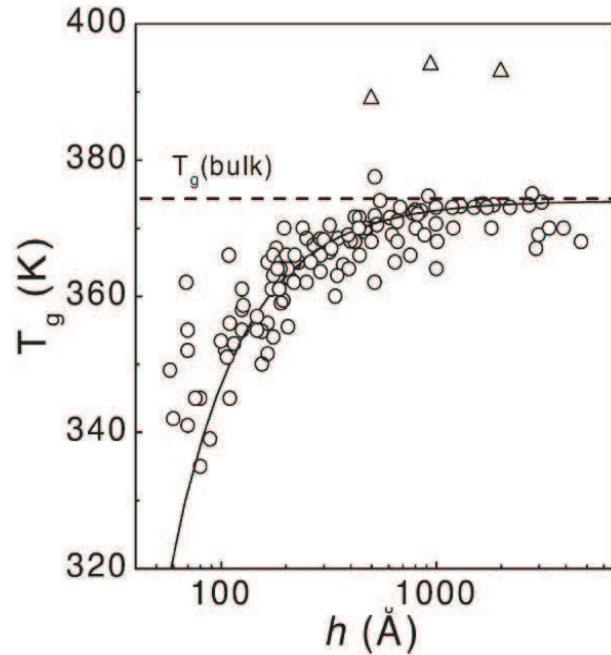
Figure 2.2: Compilation of measured T_g values for supported PS films using different methods. Adapted from ref. [62]

decreased. This could also be explained by the proposed enhanced dynamics near the free surface.

After this experiment, many similar T_g measurements have been done on thin polystyrene or other polymer films, using different techniques [52–62]. Studies on polystyrene glass transition using many different methods such as positron annihilation lifetime spectroscopy [53, 60], fluorescent intensity measurements [52] and ellipsometry [59, 61, 62], revealed that in most cases, the reduction of T_g compared to the bulk T_g is independent of molecular weight for a wide range of molecular weights below and above the entanglement threshold. Figure 2.2 shows the T_g reduction of polystyrene thin films obtained from several different studies [62]. These studies also showed that the substrate used does not seem to play any major role in the observed T_g reduction in polystyrene films. Using fluorescent intensity technique, Ellison et al. [52] showed that changing the repeat unit of polystyrene to molecules with larger persistence length (P4MS and PTBS) can enhance the T_g

reduction effect. In PTBS the onset of T_g reduction is 300 nm the largest ever seen in thin polymer films.

Unlike polystyrene, studies on PMMA showed contradictory results. In some cases the T_g was increased as the film thickness was decreased [55, 56]. It was shown that the behavior of PMMA depends strongly on the substrate used. In cases where a strong attraction between the polymer and the substrate exists, for example i-PMMA on silicon substrate, the T_g is increased, while films made on Al substrate, or Silicon substrate treated with HMDS, which are non-attractive surfaces of PMMA, show a decrease in T_g as the thickness is decreased [55–57]. Grohens *et al.* [58] also showed that the tacticity of PMMA can have an effect on the T_g values of PMMA thin films. S-PMMA on silicon substrate shows a reduction in T_g while the T_g of i-PMMA with similar molecular weight, increases as the film thickness is decreased.

The effect of sample preparation

In order to understand why the glass transition in thin films is different from that of bulk, several factors must be considered. Polymer thin films are usually made by spin-casting a solution of polymer onto a substrate. These films are highly meta-stable forms of materials, and if annealed long enough, on a non-wetting substrate, they will dewet and form spherical caps which are the preferred stable forms. Making polymers into thin films can potentially cause a reduction in the density, its degree of entanglement [63], and it can also increase the concentration of chain ends near the free surface compared to the bulk of the film [64]. Each of these factors can potentially contribute in the T_g reduction of thin polymer films. Also as mentioned before the complex interaction of the polymers with the substrates can also alter the results of the T_g measurements.

Reiter and deGennes [65] measured the behavior of ultra-thin polystyrene films made by spin-casting method when the samples were first made at room temperature. At room temperature, as the solvent evaporates, the thickness of the film is decreased under tension. It was seen that increasing the temperature up to 333K for polystyrene causes an initial increase of the film thickness due to some memory

effects. A decrease of thickness due to substrate interaction follows as the film is heated further. This process is a reversible process, and if the film is cooled down at this point the sample behaves the same way upon a repeated heating. As the temperature is increased further, a weakening of the substrate forces, causes nucleated or spinodal dewetting of the film. This study shows that the polymer samples are under a large amount of stress when they are initially made. It also suggests that when the sample is annealed, some of these stresses can be released, but in order to reach an equilibrium, the film must be dewetted, which is naturally avoided in thin film experiments, because a uniform film thickness is needed. Orts *et al.* [66] used X-ray reflectivity to measure the thickness dependence of this effect and showed that for films with thickness above 20 nm the expansivity is similar to the bulk polymer, and only for films thinner than 5 nm a shrinking of the film can be seen due to large initial stresses, which can be annealed out at 353K, about 20 degrees below bulk T_g of polystyrene. In order to avoid complications like this, in most T_g measurements the samples are annealed above bulk T_g for a period of time and measurements are done upon cooling, rather than heating. Experiments also show that the existence of oxygen during the annealing at high temperatures of some polymers (for example 2 hours at 450K for polystyrene) can cause some structural damage to the polymer surface, which could affect the dynamics and glass transition temperature of the system [67]. So it is also important that the annealing of the films be done under vacuum or a dry inert gas such as nitrogen, at only about 10-30K above bulk T_g in order to avoid complications.

In order to understand the effect of reduced entanglement on T_g reduction Simon *et al.* [68,69]measured the properties of freeze-dried polystyrene with different molecular weights. Freeze-drying from a very dilute solution is expected to reduce the entanglement of the system. Viscoelastic measurements on these samples showed that the rubbery plateau of the creep compliance decreases in successive runs at a constant temperature, indicating that the entanglement is increasing as the sample is annealed at longer times, showing that the entanglement is eventually restored in these samples. Calorimetry was used to measure the glass transition of the same samples. A T_g reduction of 4-7 degrees was observed compared to bulk T_g value, but the reduction was independent of molecular weight of the polystyrene

used (molecular weights between 4K to 196K). It was also shown that the T_g reduction is 2-5 K greater in cyclic PS compared to linear chains and with sufficient annealing bulk behavior can be restored, while entanglement is not expected to be recovered in cyclic PS systems. The authors conclude that the observed T_g reduction can not be due to reduced entanglement. Reduced density in freeze-dried polymer systems was proposed to be the cause of the observed reduction in T_g of these systems. A possible similar reduction in the density of thin films has also been proposed to be a possible factor in T_g reduction in thin films. The mass density of the thin polystyrene films were measured by Wallace *et al.* [70] using neutron scattering measurements of thin deuterated polystyrene (dPS) films with thicknesses as low as 6.5 nm on two different substrates (Si and oxide coated Si), and no difference between the thin film value and bulk value was seen. Forrest *et al.* [71] also used Brillouin light scattering, to study high frequency mechanical properties of thin freely standing polystyrene films. Within 0.5% the mass density of films as thin as 30 nm was indistinguishable from the bulk value.

As mentioned previously the T_g reduction in thin polystyrene films seems to be independent of the type of substrate used at least for the substrates that are commonly used, the reason probably being that polystyrene does not strongly interact with the substrate. One expects that modifying the PS properties to increase its interaction with the substrate would also affect its T_g reduction behavior. Pham and Green [72] used a blend of PS and tetramethylbisphenol-A polycarbonate(TMPC) with similar molecular weights (49K and 38K) to make thin films. TMPC interacts more strongly with the oxide coated silicon substrate and shows an increase in T_g values with decreasing film thickness. The films made of the mixtures of the two polymers showed that increasing the percentage of polystyrene increases the T_g reduction effect and in average the T_g of the mixture film can be obtained by averaging the T_g's of PS and TMPC according to their concentrations. In a similar experiment Rittigstein and Torkelson showed that adding nano-particles to the polymer solution has a similar effect [73]. Adding silica and alumna nano-particles can change the T_g and physical aging of the polymer. Depending on the material used and the type of interaction, T_g can increase, decrease or remain constant.

The results of these experiments and many other similar experiments show that

the confinement effect seen in thin polymer films specially polystyrene is independent of the reduced entanglement effect or the sample preparation technique. But there are some experiments in the literature which contradict these results [74]. In this thesis the effect of sample preparation on the properties of thin films is studied which can provide some possible explanation for these contradictions. The effect of substrate however is a real effect that can be eliminated in almost all cases by changing the choice of substrate. Although the substrate can have an effect in slowing down the dynamics by strong attachment to the chain monomers, it can not be the source of the reduction in T_g which indicates enhanced dynamics. This is an strong evidence that the enhanced mobility near the free surface as proposed by Keddie *et al.* can be a real cause of T_g reduction. More direct measurements of the dynamics are needed to confirm this point. One way of studying this fact is eliminating the substrate effect by completely removing the substrate and study the free standing films.

T_g measurements of thin free-standing films

Free standing films (FSF) are made by floating thin polymer films onto a water surface, and then transferring them onto a sample holder which contains an aperture [75,76]. The T_g of such films can be measured using ellipsometry [75,78] or Brillouin light scattering [76, 77]. The measurements of Mattsson *et al.* [77] on thin free standing polystyrene films showed that the films have two distinctive behaviors depending on their molecular weights. For films with molecular weights of $M_n \geq 514 \times 10^3$, the measured T_g was molecular wight dependent. The T_g reduction started from a critical thickness h_0 and the reduction could be fit to the following equation,

$$T_g(h) = \begin{cases} T_g^{bulk}[1 - (\frac{h_0 - h}{\zeta})], & h < h_0 \\ T_g^{bulk}, & h \geq h_0 \end{cases} \qquad (2.3)$$

where $h_0/R_{EE} \simeq 1$. ζ is a parameter which is a function of molecular weight. It was shown that by including the effect of molecular weight a universal curve can be obtained to explain the T_g reduction of these films [78].

$$(T_g - T_g^*) = \alpha(M_w)(h - h^*) \qquad (2.4)$$
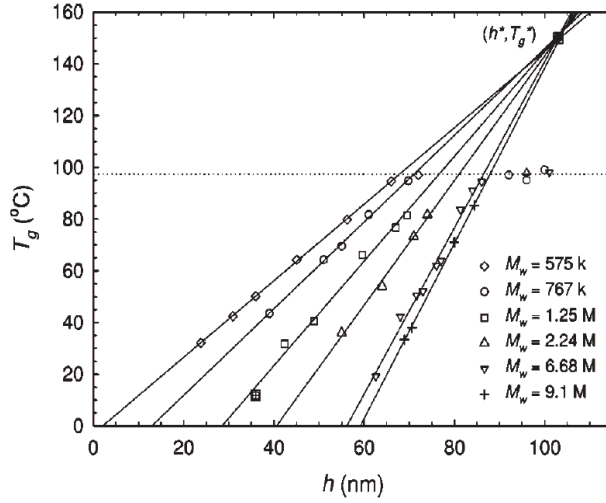
Figure 2.3: Plot of T_g vs film thickness h for high molecular weight freely standing PS films. Adapted from ref. [78]

where $h^* = 103 \pm 1$ nm, $T_g^* = 150 \pm 2$ and $\alpha(\bar{M}_w) = b \ln(M_w/M_w^*)$, where b is a constant and $M_w^* = 69 \pm 4 \times 10^3$. Figure 2.3 shows the T_g behavior of high molecular weight thin films. The straight solid lines show the best linear fits to the data in the regime in which T_g reductions are observed, and the horizontal dotted line corresponds to the bulk value of T_g. It can be seen that the extrapolation of all these linear fits coincide at the same point (h^*, T^*). de Gennes [79] proposed a model that could explain this effect based on the chain confinement of polymer chains below their radius of gyration. The details of this model will be discussed in the next section, which suggests that this effect is only a property of polymer glasses.

The confinement effects are quite different in low molecular weight free standing PS films. For films with molecular weight of $M_n \leq 347 \times 10^3$ no molecular weight dependance is observed and the T_g dependance on film thickness was similar to supported films.

$$T_g(h) = T_g^{bulk}[1 - (\frac{\alpha}{h})^\delta] \tag{2.5}$$

where $\delta = 1.8 \pm 0.2$ and $\alpha = 78 \pm 1$Å. Comparing these results with those of Keddie et al. [51] one can see that the exponent δ is the same and $\alpha_{FSF} \sim 2 \times \alpha_{supported}$.

This suggests that a free standing film with thickness h behaves like a supported film with a thickness of $h/2$, which is expected if the free surface is the main cause of T_g reduction in these films. Similar to the approach of Keddie *et al.* [51], a multi-layer film model was proposed by Forrest *et al.* There are three important layers in a free standing film. Two interface layers each with a thickness of $\xi(T)$, which are more mobile with a decreased T_g and the middle layer which has a bulk like behavior. The T_g of the film is the average T_g of these layers.

$$\langle T_g \rangle = T_g^{bulk} + \frac{2\xi(\langle T_g \rangle)}{h}(T_g^{surf} - T_g^{bulk}) \tag{2.6}$$

where

$$\xi(T) = \xi(T^*) + \alpha(T^* - T)^\gamma \tag{2.7}$$

In this equation T^* can be either T_g^{bulk} or the onset of cooperative motion obtained from other studies of cooperative motion which is about $T_{ons} \sim 485K$. The model can be solved in both situations. If $\xi_1(T) = r_0 + \alpha(T_{ons} - T)^\gamma$ with $r_0 = 6$Å the average distance between the monomer units, then $T_g(surf) = 300\pm7K$, $\gamma = 2\pm0.1$ and $\alpha = 2.95 \times 10^{-3}$. If $\xi_2(T) = \xi(T_g) + \alpha(T_g - T)^\gamma$ then, $T_g(surf) = 305 \pm 21K$, $\xi(T_g) = 26 \pm 21$Å, $\gamma = 0.95 \pm 0.15$ and $\alpha = 1.4 \pm 0.7$. Both of these models can be fit to the experimental data quite reasonably. The model can also be solved for the measurement of supported thin films of Keddie *et al.* [51], by assuming the existence of a dead layer near the substrate with constant thickness and constant T_g and a more mobile layer near the surface. By fitting the model to the data, $\lambda = 22.7\pm13$Å for the thickness of the layer near the substrate and $T_g(sub) = 391K$. Other parameters are similar to the FSF parameters.

Forrest *et al.* [62] also studied the effect of annealing on the observed T_g reductions of FSF. For low molecular weight samples $M_w = 575 \times 10^3$, the reptation time is $\tau_r = 3h$ while for $M_w = 9.1 \times 10^6$, τ_r is about 4.5 years so annealing of the samples done prior to their T_g measurements is sufficient for smaller molecular weight, but not nearly enough for higher molecular weights. But this doesn't seem to have any effect on the results, and repeated measurements also don't change the results. These annealing times are much larger than the time scale of segmental relaxation which is the same for all molecular weights (At T=388K, $\tau_{N_e} = 100s$ where N_e is the entanglement length).
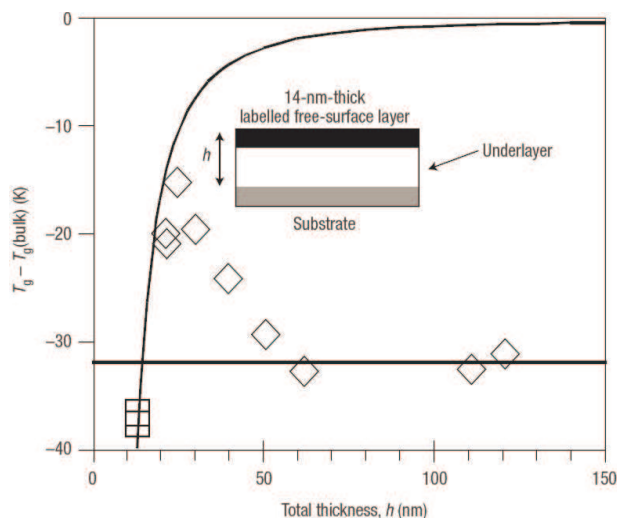
Figure 2.4: T_g for 14-nm-thick labeled PS free surface layers (diamonds) as a function of total film thickness. The solid curve is the fit to the thickness dependence of single-layer data. Two replicate single-layer T_g for 14-nm-thick labeled PS films (squares) are shown for reference. Adapted from ref. [80]

The results of experiments on free standing films strongly suggest that the behavior of the films for low molecular weight FSF and supported films are influenced by the free surface, but it can not provide further details on how exactly these effects penetrate into the bulk of the film. The three layer model gives at best an average property of the film, but one expects that in a real system the change in the behavior of the system be a gradual change rather than a discontinued one. The length scale over which this gradual change happens can provide important information about the characteristics of the system.

T_g reduction in multi-layer films

One way to study how the T_g changes as a function of the depth of the film is to make multi-layer films, and measure the T_g of different layers independently. Ellison an Torkelson [80] studied the fluorescent intensity of pyrene labeled polystyrene layers as a function of temperature in different layers of the films. It was observed

that when the T_g of the top layer of a two-layer film with a bulk like sub layer is measured, the T_g changes as a function of the thickness of the top layer are similar to the T_g reduction of thin films with similar thicknesses. As the thickness of the top layer is decreased the T_g decreases monotonically to $T_g - 40K$ for a 12 nm top layer film, the smallest thickness used in these studies. Decreasing the thickness of the bottom layer, with a fixed 12 nm top probe layer, increases the T_g of the probe layer until the thickness becomes of the order of 20 nm and then the T_g starts decreasing again, making the overall T_g of the total film the same as expected for a single-layer film (Figure 2.4). A 12 nm layer on the bottom or center of a bulk film has a bulk T_g. The T_g reduction of the layers of a tri-layer film made of three 12 nm layers is -4K, -5K, -14K from the bottom layer to the top layer. These results show that the T_g of a film is not simply made of three layers, but it gradually changes from the surface to the substrate. A surprising result of this experiment is that in thick films the dynamics are more heterogeneous through the depth of the film. As the film thickness is decreased to about 20 nm the difference between the measured T_gs of different layers decreases. The origin of this 20 nm length scale and its relevance to the glass transition phenomena is not exactly clear, and more studies are needed to define the source of this length scale.

Priestley *et al.* [81, 82] measured the physical aging of similar samples of PS and PMMA upon quenching from a temperature above T_g. In a 20 nm thick polystyrene film at $T_g - 10$ film no aging could be seen showing that the film was in an equilibrium state, while for a PMMA film with the same thickness at $T_g + 7$ physical aging could still be observed, and the film was in the glassy state. To study the effect of substrate on the aging of PMMA multi-layer films with 25 nm labeled layers on top, middle or bottom of bulk layers were used. The surface layer was seen to be more mobile as measured by the physical aging time, while the layer near the substrate showed almost complete arrest of relaxation. Using different film thicknesses it was shown that the effect of the substrate, as measured by physical aging, penetrates over 250 nm of the film thickness, while the difference seen as measured by T_g only affects 100 nm of the film thickness. These results clearly show that the T_g measurements, while a good indication of the film dynamics, do not provide a complete picture of the dynamics of the system.

The width of the transition

Another important feature of the dilatometric glass transition experiments of thin films is the reduction of the contrast [53, 59, 77, 83]. The thermal expansivity in the molten state usually remains constant while the expansivity in the glassy state increases with decreasing film thickness, resulting in a reduction of contrast. It is also seen that the transition form the rubbery state to the glassy state broadens, making the transition wider, which also increases the error in the measured T_g [51, 78]. This phenomena can be explained by increasing heterogeneity through the depth of the film. In the melt state all parts of the film are relaxing with the same relaxation time. As the film temperature is decreased below the bulk T_g value, some parts of the film freeze while the other parts are still relaxing, making the transition wider, and increasing the expansivity. Mattsson *et al.* [77] reported that for free standing films as the film thickness is decreased, the contrast decreases, to a minimum value for films of thicknesses about 26 nm. Decreasing the film thickness further, increases the contrast again. . These results are similar to the results of multi-layer film measurements which predict that the heterogeneity decreases when the film thickness is decreased below a certain value [80].

Calorimetric T_g measurements

Dilatometric T_g measurements on thin films show that unless a strong interaction with the substrate is present, the T_g of thin polymer films are decreased below their bulk value. They also provide fairly strong evidence that the T_g reduction is caused by more mobility near the free surface of the film and removing the free surface by for example coating it with a gold layer eliminates the T_g reduction completely [54]. Unlike these measurements some calorimetric measurements of the glass transition leads to different and somewhat contradictory results. Efremov *et al.* [84, 85] used nano-calorimetry to measure the glass transition of PS, poly(2-vinyl pyridine) (PVP) and PMMA thin films supported on platinum substrates. In order to get a reasonable signal, cooling/heating rates of 2-1000K/s were used. The measured T_g of films with different thicknesses were the same within the experimental error ($\pm 5K$). Huth *et al.* [86] used differential and AC calorimetry to measure the

T_g of thin PS films at different cooling rates/frequencies. The fact that the cooling rate is inversely proportional to the relaxation time was used to produce the Arrhenius plot of the relaxation for PS films in the frequency range of 0.6 to 1280 Hz. The behavior for all film thicknesses was similar to the bulk VFT behavior of polystyrene. The main difference between these measurements and dilatometric measurements is in the cooling rates used in these studies. The key to solving this contradiction would be careful measurements of T_g in different cooling rates. This will be discussed in more detail in one of the studies of this thesis.

Koh *et al.* used calorimetry technique with a step scan method which enabled them to use lower cooling/heating rates [74]. In order to increase the calorimetric signal a stack of free standing films were put together. The existence of wrinkles in between the stacked films, produces some free surface in between the films. In this experiment some T_g reduction was observed in the films, but the degree of reduction was far less than what was expected from the results of previous dilatometric T_g measurements of free stranding films [62]. The authors concluded that the T_g reduction seen in their measurements can not be due to the free surface effects. The sample preparation method used in this experiment makes it hard to interpret the data. Previous measurements showed that blocking the free surface can eliminate the T_g reduction effects [54]. It is not clear how the stacking of the free standing films would affect the amount of free surface available to the system. The fact that the holes produced by wrinkles exist in the samples even after very long annealing times makes this method of sample preparation more questionable.

2.1.2 Theories and simulations of T_g reduction

de Gennes model

de Gennes model is proposed to explain the T_g reduction in high molecular weight free standing films and it shows that confinement effects on these films are only a result of chain confinement below the radius of gyration of the films, not a property of confined glassy systems in general [79]. From free volume theory the temperature

dependance of the free volume is given by

$$v(T) = \omega\alpha(T - T_0) \tag{2.8}$$

where ω is the monomer volume, α is dilation coefficient in glassy phase and T_0 is the temperature at which $v = 0$. The time constant of a typical jump is given by, $\tau = \tau_0 \exp\left(\frac{\omega_j}{v(T)}\right)$, where ω_j is the volume required for a jump, approximately equal to $\omega = a^3$. Assume that the chain relaxation happens through the sliding motion of monomers following the relaxation of kinks which are themselves moving randomly. The time τ for such sliding motion through a sequence of N monomers, depends on the volume available to each monomer. The probability distribution of these volumes is assumed to be Gaussian

$$p(\omega) \sim e^{-\omega^2/2\omega_0^2} \tag{2.9}$$

The average relaxation time τ is thus equal to

$$\tau = \tau_0 \left\langle \exp\left(\frac{1}{v(T)} \sum_i \omega_i\right) \right\rangle \tag{2.10}$$

where the average is taken in respect of $p(\omega)$. The relaxation time is then equal to

$$\tau = \tau_0 \exp\left(\frac{N}{2}\frac{\eta^2}{2\epsilon^2}\right) p_{end}^{-1} \tag{2.11}$$

where $p_{end} = \exp\left(-\frac{\omega_e}{v(T)}\right)$ is very small. This makes the sliding motion inefficient in bulk polymer systems. In thin films however, a typical chain length between the two surfaces is of the order of $g \simeq \frac{h^2}{a^2}$ where h is the film thickness. substituting this in the relaxation time equation, and assuming that T_g is the temperature at which relaxation time reaches a constant one can easily show that

$$T_g = T_0 \left\{ 1 + \frac{\eta}{\alpha T_0} \left(\frac{g}{l}\right)^{1/2} \right\} \tag{2.12}$$

For $h < h^* \sim \eta^{-1}$. For films with higher thicknesses the bulk behavior is restored. Although a simplistic model, this model can describe the behavior of high molecular weight free standing films quite accurately. This suggest that the effect seen in these films is due chain confinement effect, and as the film thicknesses becomes smaller than of the radius of gyration of the polymer these confinement effects appear.

Multi-layer models

The three layer model discussed in the previous section is a simple model that can successfully explain some aspects of the T_g reduction in thin polymer films. The basic idea behind this model is that a length scale of cooperative motion exists and a layer with a similar thickness near the free surface has enhanced mobility

$$\xi(T) = \xi(T^*) + \alpha(T^* - T)^\gamma \tag{2.13}$$

The existence of such length scale and whether or not it diverges near the T_g has yet to be proven. Donth [87] proposed a method to estimate the size of this co-operatively rearranging region (CRR) near T_g. In this model, assuming a three dimensional CRR exists, the length scale can be obtained from a calorimetry measurement, by calculating the amount of heat that the system absorbs near T_g, to change from a frozen state into a melt that is in thermal equilibrium.

$$V_{CRR} = \xi_{CRR}^3 = K_B T_g^2 \Delta(\frac{1}{C_v})/(\rho \delta T^2) \tag{2.14}$$

Ellison *et al.* used this hypothesis to study the relationship between a length scale of CRR and the measured T_g reduction in PS, poly(4-tert-butyl styrene) (PTBS) and poly(4-methyl styrene) (P4MS) [52]. PTBS and P4MS are molecules similar to PS, with stiffer segments, and a more pronounced T_g reduction can be seen in these polymers. For PS down to very low molecular weights the length scale of CRR is constant within the experimental error and is about 3 nm. The number of units containing such a volume is about 250 segments. For both PTBS and P4BS the CRR is smaller compared to PS, which can not explain the dramatic reduction of T_g in thin films made of these polymers, so some other parameter should also play an important role. The stiffness and shape of PTBS causes a 10% reduction in its density, which means it should have more available free volume, but its CRR is only composed of 50 segmental units. It seems that the persistence length can play a more important role in the properties of the confined polymer. The reason for this can be that a larger persistence length could result in a larger volume of heterogeneous regions which can in turn result in larger penetration of heterogeneity into the depth of the film. This however needs more careful studies and theoretical work to be confirmed. Models with one dimensional CRR regions

such as Edwards model [29] or de Gennes sliding model could perhaps yield to more realistic estimation of the penetration of the surface effects into the bulk of the film. These models can potentially explain why the persistence length becomes an important parameter in the observed enhancement effects.

A percolation model

Long and Lequeux proposed a density fluctuation model to explain T_g reduction in thin films [62,88] In this model thermally induced density fluctuations are assumed to be responsible in producing dynamical heterogeneity and the glass transition in bulk and thin films. The glass transition happens when a percolation happens between more rigid areas. The T_g reduction in thin films is explained by a transition from a three dimensional percolation model to a two dimensional percolation. The model predicts that the exponent in equation 2.1 is a universal exponent and is equal to $\delta = 1.5$. Although an interesting model, it can not predict why the T_g reduction in free standing films start at a higher thickness compared to supported film, or a profile of T_gs can be seen if a multi-layer film is made. The model completely ignores the fact that a heterogeneity exists normal to the plane of the film, which unlike the heterogeneity in the bulk polymer, does not vanish if averaged over time. For example the free standing films, are stable at temperatures above their T_g and start dewetting only at temperatures above bulk T_g. If the film was uniform, one would expect the films to dewet once the temperature is increased above their measured T_g.

A mechanical response model

Another interesting model concerning T_g reduction in thin films is the mechanical model introduced by Herminghaus *et al.* [61,89–92] This model is based on the viscoelastic properties of a viscoelastic material. The equation governing the dynamics is

$$\{\partial_t + \omega_0 + \frac{E}{\eta}\}\nabla^2\phi = \frac{\nabla p}{\eta} \qquad (2.15)$$

where ω_0 is the Rouse rate of relaxation of individual chains, p is the pressure field, E is the Young's modulus and ϕ is the vector field related to the strain tensor S.

In two dimensions the stress tensor is given by

$$S = \begin{pmatrix} \partial_x \phi_x & \frac{1}{2}(\partial_x \phi_z + \partial_z \phi_x) \\ \frac{1}{2}(\partial_x \phi_z + \partial_z \phi_x) & \partial_z \phi_z \end{pmatrix} \tag{2.16}$$

The solution of this equation for a thin film with thickness h is

$$\phi_x \propto [1 + (h + q^{-1})\alpha(q)] \cosh qz - q^{-1}\alpha(q) \sinh qz \tag{2.17}$$

$$\phi_z \propto [1 + h\alpha(q)] \sinh qz - z\alpha(q) \cosh qz \tag{2.18}$$

In this equation

$$\alpha(q) = \left(\frac{q}{2}\right) \frac{e^{2qh} - 1}{e^{2qh} - 1 + qh} \tag{2.19}$$

For FSF the same analogy applies with h being half of film thickness. At the free surface the pressure is driven from surface tension $p = -\sigma \partial_{xx} \zeta$. The relaxation rate of each mode can be defined from this governing equation. In the limit of $\omega_0 \ll \frac{E}{\eta}$ the rate is given by:

$$\omega = \omega_0 + \frac{E}{\eta} + \frac{\sigma q^2}{2\eta\alpha(q)} \tag{2.20}$$

these are fast modes which contribute in surface T_g reduction. Using a mode coupling argument and memory effects one can show that the slow modes near T_g are frozen, so only the fast modes are important in enhancement of the dynamics. Also modes with q larger than h^{-1} do not penetrate into the film so only modes with $q \sim h^{-1}$ are important in defining T_g. So $T_g(h) \propto 1/\omega(h^{-1})$ thus

$$T_g(h) = T_g^0 \left(1 + \frac{1.16\sigma}{h(E + \eta\omega_0)}\right)^{-1} \tag{2.21}$$

For PS, $\sigma = 31 mN/m$ and $h_0 = 0.82$ nm. This results in $E \approx 44 MPa$ which is somewhere between the glassy (a few GPa) and liquid modulus (300KPa). This shows that capillary waves help enhance the surface fluctuations in thin films. Similarly for a bulk film, near the surface there is a smooth change of T_g from surface, because the deeper into the film the modes with shorter q become more important. This model is one of the most successful models in explaining the T_g reduction in thin films, but it does not provide details about the dynamics of the system, which as will be discussed in the next section are more complicated than the T_g behavior.

The model is also based on viscoelastic properties of the polymer, assuming that the viscoelastic properties of the film remains the same through the film. Although the density of the film remains constant, the viscosity can be different near the surface compared to the bulk of the film. Another major problem with the model is that it assumes only the fast modes are important in the dynamics, while as will be shown in this thesis, only slow modes of motion in thin films show enhancement in the dynamics and fast modes behave bulk like.

Coupling model

Ngai *et al* have a phenomenological bulk theory of the glass transition which can also be used the explain T_g reductions in thin polymer films [13, 93–95]. The coupling model relates the stretched exponent of the response function to the α relaxation time of the system. The response function of a glass forming material can be described by

$$\phi(t) = \exp[-(t/\tau_\alpha)^{1-n}] \tag{2.22}$$

where n is a fraction on one and describes the dispersion of the α-relaxation time. $n = 0$ corresponds to a single relaxation time process. τ_α is the α relaxation time of the system, which is a combination of separate single relaxation times. For each particle at times $t < t_c$ the relaxation is a single exponential relaxation $\exp(-t/\tau_0)$. At longer times the α relaxation time of the system can be described by

$$\tau_\alpha = [t_c^{-n}\tau_0]^{1/(1-n)} \tag{2.23}$$

As the temperature of the system is decreased towards the glass transition temperature, the coupling parameter changes from zero to a non-zero value, which causes the slow down of the dynamics, as well as the non-linear response function. t_c is estimated to be of the order of 2ps and is a constant. The value of τ_α depends on single exponential relaxation times and the coupling parameter n. τ_0 is also called the Johari-Goldstein relaxation time and can be calculated from experimental data. T_g reduction in thin films and also the distributions of T_gs in Ellison *et al.* measurements [80] can be explained by introducing a coupling constant that is a function of depth, and is smaller near the free surface.

$$\tau(z) = [t_c^{-n(z)}\tau_0]^{1/(1-n(z))} \tag{2.24}$$

The cross over from the bulk behavior to confinement behavior happens when τ_α/τ_0 becomes of the order of one. In thin films $n_i < n(bulk)$ for each layer of the film so the total relaxation function is less strongly dependent on the temperature, which can explain the broadening of the transition and the reduction in the contrast. This theory can also explain why the diffusion measurements which will be discussed in next section show slower dynamics, while the T_g measurements indicate enhancement in the dynamics, by explaining the different origins of the corresponding relaxation processes.

Besides the already mentioned models there are also some models based on free volume theory or configurational entropy. For example the model by McCoy *et al.* that attributes the T_g reduction to the inhomogeneous density profile though the film thickness [96]. The results of these models are not supported by the experimental data in which no changes in the mass density are seen [70,71]. Truskett and Ganesan, use a mean-field landscape model which can qualitatively explain the T_g reduction in thin films but is unable to provide more details [97].

Simulations of thin film dynamics

Monte Carlo and molecular dynamics simulations have also been used to study the T_g reduction in thin films of regular glass formers and polymers. Jackle *et al.* [98–100] used Monte Carlo simulation in a two dimensional lattice gas to study the decay of correlation function for site occupation and reorientation of two dimensional lattice gas molecules. The length scale of cooperative motion was studied by calculating the effect of the size on T_g in strips with different widths. A slow down of the dynamics was observed as the size of theses strips were reduced. Baschnagel *et al.* [101] used molecular dynamics simulation methods previously used to simulate the behavior of bulk glass formers to study the confinement effects on the dynamics. It was shown that for non-entangled polymer chains when the interaction between the polymer and the substrate is repulsive [102], or one or two free surfaces exist [103], The glass transition temperature and the mode coupling critical temperature are decreased below their bulk values. It was also shown that the behavior of free standing films is the same as those of supported films with half the thickness, similar to what has been observed in the experiments. It was seen that

with the existence of a substrate with attractive interaction, the penetration of the slow dynamics imposed by the substrate into the bulk of the film is more than the penetration of mobility caused by the free surface effect. Torres *et al.* used similar molecular dynamics simulations, but it was seen that the onset of anomalies starts at the same thickness for free standing films and supported films [104]. Butler and Harrowell used a kinetic Ising model to study the length scale of cooperative dynamics in a spin glass [105]. It was observed that as the number of layers in the film is decreased, the behavior of the system changes from VFT to Arrhenius, with a decreasing activation barrier. More details on the simulation methods and results can be found in the review article by Baschnagel and Varnik [106].

2.2 Measurements of the dynamics of confined polymer systems

The glass transition is an indirect measure of the dynamics and at best it can provide information about the average relaxation behavior of the system at the time scale of the experiment. The complex results obtained in T_g measurements of thin polymer films can not be properly explained unless more information about the dynamics of the film is obtained. There are two types of dynamical measurements that can be used to study the dynamics of thin films. Experiments measuring the equilibrium fluctuation of the system such as x-ray photon correlation spectroscopy (X-ray PCS) measurements, and experiments that measure the response of the system to a constant or oscillatory external load.

X-ray and visible light scattering measurements

Kim *et al.* used small angle X-ray photon correlation spectroscopy to measure the viscosity of the surface of polymer films with different molecular weights. [107–109] The angles were chosen to be below the total internal reflection limit. The penetration depth of the X-ray was about 9 nm. The viscosity parallel to the surface of the film was measured at different q values, at temperatures between 423-443K.

The results indicated that the surface tension is similar to the bulk, and within the error of their measurements the viscosity of the 10 nm layer near the surface could represent the bulk viscosity or a viscosity which is at most 10 times lower than the bulk value. Erichsen *et al.* used X-ray photoelectron spectroscopy to measure the T_g of thin films [110]. The T_g in this method is measured by monitoring the discharge of the positive charges, induced on the polymer surface by photoelectron emission, due to the rearrangement of dipoles. The temperature above which the discharge of the ions are observed, is defined as T_g. T_g reduction was seen in thin films, but the authors concluded that the effect seen can not be due to the free surface.

Forrest *et al.* used dynamic light scattering to measure the relaxation time of PS free standing films of high molecular weight with a thickness of 22 nm [111]. Complete relaxation was observed at temperatures above $T = 297K$. Below that temperature a complete relaxation was not seen in the time frame of the experiment. It was concluded that this temperature is the T_g of the film (about 80 degrees below the bulk T_g value of PS). The relaxation measured above this temperature could be reasonably fitted to a stretched exponential function with $\beta = 0.39$.

Dielectric relaxation measurements

X-ray and visible light photon correlation measurements of thin films that can be found in the literature are not comprehensive enough to provide enough information about the dynamics in a wide range of relaxation times and temperatures. Dielectric relaxation measurements are able to provide more details about the relaxation properties over a wider range of relaxation times and temperatures above bulk T_g. Hartmann *et al.* measured the dielectric α and β-relaxation of isotactic-PMMA films made on Al substrate, coated with a thin layer of aluminum [112]. Figure 2.5 shows the results of these experiments for films with molecular weight $M_w = 44900$g/mol along with the VFT fits to the α-relaxation data. While the β-relaxation time remains constant as the film thickness is decreased, the α-relaxation times become faster at lower frequencies. The α-relaxation strength also decreases as the film thickness is decreased. The T_g was determined as the temperature at which the relaxation time would be equal to 100 seconds as shown by the dashed
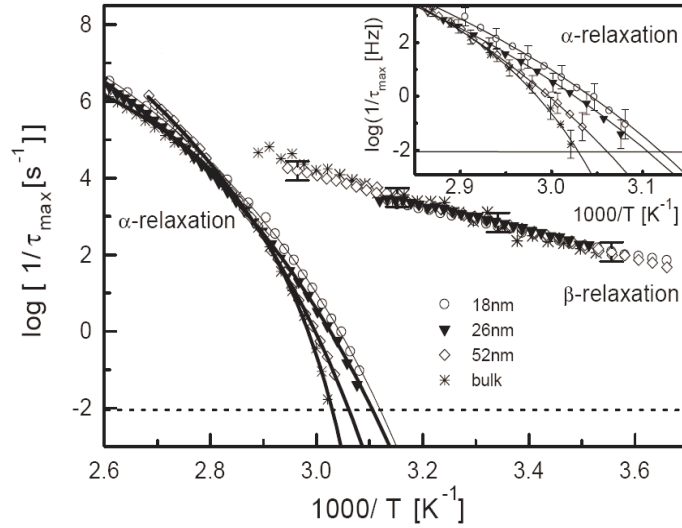
Figure 2.5: Activation plots for various film thicknesses. In the inset the α-relaxation around T_g is enlarged in order to demonstrate the shift of the relaxation rate more clearly. Adapted from ref. [112]

line in figure 2.5. It was seen that as the film thickness is decreased the T_g is also decreased. Similar samples made on Si substrate measured by ellipsometry showed an increase in the T_g as expected. Grohens *et al.* [58] used PMMA with different tacticities to make thin films and saw similar results for thin films made of i-PMMA while for s-PMMA films, the β relaxation times were also affected by confinement. Fukao *et al.* [113, 114] used dielectric relaxation and thermal expansion spectroscopy to study the behavior of PS ($3.6 \times 10^3 < M_w < 1.8 \times 10^6$), PMMA ($M_w = 49 \times 10^4$) and PVAc ($124 \times 10^3 < M_w < 237 \times 10^3$). In all systems, an enhancement of the dynamics was seen with decreasing film thickness. The T_g of the films were estimated as the temperature at which the relaxation time is equal to 100 seconds. The T_g reductions observed in this way seemed to be molecular weight dependent, a result which is not observed in any other dielectric relaxation studies or other measurements using different techniques. The behavior of the α relaxation could be fit to a VFT curves with decreasing B and T_0 value with decreasing film thickness.

Although the results of dielectric measurements are insightful, they can not necessarily be directly compared with the T_g measurement experiments. The dielectric measurements are done on samples with an evaporated Aluminum layer. Fukao *et al.* observed that as the temperature of the system is increased above bulk T_g of the polymer, the roughness of the top aluminum layer increases [113]. The effect of evaporated metals on the properties of thin films has also been studied by Sharp and Forrest [54]. It was observed that covering a thin film of polystyrene with an evaporated Au layer eliminates the T_g reduction as it is expected if the free surface is the cause of T_g reductions in thin films, but covering it with an evaporated Al layer did not change the measured T_g of the film. They dissolved the polymer films and looked at the metal-polymer interface using contact mode AFM and saw qualitative differences between the interface produced by the two different types of the metals. The interface of Al-PS seemed to be sharper, while the gold layer had penetrated about 4 nm into the polymer film, and also showed large clusters. This clearly shows that understanding the results of the dielectric measurements needs a more comprehensive understanding of the metal-polymer interactions present in the system that is being studied. Sharp and Forrest [54] showed that if instead of evaporating Al on the PS film, two layers of spin-cast PS films on Al substrates are sandwiched, the T_g reduction effect disappears, confirming the importance of the existence of the free surface. It is not clear whether or not the molecular weight dependence observed by Fukao *et al.* [113] or the roughness induced on the surface is caused by the interactions of the polymer with the evaporated Al layer.

The only dielectric study that uses a sample with at least one free surface is that of Sharp and Forrest [55, 56], where i-PMMA thin films supported on Al were used to measure the temperature of the α-relaxation peak at a frequency of 1KHz. In this study no dependance of the α-relaxation temperature to the film thickness at this frequency was observed. This result is not surprising given the fact that the dielectric measurements are done at a high frequency. One can see from figure 2.5 that there is an onset for the enhancement of dynamics. These results combined with the measurements of Hartmann *et al.* [112], or studies on molecular glass formers such as the experiments of Arndt *et al.* [40] shown in figure can potentially explain why in high frequency calorimetric measurements no T_g reductions were

observed. It seems that the anomalies in the dynamics are more enhanced at slow relaxation times or low temperatures. This will be studied in more details in this thesis.

It is also important to note that the dielectric relaxation data can not always be reliably analyzed specially when there are more than one relaxation processes in the system. For example Serghei *et al.* [115] reanalyzed the data of Hartmann *et al.* [112] and got results that showed no enhancement in the dynamics down to a frequency of 1Hz. Depending on the functional form of the α and β relaxation peaks chosen for the analysis one can get results that show enhancement in the dynamics, or bulk like dynamics. It is thus not clear how reliable the dielectric relaxation measurements are in defining the dynamics of the system.

Measurements of segmental relaxation and chain diffusion

Measuring the segmental relaxation in thin polymer films are quite challenging. In a bulk polymers, high above the glass transition, the temperature dependence of different modes of motion such as diffusion coefficient or viscosity are the same. But this is not necessarily the case in thin films. The polymer chains can be preferably aligned in one direction, which can affect different modes of dynamics in different ways. The interaction of the polymer with the substrate can also affect the behavior of the chain diffusion, but not necessarily the segmental relaxation in areas that are not close to the substrate. One should also have in mind that as mentioned in the previous chapter, even in a bulk glass former, there is a break down of the dynamics between the translational and rotational diffusion at temperatures close to the glass transition, which can also affect how the data should be interpreted in thin film experiments.

Rivillon *et al.* [116] used Deuterium-NMR to probe the orientation of C-D bounds in PDMS(D) film supported on a grafted PS layer. The PS layer was used as a wetting layer which does not interact strongly with PDMS, and it can be shown that the thickness of the interfacial layer between the two polymers is less than 3 nm. As the thickness of the films were decreased, a splitting of the NMR peak was observed, due to preferred orientation of the C-D bounds. For films made

of a low molecular weight PDMS ($M_w = 1.6 \times 10^4 < M_e = 2.4 \times 10^4$)it was seen that the order parameter is proportional to $1/h$ which is expected for a film that is in thermal equilibrium and its dynamics are affected by a hard wall interface. The chain segments are preferably aligned along the substrate, and the relation of $1/h$ shows that the fraction of the aligned segments depends on the distance of the segments from the substrate. For films made of a higher molecular weight PDMS ($M_w = 10^5 > M_e = 2.4 \times 10^4$), the orientation drops abruptly at a thickness of L which is of the order of the entanglement length, indicating that at higher distances from the substrate the segmental relaxations are not affected by the alignment imposed by the substrate. This shows that a complete chain diffusion does does not exist in these systems in the time scale of the experiment.

Jones *et al.* used small angle neutron scattering (SANS) to measure the segmental diffusion and the radius of gyration of dPS thin films parallel to the plain of the film. [117, 118] Within the error of the measurements no difference between the measured values and the bulk diffusion was observed. Tseng *et al.* used fluorescence recovery after photo-bleaching (FRAP) technique to measure the diffusion coefficient of segmental motion in PS films [119]. Rubrene was added as a dye and the films were photo-bleached with a high power laser in the form of interference patterns, the translational diffusion of the dye from other parts of the sample into the bleached areas was monitored as a function of time, at temperatures between 10-50 degrees above bulk T_g. Dramatic enhancement of dynamics at film thicknesses below 300 nm were observed. The authors used a free volume based model to estimate the T_g of the thin film and interpreted the results as an observed T_g reduction in films thinner than 300 nm. This is a much higher thickness than the onset of T_g reduction seen in direct T_g measurements which is about 50 nm for polystyrene. It was concluded that the reason that such a dramatic enhancement is seen is that the dye particles tend to segregate near the free surface, and hence enhance the effect of the free surface.

The results of segmental relaxation experiments [116–118, 120] indicate little or no change in the average α-relaxation time of the polymer thin films in the melt, the exception being the studies of Tseng *et al.* [119] which are probing the translational diffusion rather than segmental relaxation or α relaxation, and as

mentioned in the previous chapter, even in a bulk glass former near the T_g an enhancement of translational diffusion is expected [14,15]. Measurements of Hall *et al.* shows that even in the presence of strong attraction of the substrate although the segmental relaxation becomes broader it does not have an average relaxation time dramatically different from the bulk values [121, 122]. These results are often cited as measurements that indicate no T_g reductions must be observed in thin polymer films. It is important to note that the diffusion measurements are always done at temperatures above bulk T_g, where the system is in a liquid state and the relaxation times are short enough that the system can reach the equilibrium state in the time frame of the experiments. It is possible that as the temperature is decreased, this equilibrium is lost and some parts of the system show an enhancement in the dynamics while the other parts are frozen. The broadening of the transitions that are seen in T_g measurements usually correspond to the change of the expansivity in the glassy region, suggesting that the enhancement in the dynamics happens at temperatures close or below bulk T_g. In the studies presented in this thesis an evidence of such difference between the high temperature regime, where no difference between the bulk and thin film is expected and the low temperature regime, where the thin film dynamics are much enhanced compared to the bulk will be given.

Whole chain diffusion measurements usually shows a dramatic slow down of the dynamics compared to the bulk dynamics. For example the measurements of Zheng *et al.* using dynamic secondary ion mass spectroscopy (dynamic SIMS) technique showed that dPS near an attractive substrate (PVP) has a diffusion constant much slower than bulk and the diffusion changes with the molecular weight as $D \sim N^{-3/2}$ rather than $D \sim N^{1/2}$, which is consistent with a modified reptation theory which accounts for $N^{1/2}$ monomer-surface contact [123]. The penetration of this effect into the film was studied, using multi-layered films with the d-PS layer being at different distances from the substrate [124]. It was seen that the dynamics are slowed down, which was interpreted as an increase in the apparent T_g of the film. Interpreting the results of the whole chain diffusion in this way must be done with care. Although the whole chain diffusion is slower than bulk, this can be just a result of the attachment of some segments to the substrate. This does not

guarantee that the segments far away from the substrate have also a much slower relaxation. In the other hand, the fact that the segmental relaxations do not show any enhancement of dynamics at $T > T_g(bulk)$ also does not necessarily mean that no enhancement in the dynamics exists at $T < T_g(bulk)$. Kojio *et al.* [120] used dielectric relaxation to study the relaxation of normal modes and segmental relaxation of thin films of polypropylene oxide (PPO) sandwiched between two mica layers. The intensity of normal mode dielectric relaxation in chains whose dipole lies preferentially along the chain backbone is proportional to the square of the end-to-end distance, but also that the segmental relaxation mode is independent of the end to end distance. Using this method they could measure the segmental relaxation and the whole chain diffusion of PPO simultaneously. The measurements were done at $T = 233K = T_g + 30K$. As the film thickness was decreased the segmental relaxation remained the same down to a thickness of 14 nm, where the segmental relaxation were suddenly slowed down. The normal modes were slower than bulk even for 100 nm thick films. These results show that the temperature dependence of segmental relaxations, is not necessarily the same as the whole chain diffusion.

Mechanical Measurements

One way to measure the film dynamics is through direct mechanical response experiments. One example of such experiments is the method used by O'Connell and McKenna on free standing films of PS [125] and PVAc [126]. In these experiments free standing films with different thicknesses were put on filters with hole sizes of 1.2 and 5micron, and were annealed above T_g for 30 minutes. During the annealing the edges of the films sink into the holes, with more sinking observed for thinner films. The films are then put under different pressures and bubbles are made. The bubble inflations are measured using AFM as the film relaxes under a constant pressure. The creep compliance can be calculated by assuming that the film shapes follow a membrane profile with the following stress and strain functions,

$$\sigma_{11} = \sigma_{22} = \frac{PR}{2t_0} \tag{2.25}$$

$$\epsilon_{11} = \epsilon_{22} = \frac{s}{2R_0} - 1 \tag{2.26}$$

where P is the applied pressure, R is the radius of curvature of the bubble, R_0 is the initial radius of the membrane, and s is the segmental length of the bubble. $D(t) = \epsilon_{11}/\sigma_{11}$ is called the apparent creep compliance. The time dependent creep compliance is modeled to have a stretched exponential relaxation. To find the compliance value of the rubbery plateau the films were annealed at temperatures above their apparent T_g and let to reach the rubbery plateau. It was seen that the glassy compliance does not change as a function of film thickness, but the value of the rubbery compliance was decreased from its bulk value with decreasing film thickness. The rubbery compliance had a power-law dependance to the film thickness with an exponent of 1.7 for PVAc and 1.8 for PS. The bulk behavior was recovered at a film thickness equal to 200 nm. The decrease in compliance showed a stiffening of the film, which is in contradiction with the reduction in T_g, which can be determined as the temperature at which the transition between glassy to rubbery plateaus happens. This T_g reduction was only seen in the PS films, and it was seen to be as large as 42K reduction in the thinnest film measured with a thickness of 19 nm. PVAc films showed a T_g equal to the bulk value. The temperature dependance of the relaxation times were also similar to the bulk. The authors concluded that the reason the stiffening (decreasing of the rubbery compliance) is seen in these thin films is that in these systems the free surface behaves as a hard wall that the segments are reflected from, and hence the film is stiffened.

2.3 Dynamics of the surface

The measurements of segmental relaxation or mechanical measurements on the whole film, although insightful about different confinement effects on the dynamics of polymeric systems, are unable to define the exact cause of T_g reduction. In cases where such confinement effects are seen, the effects are usually related to the fact that the system under study is a polymer, with different characteristic length scales, and confinement can alter the polymer properties in different ways depending on the length scale approached by the confinement. The reduction of T_g in the other hand, with the exception of reduction in high molecular weight free standing films, seems to be independent of the fact that the system under study is a polymer, and

as seen before can even happen in confined simple glass formers as well. Many different measurements [51, 54, 71, 76, 80, 111, 112] provide strong evidence that the surface plays an important role in the T_g reduction and the related dynamics. It is then reasonable to study the surface directly and try to define its dynamics in a way that is minimally affected by the bulk of the film.

The interest in the properties of the surface of glassy polymer films was raised even before T_g anomalies was seen in thin polymer films. The surface properties are of technological interest when a polymer interface or thin film is used in a system, for example in the insulation of electronic devices or lubrication. The adhesion and friction properties can also be different from expected bulk properties, if the surface behavior is different. In 1992 Meyers *et al.* tried to answer the question, "Is the Molecular Surface of Polystyrene Really Glassy?" [127]. It was seen that if the surface of a glassy PS film is measured using contact mode atomic force microscopy (AFM), the motion of the AFM tip imposes a morphology on the surface, that depends on the molecular weight of the sample. PS surface was imaged with a constant load of 1.5×10^{-8}N. For $M_w < 24 \times 10^3$ an abrasion pattern was seen. As the M_w was increased above the entanglement threshold, the patterns did not fully develop anymore. The patterns seen at room temperature seemed to correspond to a material that was in its rubbery state rather than the glassy state.

Surface rheology experiments

Ge *et al.* used shear modulation force microscopy to probe surface T_g of PS thin films with different molecular weights [128, 129]. In this technique an AFM tip is brought to contact with the polymer surface, under a constant normal force. A sinusoidal drive signal with a frequency of 1400 Hz is applied in the X direction inducing a small oscillatory motion of the tip parallel to the sample surface. T_g was defined as the temperature at which the amplitude of the signal started decreasing from its constant value at low temperatures. The tip pressure on the surface was estimated to be about 60MPa. The measured T_gs were similar to the bulk T_g value and no dependance of the measured T_g to the tip load was found. The authors concluded that this means the load is below yield stress of the material used. Unlike these measurements, the lateral force microscopy measurements of Kajiyama *et al.*

showed enhanced dynamics on the surface of PS films [130, 131]. Enhancement in the surface dynamics were observed at all different molecular weights used in the study ($5 \times 10^3 < M_w < 140 \times 10^3$). The enhancement was more than what could be explained by chain end segregation on the surface. The normal force in these experiments was about 10nN and the scan frequency was 70Hz. The measurements were repeated at different temperatures and the time-temperature superposition plot was obtained. The temperature dependance of the surface relaxations seemed to be Arrhenius with an activation energy of 230KJ/mol. The β exponent was also found to be 0.8 rather than the bulk value of 0.36. Molecular dynamics simulation was used trying to explain the results of these experiments [132]. The simulations indicated an enhanced dynamics of the segmental relaxation, but the relaxation functions were found to be stretched exponential like the bulk dynamics, only with faster relaxation times. Reduced surface T_g was also seen in thin films of PS, PMMA and PET in friction force microscopy measurements of Hammerschmidt *et al* [133]. Fischer used thermal probe microscopy to probe the T_g of the surface of PS films [134]. Partial surface melting was seen at temperatures about 15K below the bulk T_g of PS.

Surface rheology measurements suffer from a number of problems, which can affect the results. The load of an AFM tip can easily reach the yield stress of the polymer, which could result in an observed enhancement of the dynamics even if the polymer is in the glassy state. The interaction between the AFM tip and the polymer can also affect the behavior of the surface. It is known that because of large adhesion forces the polymer tends to stick to the metal tip, and the tip can drag the polymer on the surface. The morphologies seen in the Meyers *et al.* experiments [127] can be caused by this effect. There is also a contradiction between the shear modulation force microscopy experiments [128, 129] and other AFM based surface measurements [130, 133, 134]. It seems that the only major difference is the probe frequency. It is possible that the enhanced surface dynamics are only seen in slower modes of motions, as can be confirmed by the results of dielectric measurements and high frequency calorimetry measurements. This will be discussed in more details in one of the studies of this thesis.

Surface roughness experiments

One way to measure surface relaxations is to introduce a perturbation on the surface and monitor the relaxation of the perturbed surface at different temperatures. In experiments based on surface rubbing, the surface of the polymer film is rubbed and the segments on the surface are aligned along the rubbing direction. The preferred alignment of the surface vanishes as the surface is annealed at different temperatures. In the experiments of Samant *et al.* [135, 136] near-edge X-ray absorption fine structure spectroscopy (NEXAFS) method was used to probe the relaxation of rubbed PS surfaces. The relaxation of the first 1 nm and the first 10 nm of the surface were measured through different beams simultaneously at two polarizations. The decay of the parameter $R = (I^{\parallel} - I^{\perp})/(I^{\parallel} + I^{\perp})$ indicates the relaxation of the system with $I^{\parallel}$ the intensity parallel to the direction of the surface rubbing and $I^{\perp}$ the intensity normal to that direction. A complete annealing of the surface patterns was only seen above bulk T_g. Dhinojwala *et al.* used optical retardation [137], birefringence and sum frequency generation techniques [138] to probe the surface relaxations of similarly rubbed surfaces. A decrease in the T_g values of the films were observed as the force of rubbing was decreased, making features with less depths. As the effective thickness of the rubbed surface was decreased the activation energy was also decreased slightly, showing a more enhanced dynamics on the surface.

The rubbing experiments introduce forces on the surface that are large enough that they can change the structure of the polymer near the surface at temperatures where the system is in a glassy state. These forces are thus definitely larger than the yield stress of the polymer. It is not clear how theses induced stresses affect the behavior of the system. Thus it is important to use a method that introduces the surface perturbations at a temperature above bulk T_g where the system has a chance to reach structural relaxation. An example of such experiment is the measurements of Kerle *et al.* [139]. In this study artificial roughness on Si substrate was produced using CaF_2 salt. The salt surface was covered with a thin layer of Aluminum. A polystyrene film with a thickness of 10 microns was put on top of this rough surface. The film was reversed and the salt and Aluminum were removed using HCl. The initial RMS roughness obtained in this method is about 4.5 nm at room
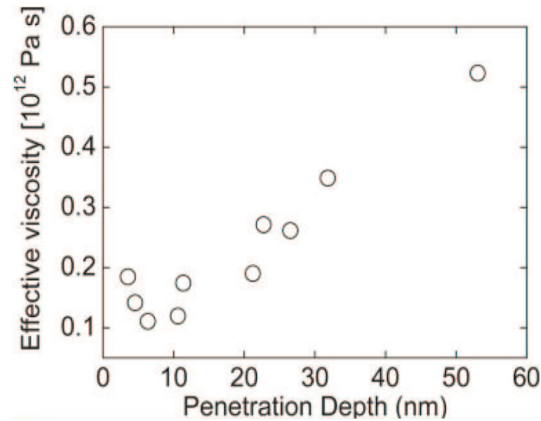
Figure 2.6: Effective viscosities as a function of penetration depth at $T = 90°C$. Adapted from ref. [141]

temperature. The films were then annealed at temperatures between 65 to 105 degrees. The more probable peak hight was about 35 nm at the beginning and the with of the peaks were approximately 50 nm. At $T > T_g$ the aspect ratio of the final roughness to the initial roughness decayed to zero, but at $T < T_g$ the aspect ratio was larger than zero, even after 2880 minutes. At 70 degrees the final aspect ratio after 2880 minutes was about 0.4. The results were similar for the two molecular weights($M_w = 96 \times 10^3$ and $M_w = 3 \times 10^6$)measured in this study. In cases where the films were covered with a layer of PI or PDMS during the annealing, no reduction in the roughness was seen below T_g. The partial relaxation of the surface roughness could not be explained by a simple two-layer model.

Johannsmann *et al.* used the decay of surface corrugations to find the viscosity as a function of penetration depth from the surface [140, 141]. Nano scale corrugations were produced by hot embossing of a stepped silicon template. The embossing was done well above bulk T_g of polystyrene to insure that the structure is relaxed and the decay is only caused by surface tension forces. The depth of the corrugations were about 10 nm, and their width was about 100 nm. The surface structure

can be described with the following equations

$$u_x(x, z, t) = u_{0,x}(t) \sin(qx) \exp(z/\xi) \tag{2.27}$$

$$u_z(x, z, t) = u_{0,z}(t) \cos(qx) \exp(z/\xi) \tag{2.28}$$

The Navier-Stokes equation for liquids in which the viscosity is dominant is given by

$$\eta \nabla^2 v = 0 \tag{2.29}$$

This leads to $\xi = 1/q = \lambda/2\pi$. Considering the effect of the surface tension one can show that $u_0(t) = u_0 \exp(-Rt)$ where $R = q\gamma/2\eta$. This shows that each fourier mode q corresponds to a penetration depth ξ. In order to make sure that the relaxation of the surface is simple exponential, only the first 3000 minutes of the data was used for analysis. Partial annealing of the surface corrugations was observed at temperatures as low as 40°C [141]. Detailed measurements at 70°C showed a decreasing viscosity as a function of penetration depth [140] while similar measurements at 90°C showed a non-monotonic decrease of viscosity. The minimum viscosity obtained at 10 nm penetration depth which was of the order of the R_g of the polymer used. Figure 2.6 shows effective viscosities obtained at 90°C.

Embedding of nano-particles

Surface roughness measurements are very successful in showing the existence of enhanced dynamics near the surface, but defining the exact shape of relaxation function and its temperature dependence in the vicinity of the surface is nearly impossible. The viscoelastic nature of the polymer surface and the fact that at different depths the relaxation times could be different, makes it hard to separate different modes of motions. The fact that the surface capillary waves may exist at all temperatures, makes it hard to see complete relaxation of the surface corrugations. The relaxation times of the surface tension driven motions are inversely proportional to the radius of curvature. In a rough surface curvatures of all length scales exist, which could have relaxation times much longer than the time scale of the experiment. So it is important to have surface perturbations with constant length scales, which makes it possible to estimate the expected annealing time, and analyze the data without having to convert the data to the Fourier space.
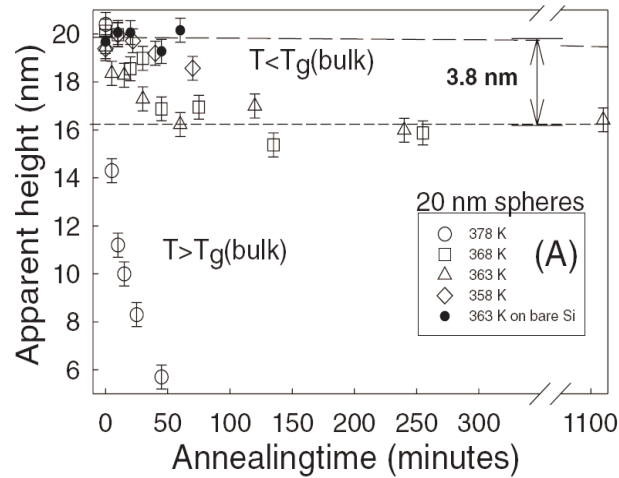
Figure 2.7: Time and temperature dependence of the apparent height of 20 nm gold nanospheres. Adapted from ref. [146]

Using indentors to measure the viscoelastic behavior of a bulk system is an standard method, and one can use viscoelastic theory to model the indentation depth as a function of time and obtain the creep compliance of the system [142]. Using AFM tip to measure viscoelastic properties of deep indentations (bulk like films) results in the bulk values of elastic modulus and yield stress in polystyrene films [143]. Gold nano-particles can be used as nano-indentors to study the properties of polymer surfaces. Weber *et al.* [144] used X-ray reflectivity to study the embedding of gold clusters on the surface of polystyrene films by measuring the apparent thickness of the gold layer at different temperatures. The gold clusters were produced by slow evaporation of a $1-2$ nm layer of gold on the surface of the polymer. During the measurements the samples were heated with a rate of 1K/min. At some temperature below bulk T_g partial covering of the gold clusters by the polymer was seen but complete embedding as measured by an increase in the apparent thickness of the gold layer, was only observed above bulk T_g. Rudoy *et al.* used the embedding of 20 nm colloidal gold particles to measure the surface glass transition using AFM [145]. The embedding of particles was monitored after 8 hours, and a surface T_g of 40 degrees was obtained below which no apparent embedding of gold particles was seen. Teichroeb and Forrest [146] used a similar

method, and monitored the time dependence of the embedding of 10 and 20 nm spheres. Figure 2.7 shows the results of their experiment for 20 nm spheres. At temperatures above bulk T_g an almost complete embedding of the spheres happened down to a final constant contact angle depending on the size of the spheres. Below bulk T_g the spheres were embedded only about 4 nm, independent of the size of the spheres and then the embedding stopped and even after long time measurements no more embedding was seen.

Hutcheson and McKenna [147] used the Lee and Radok contact mechanical analysis [142] to analyze the data obtained by Teichroeb and Forrest [146]. In this model the embedding depth of a spherical indentor as a function of time, at depths smaller than the radius of the sphere is given by

$$[h(t)]^{3/2} = \frac{3}{8\sqrt{R}} \int_0^t \phi(t-\xi) \left(\frac{dP(\xi)}{d\xi} \right) d\xi \tag{2.30}$$

where

$$\phi(t) = \int_0^t \{1 - [\nu(t-\xi)]\} \left[\frac{dJ(\xi)}{d\xi} \right] d\xi \tag{2.31}$$

here $J(t)$ is time dependent creep compliance and ν is the Poisson's ratio. The force of embedding is assumed to be mainly due to the force of adhesion between gold and polystyrene. The pressure function is given by

$$P(t) = 2\pi(\gamma_{SV} - \gamma_{SL})\sqrt{R^2 - [R - h(t) - h_m]^2} \tag{2.32}$$

where h_m is the initial meniscus depth obtained from elastic response and is equal to 0.55 and 0.84 for 10 and 20 nm spheres respectively. $\gamma_{SV} = 1.35 N/m$ and $\gamma_{SL} = 0.3 N/m$ are surface energy of gold and interfacial energy between gold and PS. Time dependent poisson ratio and time dependent creep compliance, both with a stretched exponential time dependence with $\beta = 0.7708$ were used. Poisson's ratio was chosen to vary between 0.3 to 0.5 from glassy to rubbery state. Using this model the authors could only recover the bulk data by assuming a sample temperature which was 7.2 degrees higher than the reported value. Based on this bulk behavior the authors then tried to fit the model to the low temperature embedding of the particles and showed that the results could be explained by a surface creep relaxation time, corresponding to a 4 degrees depression in the actual temperature.

It was concluded that 4 degrees depression is not sufficient to explain the larger T_g reductions seen in the previous T_g measurements of thin films.

Sharp *et al.* [148] used the same analysis method, but with a different force function

$$F = 2\pi R\gamma \sin(\phi) \sin(\theta + \phi) \tag{2.33}$$

where γ is the surface tension of polystyrene, θ is the final non-zero contact angle between the gold and PS surface and ϕ is an angle that depends on the embedding depth. Using this force the produced results were more consistent with the experimental data above bulk T_g . The force used in this method is based on the surface tension of polystyrene rather than the force of adhesion. The idea behind using this force is that, because of the large energy of adhesion between gold and PS, it is expected that once the gold particles are put on the surface, a very thin layer of polystyrene will cover the surface of the gold particle to the point that it reaches the equilibrium contact angle. This is expected to happen much faster than the actual time scale of the embedding of the sphere which is then driven by the relaxation of surface tension. Using this force it was shown that the behavior of the material at high temperatures can be reasonably explained and at temperatures below bulk T_g the surface behaves as if it is at a temperature of slightly above bulk T_g rather than 15 degrees below it. An interesting difference between the two methods is that using the method of Hutcheson *et al.* the gold particles are expected to embed completely into the surface of the polymer, while experiments show that if colloidal gold is used, because of modified surface interactions, the particles will not embed into the film completely and even at very high temperatures and annealing times, a final non-zero contact angle between the gold particles and the polymer surface is maintained [149].

Although the results of embedding experiments can be used as an evidence of enhanced dynamics near the surface, suffer from a number of problems. Considering that the ongoing debate about the mechanism of embedding can be resolved, the mere existence of the gold on the surface can be problematic, because it partially covers the free surface, and it is not exactly clear how this can affect the dynamics as we already know that the covering of the free surface can eliminate the enhanced dynamics effect. There is also a difference between the embedding of evaporated
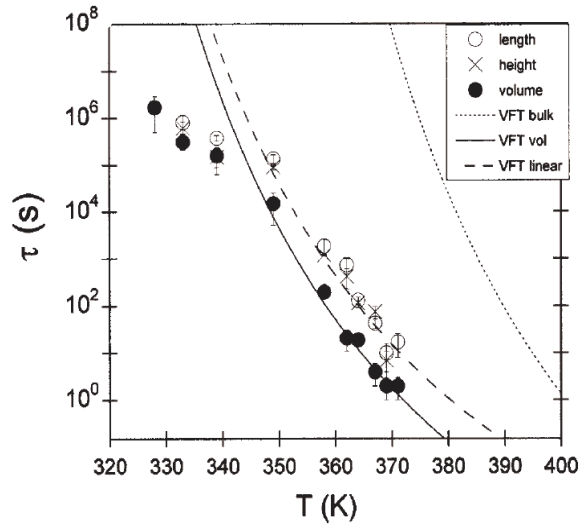
Figure 2.8: Measured relaxation times of volume, length, and height of the nano-deformations. The dotted line shows the expected bulk behavior. Adapted from ref. [152]

gold and colloidal gold, which makes it more complicated to interpret the results. The evaporated gold makes a zero contact angle with polystyrene and diffuses into the film, while colloidal gold are never completely embedded. This indicates that the type of interaction between the gold and polymer, are modified possibly due to the existence of a very thin citrate coating on the surface of the colloidal gold particles. One can imagine that the ideal mechanical response measurement would have the advantages of having a well shaped surface deformation, without having to introduce an external particle or probe.

The experiments of Papaleo *et al.* are an example of such experiments [150–152]. High energy ion bombardment was used to produce deformations on the surface of PMMA. In the point of ion contact there is a plastic deformation due to high temperature of the impact point. Away from this point, the shock waves of the impact produce bumps on the surface, with a size that depends on the molecular weight of the polymer used. It was shown that these bumps can be annealed at different temperatures above and below bulk T_g. The hight of these deformations are about 4 nm and their lengths are about 100 nm. The surface tension driven relaxation

of these structures at different temperatures showed that at temperatures above $T = 340K$ ($T_g(bulk) = 389$) the relaxation looked like a stretched exponential with $\beta = 0.4$. Below this temperature, annealing still happens, but the relaxation looks like a single exponential relaxation with an Arrhenius temperature dependence. Figure 2.8 the temperature dependence of the characteristic relaxation times for the volume, length, and height of the nano-deformations. The solid and dashed lines show the VFT fit to the high temperature portion of the experimental data. A VFT curve required to give a T_g of 389K (typical of bulk PMMA) is also displayed as a dotted line. The glass transition temperature of the surface can be defined as $\tau(T_g) = 100s$.

These results show that not only the dynamics of the surface in enhanced compared to the bulk, but the behavior of the system is changed to Arrhenius. It should be noted that the deformations obtained by the ion bombardment method are produced by extreme stresses caused by the impact shock. It is not clear how this will affect the results considering that the simulations suggest a reduction in the density of the material. Clearly more work is needed to confirm these results. It is also not clear whether or not the structural damage done by the ion impact, is changing the structure away from the point of impact. The samples used in these studies are only $80 - 100$ nm thick. It is expected that for PMMA the effect of silicon substrate, penetrate deeper than 100 nm [82] into the film. It is not clear how this can affect the results.

Summary and key questions

Despite the compeling evidence that the enhanced dynamics near the free surface is causing the observed T_g reductions in thin films, there are many questions that remain unanswered, and different contradictory results that need to be resolved. Some of the main unanswered questions are as followed.

There are many different studies that suggest that excluding the effect of substrate, the sample preparation method is not a main cause of T_g reduction in thin films, but there remains some studies that contradict this fact [74, 110]. The issue of the structure of thin film and its effect on the behavior of the film becomes

important when the dynamics of multi-layer films are compared to those of single-layer films. For example in the studies of Koh *et al.* [74] multi-layer free standing films that are stacked together are used to probe T_g. It is assumed that the dynamics of multi-layer films are similar to those of each layer, while in many other studies the dynamics are assumed to be similar to a film with a similar total thickness. [20, 80, 81] There is a major conceptual difference between these two assumptions. In the first case it is assumed that the dynamics depend on the structure of the single layers, so if the films are stacked as long as the annealing time is less than the diffusion time of the polymer chains, the film behavior follows the dynamics of each of those single layers. In the second case only the boundaries of the samples are assumed to be important in the observed anomalies of the dynamics and even though the initial structure of a multi-layer film is different from that of a single layer film with a similar total thickness, it is expected that the dynamics of these two films to be similar as long as the boundaries of the films are kept similar to each other. It is important to find out which of these two scenarios are valid. The results can both be useful to understand the behavior of multi-layer films, and to learn whether or not the thin film structure is important in the observed anomalies in the dynamics.

There seems to be a qualitative differences between the measurements of chain diffusion, measurements of viscosity and segmental relaxation, and T_g measurements. Measurements of chain diffusion in almost all cases indicate slower dynamics compared to the bulk dynamics. This slow dynamics is sometimes interpreted as increased T_g compared to the bulk T_g [128], while direct measurements of T_g in similar systems usually show lower T_g values in thinner films. Measurements of segmental dynamics and viscosity usually show that the dynamics are identical to the bulk dynamics, unless the temperature is lowered very close to bulk T_g [153]. The experimental evidence shows that at $T > T_g(bulk)$ the average segmental relaxation is not affected by the confinement even though the whole chain diffusion is slowed, probably due to the partial attachment to the substrate. But this doesn't necessarily mean that all segmental relaxations are bulk like. There is evidence that different modes of segmental motion could behave differently, leading to an average value similar to the bulk segmental relaxation. The question is then how

can we relate this behavior to the observed lowering of T_g, which indicates enhanced dynamics. The main difference between the two types of measurements is the temperatures at which the measurements are done. The measurements of segmental relaxation are always done well above T_g, while in order to do a T_g measurement, the temperature is brought below bulk T_g. Can this be the cause of the discrepancy between the two results? A complete curve of the system relaxation from temperatures above bulk T_g to well below T_g is needed to be obtained, to answer this question. It is also possible that these measurements are probing different modes of motion in the thin film [93], and these different modes of motion could be affected by confinement in different ways. It is then crucial to establish the exact type of motion that is causing the T_g reduction in thin polymer films.

The calorimetric measurements of T_g in thin films, suggest that the T_g of these films are equal to the bulk T_g, while the dilatometric measurements such as ellipsometry measurements show reduced T_g in thin films. In bulk glass formers there is often a reasonable agrement between the two types of measurements, and one expects that this agrement would exist in confined systems as well. In most calorimetric measurements, the cooling/heating rates used are much faster than what is regularly used in dilatometry measurements. This means that the relaxation times probed in these measurements are faster modes of motion compared to the dilatometric experiments. Is this the source of the differences between the results? Is there a major difference between the fast and slow modes of motion in thin films? What type of segmental relaxations are causing this difference between different modes of motion?

What is the effect of the free surface in all these observed anomalies? The T_g measurements in multi-layer films suggest that the T_g is lower near the free surface, and gradually changes towards the bulk T_g into the depth of the film. This suggests that the free surface plays an important role in the T_g reduction phenomena. More direct measurements of the dynamics near the surface indicate enhanced dynamics at temperatures below bulk T_g, but the observed enhancement at temperatures 10-30K below T_g are not so large that they can account for more than 50K reduction in the T_g of these films [141, 146, 146]. For example the measurements of Gasemjit *et al.* [141] at a temperature about 10K below bulk T_g show less than one order

of magnitude reduction in the viscosity near the free surface. In order to reconcile this discrepancy a complete curve of surface relaxation times are needed at different temperatures close or below bulk T_g. The only study that can potentially provide an answer to this question is the measurements of Papaleo *et al.* [152] for PMMA. The results of this experiment suggest that there is a transition from the usual stretched exponential relaxations of the surface deformations with VFT temperature dependence to a single exponential relaxation with Arrhenius temperature dependence at a temperature about 50K below the bulk T_g of PMMA. It is however hard to directly interpret these results, as there are major concerns about the sample preparation technique used in this study which involves structural damage to some parts of the surface due to high energy ion bombardment. There is also a possible reduction of the density of the surface deformations as they are produced by the shock wave of the impact propagating into the film.

If these questions are answered, then one would expect to be able to answer the more important question that whether or not these observed anomalies are caused by approaching the characteristic length scales of the system for polymers or glass formers in general. Is this a universal behavior of all polymers, and if it is, how can we explain the fact that the strength of the observed effects are different in different polymers? What is the relevance of parameters such as the chain stiffness in the observed T_g reductions? Does this mean that the observed differences are only happening because a polymeric system is being used, or this is a general behavior of a molecular glass former, and the effects are only larger in polymers, because larger length scales are involved? Can we define any length scales, such as the length scale of cooperative motion or dynamical heterogeneity using thin polymer films? At the end do these studies lead to a better understanding of the glass transition phenomena in general?

In this thesis we try to answer some of these key questions such as the difference between different modes of motion, and how many discrepancies in the literature can be resolved by considering different behavior at different temperatures and time scales. A direct relationship between the thin film dynamics and the surface relaxation is established, which helps build a universal picture that can be used as a base for more detailed theoretical models.

Chapter 3

Experimental techniques

3.1 Sample preparation

3.1.1 Material

The material used in the studies of this thesis is atactic polystyrene, with the molecular weight of $M_w = 641 \times 10^3$, $M_n/M_w = 1.11$ or $M_w = 221 \times 10^3$, $M_n/M_w = 1.03$ obtained from the Polymer Source Inc [155]. Figure 3.1 shows the molecular structure of polystyrene, composed of styrene monomers. Atactic polystyrene does not have a crystalline phase, which makes it easy to use for T_g studies. The glass transition temperature of polystyrene at high molecular weights is about 373K [156]. Table 3.1 shows some of the important physical constants of polystyrene that are referred to in this thesis.

3.1.2 Thin film preparation

Preparation of single layer films

Thin polystyrene films are prepared by spin-casting a solution of polystyrene (PS) in toluene onto a substrate. The thickness of the film is controlled by changing the concentration of PS solutions and the spin speed. Films with thicknesses between
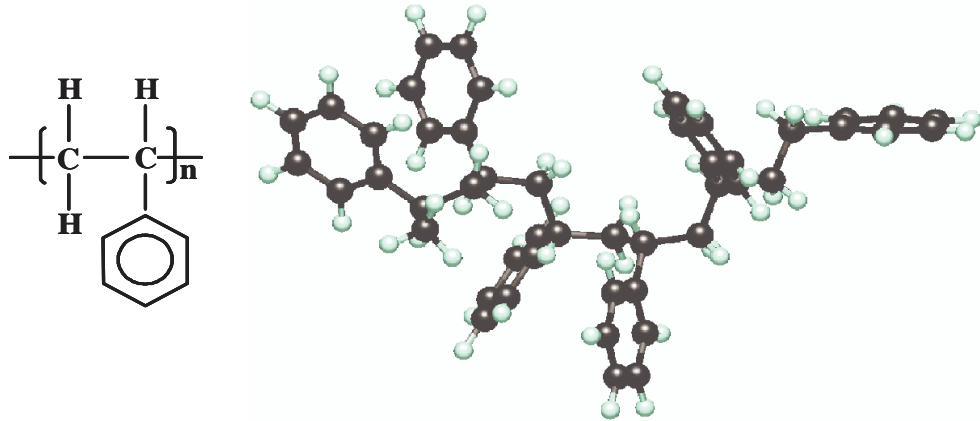
Figure 3.1: Chemical structure of polystyrene [154]

Physical property		Value
Density		$1.04 - 1.065$ Kg/m^3
Coefficient of thermal	$< T_g$	$1.7 - 2.1 \times 10^{-4}$ K^{-1}
expansion (volume)	$> T_g$	$5.1 - 6.0 \times 10^{-4}$ K^{-1}
Refractive index	$\lambda = 589.3$ nm	$1.59 - 1.6$
Entanglement molecular weight		19100 Kg/mol
Elastic Modulus		3200 MPa
Poisson's ratio		$0.325 - 0.33$
Surface tension	293K	40.7 mN/m
Yield stress	298K	88.5 MPa

Table 3.1: Physical properties of polystyrene [143, 156]

3 nm to 200 nm were made and used in our studies. The films were then annealed 20-40 degrees above T_g between 10 to 24 hours to make sure that the solvent is completely removed from the sample and to partially anneal the stresses induced in the sample upon spin-casting. Annealing was done under dry nitrogen to avoid structural damage to PS due to the existence of oxygen.

Preparation of multi-layer films

In order to make multi-layer films, each layer was prepared separately on either silicon, for the first layer, or NaCl salt crystal for other layers. Each layer was treated in the same manner as a single layer film, to make sure that the layers have similar structures and properties. The layers were then put together using the following procedure; the second layer made on salt was put upside down on top of the first layer made on silicon. A drop of water was brought in contact to the salt crystal. The water wetting the salt surface, would rapidly detach the salt crystal from the polymer layer. The polymer layers stick together by the surface adhesion forces. The third and forth layers were put on the sample with the same method if necessary. Once the multi-layer films were made, they were annealed for a second time under dry nitrogen to evaporate the water trapped in between the layers. The second annealing was done at 30 degrees below bulk T_g and any other measured T_gs of thin films, to make sure that the layers remained separated from each other. Figure 3.2 shows this procedure schematically.

3.1.3   Sample preparation methods involving gold nano-spheres

Synthesizing gold nano-spheres

The recipe used to make gold nano-spheres was obtained from university of Wisconsin's interdisciplinary education group [157]. The recipe is as followes,

1. A 1.0mM solution of the gold salt, $HAuCl_4$(0.034gr in 100mL water) is prepared.
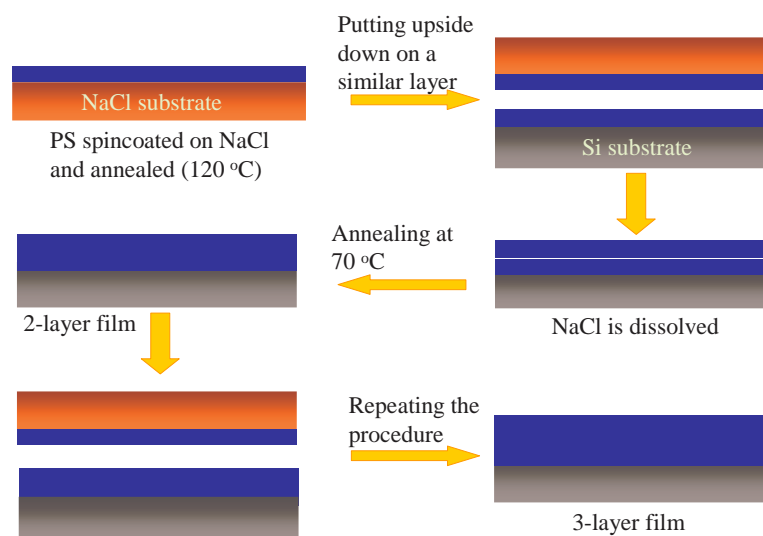
Figure 3.2: Schematic diagram of the preparation of multiple-layer thin films

2. 20ml of this 1.0mM solution is brought to boiling while being stirred.

3. 2mL of 1% solution of tri-sodium Citrate is added to the boiling solution.

4. The color change of the solution is monitored as it changes from yellow to clear, to dark grey, to dark purple and then to dark red within about 15 minutes.

5. The boiling is continued for an extra 5 minutes to make sure that the suspension is stabilized.

Prepared properly, the solution has a shelf life of more than one month. Depending on the concentration of the citrate solution used, gold spheres with sizes between $10 - 100$ nm can be made with this recipe. Decreasing the citrate concentration results in larger size spheres. The solutions prepared with this recipe are about 10 times more concentrated than the commercially available nano-spheres as measured by absorption spectroscopy, so it is easier to spread them onto the surface of thin films. The size dispersion however is not as good. Depending on how carefully the solution is prepared the dispersion can vary between ± 2 nm to

± 4 nm for small spheres to ± 10 nm to ± 30 nm for larger spheres (As opposed to 10% of the sphere size for commercially available spheres).

Putting gold nano-spheres on the polymer surface

Gold nano-spheres are made as charged stabilized colloidal particles in a water based solution. This solution can not wet the PS surface and as a result if one tries to spincast the particles onto the PS surface, the gold particles will not stick to the surface. Methanol can be added to the solution to make it more wetable. It is important to choose the right concentration of methanol added to the solution. Adding too much methanol can cause the aggregation of the particles and adding too little will not produce a wetting solution. The concentration of methanol needed in the solution depends on the type of spheres used and their sizes and is obtained for each batch of spheres separately. For 20 nm spheres synthesized in the lab, the concentration of methanol needed is approximately 25%.

Producing surface nano-deformations

In order to make holes with constant depth and radius of curvature a novel method for embedding of gold particles was developed. Thick films of polystyrene (approximately 100 nm) are made as described before. Gold spheres (approximately 20 nm in diameter)are then put on the sample and are embedded above T_g (378K)for different times to get different embedding depths. The approximate embedding times for different embedding depths can be obtained from reference [146] for 20 nm spheres. The temperature of the samples is then brought back to room temperature and the gold spheres were dissolved using mercury [158]. Gold can be dissolved in mercury in any proportion, similar to the way sugar is dissolved in water. In fact gold nano-particles or gold surfaces can be used as mercury sensors, [159] because gold can completely absorb all the mercury present in the air or water.

The advantage of using mercury in removing gold particles is that mercury does not interact with polystyrene and because of its high surface tension it can be completely removed from the surface once the gold particles are dissolved. To make

Put gold nano-spheres
on the surface

Anneal at 379K
for 10 minutes.

Dissolve gold nano-
spheres in mercury

Produced nano-deformations

1000nm

25.5nm

0.0nm

0nm
0nm   1000nm

1000nm

19.0nm

0.0nm

0nm
0nm   1000nm

1000nm

7.0nm

0.0nm

0nm
0nm   1000nm
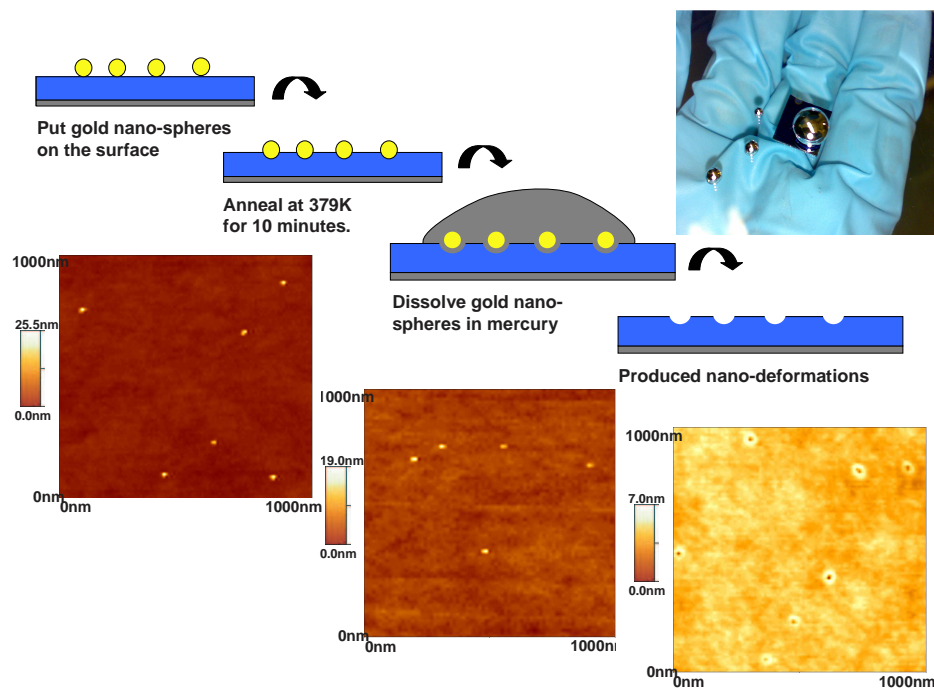
Figure 3.3: Schematic procedure of producing nano-deformations on the surface.

sure that the mercury did not have any effects on the PS films, the T_g of a film was measured after being soaked in mercury for a long time, and it was confirmed that the T_g was the same before and after soaking, (378K for a 100 nm film of PS). Energy dispersive x-ray analysis (EDX) was also done on a similar sample, with an accuracy that was enough to detect the oxide coating of the silicon substrate (less than 2 nm as measured by ellipsometry) and no residue of mercury was found on the sample within this accuracy. This confirms that the mercury is not penetrating into the polymer film. Figure 3.3 shows the schematic of this process. The atomic force microscopy (AFM) images from left to right show the surface of the sample with gold nano-particles, after the gold particles are embedded, and when the nano-deformations are produced respectively. The image on the top right corner shows an image of the sample with the mercury.
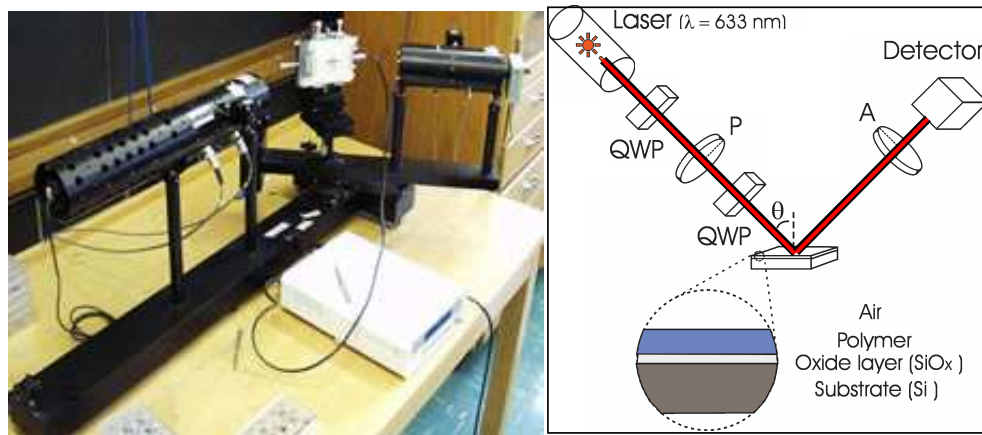
Figure 3.4: Left: An image of the ellipsometer used in this thesis, the EXACTA 2000 Faraday modulating fast nulling ellipsometer. Right: Schematic drawing of the ellipsometer. The first quarter-wave plate and the Faraday rods are not illustrated.

3.2   Ellipsometry

When light is reflected from a surface, its polarization changes depending on the properties of the reflecting surface. Ellipsometry is a method to use the ellipticity induced by the surface properties to find information about the system, such as the film thickness and index of refraction in a film/substrate system. The ellipsometer used in different studies of this thesis is a nulling ellipsometer [160]. In this section the basic calculations required to analyze the data obtained in a nulling ellipsometric measurement will be explained for different types of samples and measurements.

3.2.1   Nulling ellipsometer

Figure 3.4 shows an schematic picture of a nulling ellipsometer. First, a quarter-wave plate converts the linear polarization of the laser light into a circular polarization. The light then hits the polarizer prism, which produces a linearly polarized light in the direction of the polarizer. The light becomes elliptically polarized after passing the second quarter-wave plate and then is reflected from the sample. The light hits the detector after passing the analyzer. If the light reflected from the

surface is linearly polarized, the intensity of light on the detector would be zero, otherwise the two motors mounted on the polarizer and analyzer, will turn the P (polarizer) and A (Analyzer) angles until the intensity becomes zero. One can then use the corresponding P and A values to find the properties of the reflecting surface such as film thickness and index of refraction. The ellipsometer used in this study [160] also uses two modulated Faraday rods for the polarizer and analyzer which change the polarization of the light passing through the polarizer and the analyzer with a small quadrature sinusoidal modulation form. The detected signal at the detector is modulated and fed back to the motors that rotate the polarizer and the analyzer to detect slight changes in the null and keep the ellipsometer at null at all times. This method enables the user to measure slight changes in the P(polarizer) and A(analyzer) values accurately and with a fast speed. If the changes in the null are small new null values can be obtained in less than 0.3 seconds, with an angle accuracy of 6×10^{-4} degrees [160].

3.2.2 The optics of ellipsometry

Jones matrices

In this section the Jones matrices are introduced which are the basic mathematical tool used to calculate the polarization of light as it passes through the system and is reflected off different types of samples. Since the only property of light that is important here is its polarization other parameters such as intensity can be ignored in this discussion.

Assume that the laser light is traveling in the $+z$ direction (Figure 3.5), then the electric field lies in the $x - y$ plane (the p and s polarized light respectively) and and the electric field vector can be written as a two component column matrix,

$$\begin{pmatrix} E_{0,x} \\ E_{0,y} \end{pmatrix} \exp(i\omega t) \tag{3.1}$$

Where E_0 is the amplitude of the electric field at time zero. Without losing any accuracy, one can ignore the time dependant part of the matrix. For a linearly

polarized light in the angle of θ compared to the x axis, the x and y components of the electric field are in phase, and the Jones matrix for the light will be equal to,

$$\begin{pmatrix} E_0 \cos\theta \\ E_0 \sin\theta \end{pmatrix}$$

similarly the Jones matrix of a circularly polarized light, with a phase difference of $\pm\pi$ between its x and y components is given by,

$$\begin{pmatrix} E_0 \\ \pm iE_0 \end{pmatrix}$$

As mentioned before, we are only interested in the polarization of the light, so one can change the components of the Jones matrices as long as the relative phase and the ratio of the two components are conserved. So the following matrix can also be used as the Jones matrix in equation 3.1 [161].

$$\begin{pmatrix} A_x \exp(i\phi_x) \\ A_y \exp(i\phi_y) \end{pmatrix}$$

Where if, $E_{x,r}, E_{x,i}, E_{y,r}$ and $E_{y,i}$ are the real and imaginary parts of the x and y components of the electric field, then $\tan\phi_x = E_{x,i}/E_{x,r}, \tan\phi_y = E_{y,i}/E_{y,r}, A_x = (E_{x,r}^2 + E_{x,i}^2)^{1/2}$ and $A_y = (E_{y,r}^2 + E_{y,i}^2)^{1/2}$. The normal unit vectors for the system are the electric field vectors of linearly polarized light in the x and y directions. Any transformation that conserves the polarization of light is proportional to a 2×2 unity matrix.

Now one can construct the Jones matrices representing a polarizer and a quarter-wave plate and the Jones matrix of reflection. If the light passes through a polarizer with an angle of zero, the y component of the electric field would be completely absorbed by the polarizer and only the x component will pass, so the corresponding Jones matrix would be equal to,

$$\begin{pmatrix} 1 & 0 \\ 0 & 0 \end{pmatrix}$$

To find out the Jones matrix for a polarizer that is set in an angle of P one can simply rotate the coordinate system by the same angle, using the above Jones
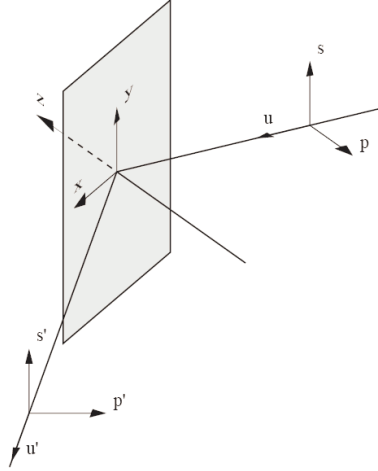
Figure 3.5: The schematic diagram of the light reflecting from a surface. Figure from ref. [161]

matrix and then use an inverse rotation to convert the coordinate system back to the original system. So the Jones matrix will be given by,

$$
\begin{pmatrix}
\cos^2 P & \sin P \cos P \\
\sin P \cos P & \sin^2 P
\end{pmatrix}
\tag{3.2}
$$

Similarly, a quarter wave-plate with its fast axis along the x direction, is represented by a Jones matrix that introduces a $\pm 90°$ phase delay in the y direction [161]

$$
\begin{pmatrix}
1 & 0 \\
0 & -i
\end{pmatrix}
$$

Using the same rotation as used for the polarizer matrix, the Jones matrix of a quarter wave-plate with its a fast axis along the angle Q is,

$$
\begin{pmatrix}
\cos^2 Q - i \sin^2 Q & (1+i) \sin Q \cos Q \\
(1+i) \sin Q \cos Q & \sin^2 Q - i \cos^2 Q
\end{pmatrix}
\tag{3.3}
$$

Finally, if one chooses the coordinate system so that the x and y directions are the directions of a p and s polarized light hitting a surface, the Jones matrix

representing reflection would be equal to,

$$\begin{pmatrix} r_p & 0 \\ 0 & r_s \end{pmatrix} \tag{3.4}$$

Light passing through the ellipsometer

Using the Jones matrices one can follow what happens to the polarization of light as it passes through the ellipsometer as schematically shown in figure 3.4. The initial laser light $\begin{pmatrix} E_x \\ E_y \end{pmatrix}$, changes to a circularly polarized light as it passes through the first quarter-wave plate with its fast axis along the x direction $\begin{pmatrix} E_x \\ -iE_y \end{pmatrix}$ (not illustrated in figure 3.4). After passing the polarizer P and the quarter wave plate QWP, the incident light that hits the sample is represented by, [161]

$$\begin{pmatrix} E_{p,i} \\ E_{s,i} \end{pmatrix} = \begin{pmatrix} \cos Q \cos(P - Q) + i \sin Q \sin(P - Q) \\ \sin Q \cos(P - Q) - i \cos Q \sin(P - Q) \end{pmatrix} \tag{3.5}$$

The relationship between the incident light and reflected light is given by,

$$\begin{pmatrix} E_{p,r} \\ E_{s,r} \end{pmatrix} = \begin{pmatrix} r_p & 0 \\ 0 & r_p \end{pmatrix} \begin{pmatrix} E_{p,i} \\ E_{s,i} \end{pmatrix} \tag{3.6}$$

When the light passes through the analyzer A, in a nulling ellipsometer, it is completely absorbed, which means the light in equation 3.6 is linearly polarized. This constraint can be written as,

$$\Im(\frac{r_p}{r_s} E_{p,i} E_{p,s}^*) = 0$$

where $\Im$ shows the imaginary value of the function. If the ratio of the reflection coefficients is written as a complex number,

$$\frac{r_p}{r_s} = \tan\psi \exp(i\Delta)$$

Then using equation 3.5 one can show that

$$\Im(\frac{r_p}{r_s} E_{p,i} E_{p,s}^*) = \frac{1}{2} \sin(2P - 2Q) \tan\psi \cos\Delta + \frac{1}{2} \sin 2Q \cos(2P - 2Q) \tan\psi \sin\Delta = 0$$

The solution to this equation is

$$\tan(2P - 2Q) = -\sin 2Q \tan \Delta \tag{3.7}$$

There are four different values of P which satisfy the above equation. For each of these values the corresponding A angle which leads to a zero intensity in the detector is given by,

$$\tan A = \tan \psi \frac{\cos(2P - 2Q) \cos \Delta \sin 2Q - \sin(2P - 2Q) \sin \Delta}{\cos(2P - 2Q) \cos 2Q - 1} \tag{3.8}$$

In the special case where $Q = \pm\pi/4$ which is the angle of the quarter wave plate usually used in conventional ellipsometers, one can greatly simplify equations 3.7 and 3.8,

$$P_{1,2} = \mp\Delta/2 - \pi/4 \quad \text{and} \quad A_{1,2} = \psi \tag{3.9}$$

$$P_{3,4} = \mp\Delta/2 + \pi/4 \quad \text{and} \quad A_{3,4} = -\psi \tag{3.10}$$

P and A are the properties that are measured by a nulling ellipsometer. If the measured samples are isotropic, then the measurements in different zones will not lead to any extra information about the sample, but they are useful in eliminating systematical alignment errors in the ellipsometer. From these values, one can calculate the real and imaginary part of the ratio of the reflection coefficients.

The easiest system that can be studied using a nulling ellipsometer is an isotropic reflecting half space. For this system the Fresnel reflection and transmission coefficients for p and s polarized lights are given by [162],

$$r_p = \frac{n_t \cos \theta_i - n_i \cos \theta_t}{n_t \cos \theta_i + n_i \cos \theta_t} \tag{3.11}$$

$$t_p = \frac{2n_i \cos \theta_i}{n_t \cos \theta_i + n_i \cos \theta_t} \tag{3.12}$$

$$r_s = \frac{n_i \cos \theta_i - n_t \cos \theta_t}{n_i \cos \theta_i + n_t \cos \theta_t} \tag{3.13}$$

$$t_s = \frac{2n_i \cos \theta_i}{n_i \cos \theta_i + n_t \cos \theta_t} \tag{3.14}$$

Where n_i and n_t are the refraction index of the medium containing the incident light and the medium containing the transmitted light respectively. θ_i and θ_t are the
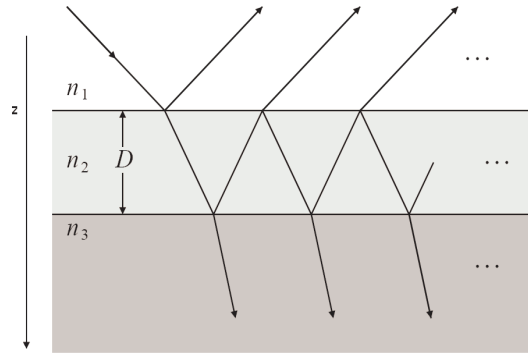
Figure 3.6: Reflection of light from a thin film on a substrate. Figure from ref. [161]

incident and transmission angles which are related through Snell's law $n_i \sin \theta_i = n_t \sin \theta_t$ [162]. Using these equations the index of refraction of the medium can be obtained,

$$n_t = n_i \tan \theta_i \sqrt{1 - \frac{4\rho \sin^2 \theta_i}{(1 + \rho)^2}} \qquad (3.15)$$

Where $\rho = r_p/r_s$ can be calculated from the P and A values obtained from equation 3.9 or 3.10.

3.2.3 Reflection coefficient of thin films

The samples we are interested to study are often more complicated than just isotropic half spaces, they are usually made of one or multiple layers of polymer films, on top of silicon substrate which usually contains a very thin layer of native silicon oxide. All layers are isotropic and have roughly the same thickness every were on the substrate. In this section the reflection coefficients for multi-layer thin films are calculated which can be then used in different ways in different studies.

One-layer films

Figure 3.6 shows how light is reflected from the surface of a thin film with the thickness D on a substrate. In order to calculate the reflection and transmission

coefficients one needs to add all the components that are reflected or transmitted. When the electric field with an amplitude E hits the surface of a thin film, the intensity of the reflected light is equal to $r_{12}E$, and the intensity of the transmitted light is equal to $t_{12}E$. After traveling a distance D inside the thin film the the electric field will have a phase delay equal to $\exp(-i\delta) = \exp(-ik_z D)$. When it is reflected back from the substrate and reaches the surface, its intensity is further reduced by a factor of r_{23} accounting for the reflection from the substrate and another phase shift of δ accounting for the distance it has traveled. The part of the electric field that is transmitted is added to the initial reflected field and the part that is reflected continues this process over and over again. The total reflection coefficient is then given by,

$$R_{total} = r_{12} + t_{12}t_{21}r_{23}e^{-2i\delta}[1 + r_{21}r_{23}e^{-2i\delta} + (r_{21}r_{23}e^{-2i\delta})^2 + ...]$$

Using the Fresnel coefficients one can show that,

$$r_{12} = -r_{21} \quad \text{and} \quad t_{12}t_{21} = 1 - r_{12}^2$$

The summation can be calculated and it can be shown that the total reflection coefficient is equal to, [162]

$$R_{total} = \frac{r_{12} + r_{23}\exp(-2i\delta)}{1 + r_{12}r_{23}\exp(-2i\delta)} \tag{3.16}$$

The total transmission coefficient can be calculated in the same manner,

$$T_{total} = \frac{t_{12}t_{23}\exp(-i\delta)}{1 + r_{12}r_{23}\exp(-2i\delta)} \tag{3.17}$$

Note that for the s and p polarized lights the calculation of the total reflection and transmission coefficients are the same, as long as the the proper index r or t is used. Now that the total reflection coefficients are calculated, one can use the P and A data from the ellipsometric measurements to calculate the index of refraction of the thin film, if the index of refraction of the substrate is known. The thickness of the film can also be calculated, as it is related to the phase lag $\delta = 2\pi n_2 D \cos\theta_2/\lambda$. It is however not as straight forward to obtain these values as it is in a system of infinite half space. Here the number of unknown variables
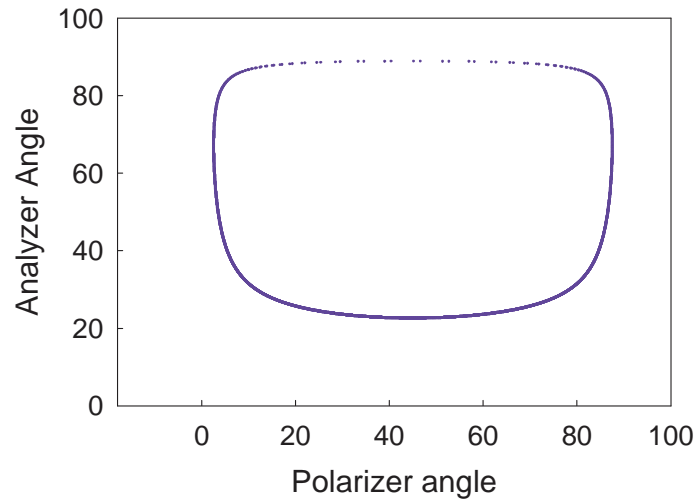
Figure 3.7: Plot of A vs P for polystyrene.

are more than the number of independent equations. The proper way to obtain the index of refraction from an ellipsometeric measurement is to measure films of the same material with different thicknesses. For a constant, real index of refraction the plot of P vs. A obtained from different thickness values produces a closed curve. Figure 3.7 shows an example of such plot for polystyrene produced using an index of refraction equal to $n = 1.595$, on a silicon substrate with the complex index of refraction $n_s = 3.74 + 0.019i$ [163]. It is assumed that the substrate is coated with a 2 nm oxide layer with the index of refraction of $n_{oxide} = 1.46$ [163]. The value of the oxide layer thickness can be measured independently using a bare silicon substrate and a one-layer model. The measured thickness of this layer is usually about 2nm. The data can be fit to a model to find the best fit to this curve with a single parameter which is the index of refraction. If done properly this method can define the index of refraction of a system with an accuracy of about 0.005. Once the index of refraction is determined, one can find the thickness of each film since the set of equations are now enough to define them.

Multi-layer Films

Figure 3.8 shows a two-layer film, with two different thicknesses and indexes of refraction. Finding the total reflection coefficient of the top layer is straight forward. This coefficient is still represented by equation 3.16 except that instead of r_{23} the total reflection from that surface (R_{23}) is used and to calculate the phase delay, the thickness of the second layer is used. R_{23} is a combined reflection coefficient from a multi-layer film, and is again calculated using equation 3.16

$$R_{23} = \frac{r_{23} + r_{34}\exp(-2i\delta_3)}{1 + r_{23}r_{34}\exp(-2i\delta_3)}$$

Where $\delta_3 = 2\pi n_2 D_3 \cos\theta_2/\lambda$ is the phase corresponding to the thickness of the third layer. And similarly, if there are more layers, the coefficient r_{34} is replaced with the total reflection R_{34} using the appropriate film thickness for the phase difference. This procedure continues until there are no more layers left unaccounted for. The general recursive relation for the total reflection coefficient of an n layer film can be written as

$$R_{i,i-1} = \frac{r_{i,i-1} + R_{i-1,i-2}\exp(-2i\delta_{i-1})}{1 + r_{i,i-1}R_{i-1,i-2}\exp(-2i\delta_{i-1})} \tag{3.18}$$

Although finding the reflection coefficients is not hard, interpreting the data is much harder for a multi-layer film as the number of unknown variables could be much more than the number of experimental data obtained from a single measurement, and one may need to develop models to fit the data.

3.2.4   Using ellipsometry in thin film measurements

In this section we describe the application of ellipsometry technique in measuring the thickness, T_g and dynamics of thin films.

Measuring film thickness

Measuring film thickness is one of the main applications of the ellipsometry technique. Polystyrene is a transparent material with a real index of refraction. The
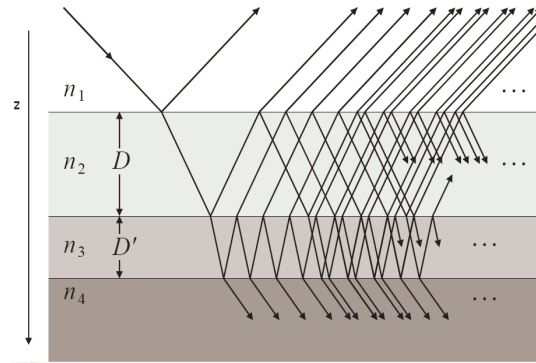
Figure 3.8: Reflection of light from a four layer sample, with the first layer being the ambient and the fourth layer an infinite half space. Figure from ref. [161]

plot of figure 3.7 can be used to obtain the thickness of thin polystyrene films. A thin PS film is made from three different layers, the substrate is Silicon with a well known index of refraction. The oxide layer on top has a well known index of refraction, but its thickness could vary depending on the type and age of the silicon wafer. In order to find an accurate thickness of this layer one can measure the P and A values for a bare silicon wafer and since it is a one-layer film on a substrate the data can be easily converted to the film thickness, using equations obtained in section 3.2.3. The thickness of this layer is usually of the order of 2 nm.

Knowing the thickness of the oxide layer, the only unknown fit parameter to the P vs A plot is the index of refraction of PS. Once the index of refraction is determined, the P and A data for each individual film can be converted to the film thickness. But a small error in the measured P and A values can lead to a much larger error in the thickness measurement because of the nonlinear relation between the thickness and the $P\&A$ values, so it is usually better to make an array of $P\&A$ values vs film thickness for the obtained index of refraction, and compare the values with the experimental values obtained for $P\&A$. This could also produce an estimation of the error in the thickness measurement.

In some cases a two-layer model can be used instead of the three- layer model, with an effective index of refraction for silicon and ignoring the existence of the oxide layer. This method can only be used for films that are much thicker than
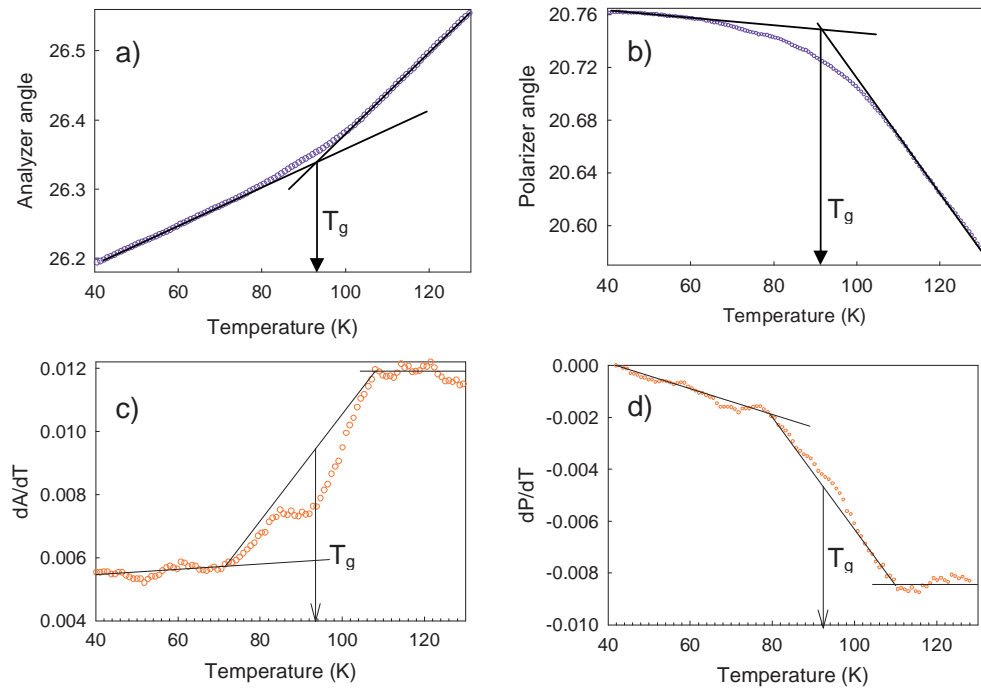
Figure 3.9: a)A , b)P , c)dA/dT and d)dP/dT vs T for a 40 nm polystyrene thin film. A T_g value is obtained from each of these graphs.

the oxide layer. For ultra thin films with thicknesses that are comparable with the thickness of the oxide layer (< 10 nm) the error in the thickness measurement is larger and this could lead to a systematic error in the thickness measurement which is not linearly dependent on the film thickness.

Measuring the glass transition temperature

Measuring the absolute film thickness with the ellipsometer has an accuracy between $1 - 10$ nm depending on the film thickness and quality. There are a number of reasons that this accuracy can not be improved. Variations in the film thickness at different points on the sample, the capillary roughness of surface which increases with the film thickness and also systematic errors in the $P\&A$ measurements could play an important role in defining the accuracy of the film thickness measurements.

But once the sample is in a steady position and a null is achieved, the changes in the film thickness can be detected more accurately. The ellipsometer used in these studies has a precession of 6×10^{-4} degrees in P or A angles which translates to a sub angstrom measurement of the thickness variations. This enables the user to measure the coefficient of linear expansion in ultra-thin films in the glassy or liquid states.

In order to measure T_g the sample is mounted on a Linkam temperature controller, and the temperature is ramped up and down with a constant rate. The P and A values are measured continuously during the ramp, and the plots of P vs T (temperature) and A vs T are generated. It is important to measure the T_g on the cooling cycle from an equilibrium temperature well above T_g. When measured on a heating cycle, the changes in the thickness could depend on previous stresses induced on the sample during previous cooling or heating cycles.

Figure 3.9 shows a typical plot of P, A, dP/dT and dA/dT vs T. It can be seen from the plots that changes in the A values are small enough that can be assumed to be changing linearly with the temperature in the liquid and glassy phases. This is also clear in the dA/dT plot. Changes in the P value slightly deviate from linear behavior in the glassy region. It is thus not necessary to convert this data to a plot of thickness (h) versus temperature (T) to determine the T_g of the film. The change in the slope shows the glass transition temperature. From the derivative plots the midpoint of the transition can also be defined as T_g. In some cases if both P and A values are near a turning point in the P vs A graph, the changes of both values could be nonlinearly dependent to the thickness and converting the data to a plot of h vs T would be necessary to find T_g [54]. In all cases concerned in this thesis, obtaining the T_g values from either P or A vs T plots was possible, and no conversion was done. The value of the T_g using ellipsometry can be obtained with a typical accuracy of $\pm 2°C$, due to uncertainty in defining the onset of changes in the behavior in the liquid and glassy region, in a single measurement and $\pm 4°C$, due to alignment and other systematic errors, from repeated measurements.

A model of interface healing

To measure interfacial healing of two PS layers we needed to develop a more complicated model compared to models used for measurements of single or double layer films [164]. The samples in this study are films with 5 different layers. The silicon substrate, the oxide layer, two PS layers with the same thickness which are mounted on top of each other and the interfacial layer which has an initial density less than the PS density, which gradually changes to the density of polystyrene during the annealing procedure. This interfacial layer is produced when the two PS layers are brought to each other, due to the surface asperities of both layers which causes a distance between the two surfaces. There is also a possibility that the near surface layer has a lower density compared to the bulk PS. The thickness of this layer and the initial average density of this layer are not independent parameters, and can not both be used as fit parameters. A number of different measurements and different fitting models showed that choosing an initial average density of $\rho_0 = 0.4 \times \rho_{bulk}$ is a reasonable initial condition for the interface layer. This value leads to an interface region of $3 - 5$ nm, which is consistent with what is expected from the AFM measurements of the initial surface roughness of the films, which are about $0.9 - 1.5$ nm for individual layers depending on their size. It is assumed that the density of this layer changes with time to a maximum value of ρ_{bulk} with an stretched exponential relation $\rho(t) = \rho_{bulk}(1 - a \exp[-(\frac{t}{\tau_0})^\beta])$ where $\rho(0) = 0.4 \times \rho_{bulk}$, τ_0 is the characteristic relaxation time of the system and one of the fit parameters and $\beta = 0.3$ is the exponent of the stretched exponential. The index of refraction of the interface can be related to the density using the Lorentz-Lorenz relation [162],

$$\frac{n^2 - 1}{n^2 + 1} \simeq \alpha\rho \tag{3.19}$$

The constant α can be obtained from the limit of $\rho = \rho_{bulk}$ and $n = n_{bulk}$. Using this index of refraction, the reflection coefficients can be calculated using equation 3.18 for a five-layer film, which in turn can be used to find the P and A values. The values obtained are fitted to the experimental data using a Matlab function that uses the Nelder-Mead [165] simplex direct search method to minimize the sum of the magnitudes of differences between the calculated and the measured values. This algorithm does not need minimized function derivatives and is among the best and
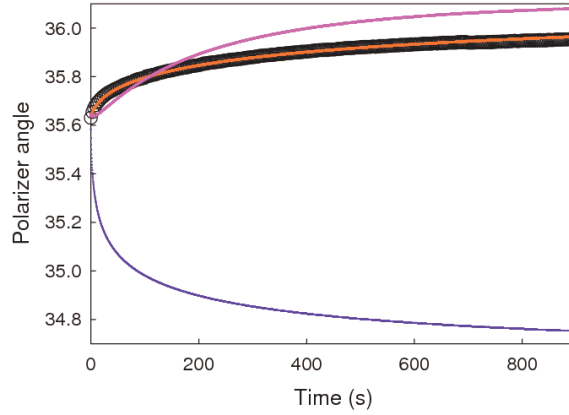
Figure 3.10: The plot of P vs time for a bi-layer film (○) made of two 5 nm layers annealed at 393K. The red curve shows the stretched exponential fit to the data the pink curve is the single exponential curve with the same relaxation time and the blue curve is generated using the same parameters as the red curve, but without the conservation of mass.

fastest algorithms for numeric optimization when the minimized function is well behaved, and does not have many adjacent local minima. The only independent fit parameter used are then the time constant τ_0, The initial film thickness of PS layers, and the initial thickness of the interfacial layer. The average relaxation time of the interface healing is then proportional to the time constant τ_0

$$\tau = \frac{\tau_0}{\beta} \times \Gamma(\frac{1}{\beta}) \tag{3.20}$$

It is important to notice that only a realistic model could lead to results that could even qualitatively be fitted to the data. For example in order to obtain reasonable fit, one has to keep the total mass of the system constant at each time, which means that as the density of the interfacial layer is increased, the thickness of the two PS layers should be decreased correspondingly to adjust for the mass of the system. If the conservation of mass is not considered, the changes in the P value would qualitatively different from what is measured. Figure 3.10 shows an example of a bi-layer film made of two 5 nm layers. The fit to the data using the above model is shown, along with a curve that represents a model with similar parameters, but

without considering the conservation of mass. One can also see that if a single relaxation model is used instead of stretched exponential, the best fit to the data, is still far different from the experimental data. These examples confirm that using a realistic model is necessary to analyze the data, and that the model used here can reasonably explain the experimental data. The matlab program used to calculate the P and A values of this model is given in appendix A.

3.3 Atomic force microscopy

Scanning probe microscopy (SPM) is a technique to measure surface properties such as topography and structure with nanometer scale depth and spatial resolution. A SPM device is usually composed of a sensing sharp tip with different properties depending on the type of measurements. In the studies of this thesis only non-contact atomic force microscopy (AFM) technique was used, which uses the interaction force between the probe and the surface to create a topography image of the surface. Figure 3.11 shows an schematic illustration of an AFM device. The probe tip is connected to the end of a cantilever which oscillates at its resonant frequency. The reflected laser light from the tip of the cantilever is send through a mirror to a four section photo-detector, which detects the motion of the tip in the left and right, and the up and down directions. The motion in the up and down direction of the cantilever is modulated to monitor the amplitude and the phase of oscillation. When the tip is brought close to the surface, the interactions between the sharp tip and the surface damps the resonant oscillation of the cantilever, and this damping of the signal, or the changes in the phase of the signal can be detected and controlled by the AFM controller device using a PID controller. The controller keeps the distance between the tip and the surface at a constant level by maintaining the modulation amplitude at a constant level. As the position of the tip is changed by the X and Y piezos, the surface topography can be generated by measuring the motion of the Z piezo that is necessary to keep the distance between the tip and the surface constant.

The resolution of an AFM device in the X and Y directions depends on the radius of curvature of the tip and for sharp tips this could be as small as 10 nm.
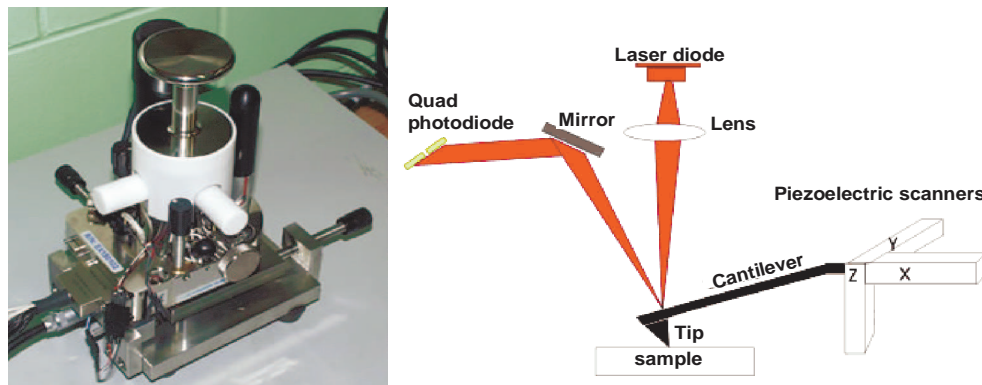
Figure 3.11: Left: An image of the atomic force microccopy device used in this thesis, a Veeco explorer. Right: Schematic illustration of an AFM device [166].
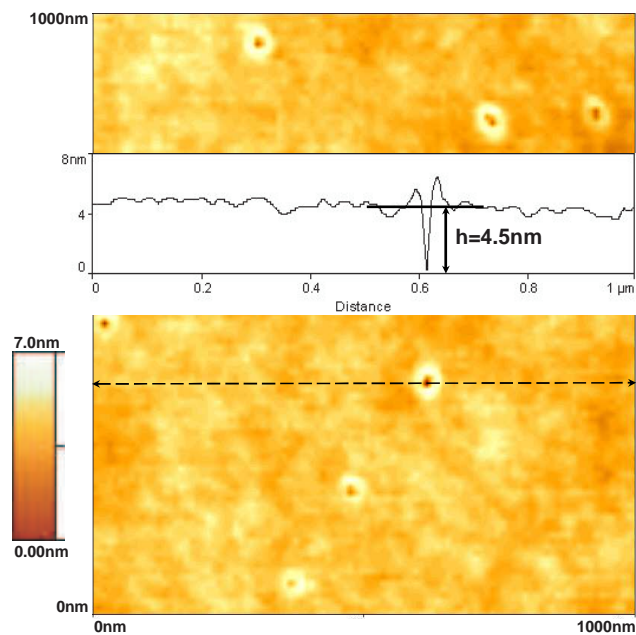
Figure 3.12: An AFM image of surface nano-deformation taken with the resolution of 500 points in a $5\mu m \times 5\mu m$ scan range (Only a $1\mu m \times 1\mu m$ part of the image is shown here for clarity). The inset shows the line scan of the indicated line (dashed line) used to measure the depth of the hole.

The accuracy in the height measurement can be less than a nanometer, which makes the AFM a good tool in measuring features such as gold nano-spheres on the surface or very small surface nano-deformations.

Using AFM to measure surface nano-deformations

When small features are measured using AFM, the shape and length of the AFM tip can become an important factor, especially when the deformation being measured is a hole where the tip may not get into the bottom of the hole. In order to get an accurate depth, it is necessary that the tip reaches the bottom of the hole. The obtained shape of the hole will be a convolution of the tip shape and the actual shape of the hole. In the measurements of nano-deformations in this theses the diameter of the holes are about 20 nm. The radius of curvature of sharp AFM tips are between 7 nm to 10 nm. If a tip is used more than once, the tip radius can easily exceed 20 nm. So using a sharp tip and replacing the tips often are important to obtain an accurate measurements. The measured depths of the holes can not exceed the tip size or the radius of curvature of the hole (meaning that the spheres were embedded more than half way into the surface of the film) both of the order of 10 nm. In order to avoid that, the depth of the holes (controlled by the embedding depths) were chosen to be less than 4 nm in average in all cases. The other parameter that can be important in the measurements are the resolution of the image. If the resolution is chosen so that a hole occupies less than a pixel, one would not expect to obtain the depth accurately. In all measurements the image sizes were chosen to be $5\mu m \times 5\mu m$ or less, and the resolution was chosen to be 500×500 or 1000×1000. Repeated measurements showed that no difference between the measured sizes of the two resolution was seen, confirming that the tip can reach the bottom of the hole properly. The average size of the holes were also confirmed to be equal to the average embedding depth of the gold nano-spheres within the error of the measurements. In order to make more accurate measurements, two scans of each samples were taken, in the forward and backward motion of the X piezo, to eliminate possible errors of depth measurements caused by possible tilt of the tip. Figure 3.12 shows and example of hole measurements along with a line scan of one of the holes and the measurement of the hole depth.

Chapter 4

Summary of the papers and conclusion

Paper I: Effect of Sample Preparation on the Glass-Transition of Thin Polystyrene Films

In this paper the effect of sample preparation on the T_g reduction of thin films of polystyrene was investigated. Multi-layered films of polystyrene were produced with the procedure described in chapter 3. The T_g of these samples were measured using ellipsometry. If the T_g reduction in thin films is caused by chain end segregation, reduced entanglement or the structural damage due to spin coating, it is expected that the T_g of multi-layer films before the annealing of the films, be equal to the T_g of separate layers, while if the T_g reduction is an effect that is related to the total film thickness or the existence of the free surface, the T_g is expected to be equal to the T_g of a film with a thickness equal to the total film thickness.

It was seen that in fact the T_g of multi-layer films reaches a steady state value equal to the T_g of a film with an equal total film thickness after three T_g measurements cycles, equal to only 15 minutes of annealing at $T_g(Bulk) + 20K$. This time is much less than the reptation time of the chains used in this study and it is expected that the structure of these films are not changed after this annealing time. However this annealing time is comparable with the Rouse relaxation time of

the segments, which indicates that it is only enough to heal the interface between the layers. This also shows that the T_g reduction is caused by the free surface of the films.

This result can also provide a reason to believe that the results of the measurement done on multi-layer films, can be directly compared with the properties of single-layer films with a similar total thickness. This provides a possible answer to the contradictory results of Koh *et al.* [74], in which they used stacked free standing films in a calorimetric T_g measurements. If the films were stacked properly without the wrinkles, then the interface would be annealed in less than 15 minutes, and no T_g reductions would have been observed. The fact that a T_g reduction can be observed even after repeated annealing cycles, shows that the voids produced by the wrinkles can not be annealed easily, and even after repeated annealing cycles, the system still has partial available free surface, which causes a partial T_g reduction compared to free standing films that have two complete free surfaces.

Paper II: Qualitative discrepancy between different measures of dynamics in thin polymer films

The results of paper I indicated that the interface healing is important in recovering the expected T_g values in multi-layer thin films. Before the annealing of the samples above bulk T_g the behavior of the interface is similar to a partial free surface. It was also seen that after a short annealing time the effect of the interface disappeared, indicating that the local diffusion of the segments was enough to heal the interface. In this study the interface healing of bi-layer films was used as a probe of local segmental dynamics. Using ellipsometry, the time dependence of interface healing at 393K ($T_g(Bulk) + 20K$) was monitored for films made of two layers with similar thicknesses. The T_g of the bi-layer films were also measured after a long annealing time.

The results of this experiment showed that the relaxation time for bulk-like bi-layer films was comparable to the Rouse relaxation time of polystyrene, and as the film thickness was decreased the relaxation time was increased indicating a slowing down of dynamics in the direction normal to the plane of the film. These

results are similar to the simulation [167] and experimental results of segmental relaxations [120]. The T_g of the same films were reduced below bulk T_g as the film thickness was decreased, which is an indication of enhanced dynamics in the same films. The difference between the results of the two measurements done on the same sample clearly show that different modes of dynamics are not necessarily affected by confinement in the same manner. The enhanced mode of motion which causes the T_g reduction in thin films can only be detected at temperatures close or below bulk T_g. As discussed in Chapter 2 at temperatures above bulk T_g it is expected that the segmental motion be equal or slower than bulk depending on the type of motion probed. This results show that not all type of measurements and probes of dynamics can be interpreted as a reduction or increase in the T_g of thin films.

Paper III: Probing Slow Dynamics in Supported Thin Polymer Films

In this study T_g measurements at different cooling rates were used as a probe of dynamics of thin films below bulk glass transition temperature. The results of T_g measurements at the lowest cooling rate (1K/min) showed a T_g reduction with decreasing film thickness that was about 30K below bulk T_g for the thinnest film measured with $h = 6$ nm. As the cooling rate was increased the T_g reduction effect was less pronounced such that for the cooling rate of 130K/min the maximum T_g reduction measured was less than 10K for the same film. This shows that the enhanced dynamics is strongly dependent on the probed relaxation time. The results were converted to a VFT plot using the results of ref. [9] that the calorimetric cooling rate of 10K/min corresponds to the relaxation time of 100 seconds and that the relaxation time is proportional to the inverse of cooling rate. Figure 4.1 shows the results of this experiment. The solid curve shows the bulk VFT curve for polystyrene. It can be seen that the thin film relaxation deviates strongly from this behavior starting from a common point at a temperature T^*. The data points at high cooling rate are taken from the calorimetric measurement of Ref. [14] for three different film thicknesses. The existence of this common coincidence point at which all Arrhenius curves meet is one of the most surprising results of this experiment. This means that at temperatures above this point ($T^* = 378$K) or frequencies higher than this frequency, dynamical measurements will not indicate
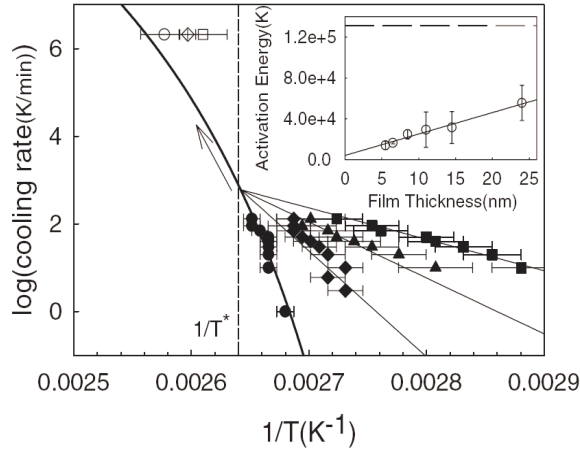
Figure 4.1: The log(cooling rate) vs $1/T$ for 90 ($\bullet$), 24 ($\blacklozenge$), 11 ($\blacktriangle$), and 6 nm ($\blacksquare$) films, along with the bulk VFT curve for PS. The inset shows the plot of activation energy vs film thickness.

the enhanced dynamics that are causing T_g reductions in thin films. Using this a unified picture can be possibly built that explains many of the controversies in the literature. Recent XPCS and Fluorescent measurements [153, 168] also show evidence of this enhanced dynamics as the temperature is decreased towards bulk T_g from above or measurements are done at lower frequencies respectively. The inset of figure 4.1 shows the activation energies at different thicknesses. The dashed line shows the activation energy that is tangent to the VFT curve and corresponds to a film thickness of 61 nm. No confinement effect is expected to be seen at films with thicknesses larger than this thickness.

These results are able to answer some contradictions in the literature. For example the reason why no T_g reductions are seen in calorimetric measurements with large heating/cooling rates is that these measurements are done at frequency/temperatures above the onset of anomalies. The reason for the existence of this point however and the reason why it is so close to the bulk T_g remains unknown and can not easily be explained by common glass transition theories and is not predicted by any simulations in the literature. A theory that predicts the existence of a length scale which increases with decreasing temperature, predicts that as the film thickness

is decreased, the system size will reach this length scale at a higher temperature, so the deviation from bulk behavior should happen at a higher temperature for thinner films. Based on such theories the length scale of cooperative motion is expected to be of the order of a couple of nanometers at T_g. The deviation from bulk behavior seen in thin polystyrene films starts at thicknesses much larger than these predictions and it starts at the same temperature for all film thicknesses. So a different explanation is needed for such behavior. This point will be discussed more in the next study.

Paper IV: Surface dynamics of thin polymer films

In this study the relaxation of surface nano-deformations as made with the procedure introduced in chapter 3, at constant temperatures below bulk T_g of polystyrene was measured. As shown in the previous study the enhanced dynamics is only expected to happen at temperatures close and below bulk T_g. It is then important to design a measurement to probe the surface dynamics at these temperatures to see whether or not a connection can be made between the enhanced surface dynamics and T_g reduction in thin films. It was seen that at all temperatures the time dependence of the annealing of the surface deformations follows a single exponential relaxation rather than the expected stretched exponential relaxation. Using this single exponential annealing of the nano-deformations one can find a relationship between the characteristic relaxation time of the surface and the life time of the annealing. The depth of the holes changes with time with a single exponential time dependence,

$$h = h_0 \exp(-t/\tau) \tag{4.1}$$

and the initial stress on the system is from the surface tension force,

$$\sigma_0 = \frac{2\gamma}{R} \tag{4.2}$$

where R is the radius of curvature of the nano-deformations. One can assume that since the time dependence of the annealing of nano-deformations are single exponential the time dependence in the stress and strain functions can be separated

from the position dependencies,

$$\epsilon_{ij}(x_i, t) = \epsilon_{ij}(x_i) \exp(-t/\tau) \tag{4.3}$$

$$\sigma_{ij}(x_i, t) = \sigma_{ij}(x_i) \exp(-t/\tau) \tag{4.4}$$

It is thus a reasonable estimation to assume that the system has a single exponential relaxation behavior so the creep modulus can be defined as

$$G = G_0 \exp(-t/\tau_\alpha) \tag{4.5}$$

where τ_α is the α-relaxation time of the system or a characteristic relaxation time that is governing the behavior of the system. Ignoring the position dependencies, one can write the time dependence part of the differential equation of the system [5],

$$\frac{1}{\tau_\alpha}\sigma(t) + \frac{d\sigma(t)}{dt} = G_0\epsilon(t) \tag{4.6}$$

Using this equation and the fact that the time dependencies are exponential functions it can be shown that

$$\tau = \tau_\alpha \left(1 + \frac{RG_0}{2\gamma}\right) \tag{4.7}$$

Using this relationship and information in table 3.1 one can find the values of this characteristic relaxation time at different temperatures and it can be seen that the behavior of the surface dynamics deviates strongly from bulk α-relaxation. Figure 4.2 shows the surface relaxation as compared with the bulk α and β relaxations.

The fact that the relaxation behavior suddenly changes from stretched exponential to a single exponential relaxation, also observed in recent viscosity measurements of the surface [153] and the strong deviation from bulk behavior suggest that there is probably either a large change in the α/β relaxations behavior or the present of a new relaxation mechanism near the surface, which becomes faster than bulk α relaxation at this temperature with a weaker temperature dependence compared to the bulk α relaxation.

It is also interesting to compare these results with the results of the T_g measurements at different cooling rate. In order to do that the same relation that was used before to convert the bulk VFT relaxation to a cooling rate plot, can be used
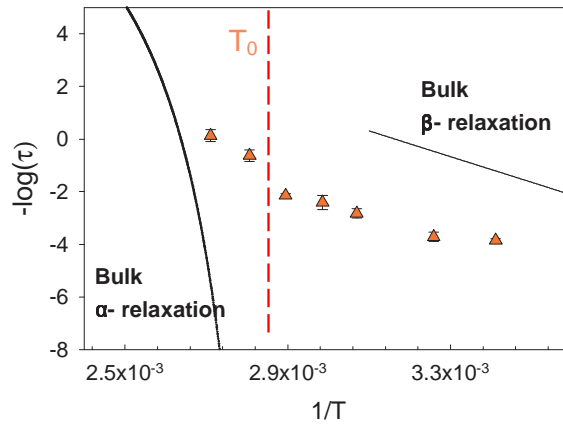
Figure 4.2: The VFT plot of the surface relaxation compared to the bulk α and β relaxations. The dashed line shows the temperature T_0 where the bulk α relaxation is expected to diverge.

for the surface relaxations. Figure 4.3 shows the combined plots of figure 4.1 and 4.2. For simplicity, only the fit to the T_g measurements data is shown as Arrhenius lines. The similarities between the two results obtained from two different types of measurements are compelling. This is a very strong evidence that the T_g reduction in thin films are in fact a direct result of an enhanced relaxation mode near the free surface. This results can also explain the broadening of the transition, as this new relaxation mode in only dominant at $T < T_g(bulk)$. At $T > T_g(bulk)$ the bulk α-relaxation is dominant, thus the expansion coefficient of melt remains similar to the bulk. At temperatures $T < T_g(bulk)$ this new relaxation mode continues down to very low temperature with a much weaker temperature dependence compared to the bulk behavior causing a broadening of the transition, and a reduction in the contrast.

It is really important to note that this mode of relaxation, only happens at temperatures close and below bulk T_g, and it is more enhanced as the temperature is decreased well below bulk T_g. This can provide an answer to most of the questions, concerning the segmental diffusion measurements and calorimetric measurements, which are usually done at temperatures above bulk T_g or high frequencies. It is also possible that some experiments, that are only sensitive to the bulk α relaxation,
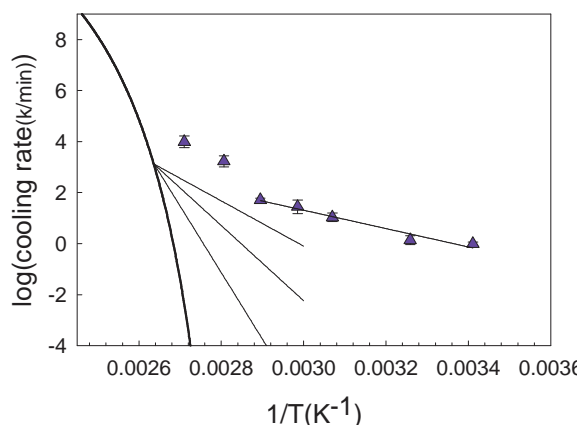
Figure 4.3: The VFT plot of the surface relaxation compared to the thin film T_g measurements.

are not sensitive to this new mode of relaxation, and as a result not sensitive to the enhancement of dynamics in thin polymer films.

The combined results of these four studies can answer some of the questions asked at the end of chapter 2. It is clear that the sample preparation, and the exact structure of thin films are not major cause of anomalies in the dynamics and T_g of surfaces or thin films. There is compelling evidence that the faster relaxation near the free surface are defining the dynamics throughout the rest of the film. It seems that the relaxation of the surface is different from the bulk α-relaxation only at very low temperatures or frequencies, as a result anomalies in the dynamics of thin films are also only seen below the onset of anomalous dynamics, which happens at a temperature only 5K above bulk T_g and a frequency of about 1-10Hz. The segmental dynamics in different directions are not necessarily similar, and not all measurements of dynamics can be used as a probe of T_g in thin films. Because of the existence of this onset of observed anomalies, measurements at temperatures above this point can not be used to interpret the value of the T_g of thin films. Almost all measurements in the literature, depending on the time scale and temperatures used, agree with this picture. In case of polystyrene this seems to be a universal picture that can be used to predict the behavior of the system in the experimental time scale and temperature range. In the few measurements that are not in agreement

with this picture, either there is no free surface, or the free surface is partially covered by other films, or a liquid. The dielectric measurements, show a different behavior, in those measurements there a sharp onset of the enhanced dynamics is not seen [113], but in all those cases the free surface is also covered with Al.

The questions to be answered, which need more careful studies are then the exact nature of this new mode of relaxation and how it changes in different polymeric systems. Answering this question can be the key in understanding the T_g anomalies in thin films. For example it is not clear whether or not the cross over temperature is always this close to bulk T_g or it is just a coincidence which makes the T_g reductions more pronounced in thin polystyrene films compared to other polymers. One can imagine that if this cross over point happens at a temperature below bulk T_g then no anomalies in the T_g measurements will be seen. The important parameters that can affect the observed enhanced dynamics are the position of this point and the activation energy of the surface mode compared to the activation energy of the α relaxation at this cross over temperature. The thickness dependence of the activation energy can also be a key in determining the thickness below which the T_g anomalies can be detected. A clear theory is needed to predict these parameters and also similar measurements using different polymers are needed to be done to confirm the universality of this behavior. There is some evidence in the literature that this behavior might be observed in other molecular glass formers as well [40, 169]. de Gennes theory of sliding motion [79] can perhaps be a good candidate to explain how the effects are propagated into the bulk of the film. It also has potential to explain why the onset of the observed anomalies depends so strongly on the stiffness of the polymer chains used [52]. But this theory would not be complete without a model that explains why this simple activated motion exists near the free surface, and why does it become faster than the bulk α relaxation only at temperatures close or below bulk T_g. It is also important to understand how covering the free surface affects the existence of this new mode of motion near the free surface and why different metals behave differently if put on this free surface.

Another puzzling question in my mind, which may not be that important after all, is that the thickness of about 20 nm seem to be an important thickness in the film dynamics for polystyrene. Below this thickness, the film more behaves like a

single layer [80], while above that a gradual change of the dynamics is expected from the free surface to the bulk of the film. At this thickness the films also partially recover the loss of contrast and broadening of the transition [77] (only observed in free standing films). There is no indication of why this should happen based on the experimental data of paper III. Perhaps any proposed model should also be able to define the importance of this thickness.

Appendix A

Matlab Codes for Ellipsometry

In this appendix you can find the matlab codes necessary to simulate the 6 layer model and fit the model to the experimental data.

The following file initiates the process and defines the constants

```
clear;
global P;
global Pdata;
global L;
global T1;
global n6;
global n5;
global n4;
global n2;
global n1;
global h5;
global rops;
global result;
global k;
global Ro;
```

```
global N3;
k=3000;                  % number of data reading from the file
L=6328;
T1=60*pi/180;           %Angle of incident
n6=3.740-0.019*i;       %Indexes of refraction of the layers
n5=1.460;
n4=1.595;
n2=1.595;
n1=1;
h5=20;
rops=(n2^2-1)/(n2^2+2);      %Lorentz-Lorenz relation
filename='5-5.m';
result=importdata(filename);   % importing the experimental results
```

This is a matlab code which generates the error function for nelder-mid fit.

```
function E=displ(V);
global P;
global Pdata;
global L;
global T1;
global n6;
global n5;
global n4;
global n2;
global n1;
global h5;
global rops;
global result;
```

```
global k;
global Ro;
global N3;
ti=-V(3)/.3;          %vector variable V is defines the fit parameters
Time=V(1);
n3=1.2;
h3=50;
h2in=V(2);
h4in=V(2);
B=.3;                 %The exponent of the stretched exponential
if n3<1
  n3=1;
end
Pdata=result(1:k,2);
roin=(n3^2-1)/(n3^2+2);


% defining the thickness of PS layers and the density of the interface
for j=1:k
  h2=h2in-(rops-roin)/rops*h3/2*(1-exp(-((j-ti)*.3/Time)^B));
  h4=h4in-(rops-roin)/rops*h3/2*(1-exp(-((j-ti)*.3/Time)^B));
  ro=roin+(rops-roin)*(1-exp(-((j-ti)*.3/Time)^B));
  n3=sqrt((2*ro+1)/(1-ro));
  T2=asin(n1*sin(T1)/n2);
  T3=asin(n2*sin(T2)/n3);
  T4=asin(n3*sin(T3)/n4);
  T5=asin(n4*sin(T4)/n5);
  T6=asin(n5*sin(T5)/n6);

%fresnel reflection coefficients for the s and p components of light
  r5p=(n6*cos(T5)-n5*cos(T6))/(n6*cos(T5)+n5*cos(T6));
  r5s=(n5*cos(T5)-n6*cos(T6))/(n5*cos(T5)+n6*cos(T6));
  r4p=(n5*cos(T4)-n4*cos(T5))/(n5*cos(T4)+n4*cos(T5));
  r4s=(n4*cos(T4)-n5*cos(T5))/(n4*cos(T4)+n5*cos(T5));
```

```
r3p=(n4*cos(T3)-n3*cos(T4))/(n4*cos(T3)+n3*cos(T4));
r3s=(n3*cos(T3)-n4*cos(T4))/(n3*cos(T3)+n4*cos(T4));
r2p=(n3*cos(T2)-n2*cos(T3))/(n3*cos(T2)+n2*cos(T3));
r2s=(n2*cos(T2)-n3*cos(T3))/(n2*cos(T2)+n3*cos(T3));
r1p=(n2*cos(T1)-n1*cos(T2))/(n2*cos(T1)+n1*cos(T2));
r1s=(n1*cos(T1)-n2*cos(T2))/(n1*cos(T1)+n2*cos(T2));

%the reflection coefficients for oxide layer
E=exp(-4*pi*i*h5*n5*cos(T5)/L);
R4p=(r4p+r5p*E)/(1+r4p*r5p*E);
R4s=(r4s+r5s*E)/(1+r4s*r5s*E);

%the reflection coefficients for the first PS film
E=exp(-4*pi*i*h4*n4*cos(T4)/L);
R3p=(r3p+R4p*E)/(1+r3p*R4p*E);
R3s=(r3s+R4s*E)/(1+r3s*R4s*E);

%the reflection coefficients for interface
E=exp(-4*pi*i*h3*n3*cos(T3)/L);
R2p=(r2p+R3p*E)/(1+r2p*R3p*E);
R2s=(r2s+R3s*E)/(1+r2s*R3s*E);

%the reflection coefficients for the second PS film
E=exp(-4*pi*i*h2*n2*cos(T2)/L);
R1p=(r1p+R2p*E)/(1+r1p*R2p*E);
R1s=(r1s+R2s*E)/(1+r1s*R2s*E);

% finding P and A
Psi=atan(abs(R1p/R1s))*180/pi;
D=atan(imag(R1p/R1s)/real(R1p/R1s))*180/pi;
if (real(R1p/R1s) < 0.0)
  D=D+180;
elseif (imag(R1p/R1s) < 0.0)
```

```
    D=D+360;
  T(j)=j*.3;
  P(j)=D/2-45;
  error(j)=(P(j)-Pdata(j))^2;
end;
plot(T,P(1:k),T,Pdata(1:k));
E=sum(error);
```

Bibliography

[1] G. R. Strobl, "*The Physics of Polymers: concepts for understanding their structures and behavior*", Springer, (1996).

[2] M. Rubinstein, and R. Colby, "*Polymer Physics*", Oxford University Press, (2003).

[3] D. S. Pearson, G. Ver Strate, E. von Meerwall, and F. C. Schillingld, "*Viscosity and Self-Diffusion Coefficient of Linear Polyethylene*", Macromolecules **20**, 1133-1141 (1987).

[4] M. Doi, and S. F. Edwards, "*The Theory of Polymer Dynamics*", Oxford University Press, (1986).

[5] R. M. Christensen, "*Theory of Viscoelasticity*", Academic Press, New York and London, 1971.

[6] P. W. Anderson, "*Through the Glass Lightly*", Science **267**, 1615 (1995).

[7] P. G. Debenedetti, and F. H. Stillinger, "*Supercooled liquids and the glass transition*", Nature **410**, 259-267 (2001).

[8] M. D. Ediger, C. A. Angell, and S. R. Nagel, "*Supercooled Liquids and Glasses*", J. Phys. Chem. **100**, 13200-13212 (1996).

[9] C. M. Roland, and R. Casalini, "*Temperature dependence of local segmental motion in polystyrene and its variation with molecular weight*", J. Chem. Phys. **119**, 1838-1842 (2003).

[10] E Donth, "*The Glass Transition relaxation dynamics in liquids and disordered materials*", Springer, (2001).

[11] D. Kivelson, S. A. Kivelson, X. Zhao, Z. Nussinov, and G. Tarjus, "*A thermodynamic theory of supercooled liquids*", Physica A. **219**, 27-38 (1995).

[12] G. P. Johari, and M. Goldstein, "*Viscous liquids and the glass transition, III secondary relaxation in aliphatic alcohols and other nonrigid molecules*", J. Chem. Phys. **55**, 4245-4252 (1971).

[13] K. L. Ngai, A. K. Rizos, and D. J. Plazek, "*Reduction of the glass temperature of thin freely standing polymer films caused by the decrease of the coupling parameter in the coupling model*", Journal of Non-Crystalline Solids **235-237**, 435-443 (1998).

[14] C. T. Thurau, and M. D. Ediger, "*Influence of spatially heterogeneous dynamics on physical aging of polystyrene*", J. Chem. Phys. **116**, 9089-9099 (2002).

[15] C. T. Thurau, and M. D. Ediger, "*Change in the temperature dependence of segmental dynamics in deeply supercooled polycarbonate*", J. Chem. Phys. **118**, 1996-2004 (2003).

[16] G. Adam, and J. H. Gibbs, "*On the temperature dependance of cooperative relaxation properties in glass-forming liquids*", J. Chem. Phys. **43**, 139-146 (1965).

[17] W. K. Kegel, and A. van Blaaderen, "*Direct Observation of Dynamical Heterogeneities in Colloidal Hard-Sphere Suspensions*", Science **287**, 290-293 (2000).

[18] M. D. Ediger, "*Movies of the Glass Transition*", Science **287**, 604-605 (2000).

[19] M. D. Ediger, and J. L. Skinner, "*Single Molecules Rock, and Roll Near the Glass Transition*", Science **292**, 233-234 (2001).

[20] S. F. Swallen, M. K. Mapes, Y. S. Kim, R. J. McMahon, and M. D. Ediger, "*Neutron reflectivity measurements of the translational motion of tris(naphthylbenzene) at the glass transition temperature*", J. Chem. Phys. **124**, 184501 (2006).

[21] S. C. Glotzer, "*Spatially heterogeneous dynamics in liquids: insights from simulation*", J. Non-Crys. Solids **274**, 342-355 (2000).

[22] C. A. Angell, K. L. Ngai, G. B. McKenna, P. F. McMillan, and S. W. Martin, "*Relaxation in glassforming liquids and amorphous solids*", J. Appl. Phys. **88**, 3113-3157 (2000).

[23] M. H. Cohen, and D Turnbull, J. Cbem. Pbys. **31**, 1164 (1959).

[24] J. Jäckle, "*Models of the glass transition*", Rep. Prog. Phys. **49**, 171-231 (1986).

[25] M. D. Ediger, "*Spatially Heterogeneous Dynamics in Supercooled Dynamics*", Annu. Rev. Phys. Chem. **51**, 99-128 (2000).

[26] E. A. DiMarzio, and A. J. M. Yang, "*Configurational entropy approach to the kinetics of glasses*", Journal of Research of the National Institute of Standards and Technology **102**, 135-157 (1997).

[27] P. A. O'Connell, and G. B. McKenna, "*Arrhenius-type temperature dependence of the segmental relaxation below Tg*", J. Chem. Phys. **110**, 11054-11060 (1999).

[28] S. F. Edwards, and K. E. Evans, "*Dynamics of Highly Entangled Rod-Like Molecules*", J. Chem. Soc. Faraday Trans. **78**, 113-121 (1982).

[29] S. F. Edwards, and Th. Vilgis, "*The dynamic of glass transition*", Physica Scripta **T13**, 7-16 (1986).

[30] S. F. Edwards, "*The glass transition in polymers*", Polymer **35**, 3827-3830 (1994).

[31] E. R. Weeks, J. C. Crocker, A. C. Levitt, A. Schofield, and D. A. Weitz, "*Three-Dimensional Direct Imaging of Structural Relaxation Near the Colloidal Glass Transition*", Science **287**, 627-631 (2000).

[32] W. Götze, and L. Sjögren, "*Logarithmic decay laws in glassy systems*", J. Phys.: Condens. Matter **1**, 4203-4222 (1989).

[33] G. Tarjus, D. Kivelson, and P. Viot, "*The viscous slowing down of super-cooled luquids as a temperature-controlled super-Arahenius activated process: a description in terms of frustration-limited domains*", J. Phys.:Condens. Matter **12**, 6497-6508 (2000).

[34] P. Viot, G. Tarjus, and D. Kivelson, "*A heterogeneous picture of a relaxation for fragile supercooled liquids*", J. Chem. Phys. **112**, 10368-10378 (2000).

[35] C. L. Jackson, and G. B. McKenna, "*The glass transition of organic liquids confined to small pores*", Journal of Non-Crystalline Solids **131-133**, 221-224 (1991).

[36] J. Schüller, Yu. B. Mel'nichenko, R. Richert, and E. W. Fischer, "*Dielectric studies of glass transition in porous media*", Phys. Rev. Lett. **73**, 2224-2227 (1993).

[37] P. Pissis, D. Daoukaki-Diamanti, L. Apekis, and C. Christodoulides, "*The glass transition in confined liquids*", J. Phys.: Condens. Matter **6**, L325-L328 (1994).

[38] R. Richert, and M. Yang, "*Solvation dynamics of molecular glass-forming liquids in confinement*", J. Phys.: Condens. Matter **15**, S1041-S1050 (2003).

[39] S. L. Simon, J. -Y. Park, and G. B. McKenna, "*Enthalpy recovery of a glass-forming liquid constrained in a nanoporous matrix: Negative pressure effects*", Eur. Phys. J. E. **8**, 209-216 (2002).

[40] M. Arndt, R. Stannarius, H. Groothues, E. Hempel, and F. Kremer, "*Length scale of cooperativity in the dynamic glass transition*", Phys. Rev. Lett. **79**, 2077-2080 (1997).

[41] A. Schönhals, H. Goering, Ch. Schick, B. Frick, and R. Zorn, "*Glassy dynamics of polymers confined to nanoporous glasses revealed by relaxational and scattering experiments*", Eur. Phys. J. E. **12**, 173-178 (2003).

[42] . Schönhals, H. Goering, Ch. Schick, B. Frick, and R. Zorn, "*Polymers in nanoconfinement: What can be learned from relaxation and scattering experiments*", Journal of Non-Crystalline Solids **351**, 2668-2677 (2005).

[43] T. Sasaki, A. Shimizu, T. H. Mourey, C. T. Thurau, and M. D. Ediger, "*Glass transition of small polystyrene spheres in aqueous suspensions*", J. Chem. Phys. **119**, 8730-8735 (2003).

[44] P. Scheidler, W. Kob, and K. Binder, "*The relaxation dynamics of a simple glass former confined in a pore*", Europhys. Lett. **52**, 277-283 (2000).

[45] L. Wang, F. He, and R. Richert, "*Intramicellar Glass Transition and Liquid Dynamics in Soft Confinement*", Phys. Rev. Lett. **92**, 095701 (2004).

[46] M. S. Wilson, and S. Gottesfeld, "*Thin-film catalyst layers for fuel cell electrodes polymer electrolyte*", J. Applied Electrochemistry **22**, 1-7 (1992).

[47] P. C. Beard, and T. N. Mills, "*Extrinsic optical-fiber ultrasound sensor using a thin polymer film as a low-finesse Fabry-Perot interferometer*", Applied Optics **35**, 663-675 (1996).

[48] V. Maquet, D. Martin, B. Malgrange, R. Franzen, J. Schoenen, G. Moonen, and R. Jérôme, "*Peripheral nerve regeneration using bioresorbable macroporous polylactide scaffolds*", Journal of Biomedical Materials Research **52**, 639-651 (2000).

[49] R. W. Jaszewski, H. Schift, B. Schnyder, A. Schneuwly, and P. Groning, "*The deposition of anti-adhesive ultra-thin teflon-like films and their interaction with polymers during hot embossing*", Applied Surface Science **143**, 301-308 (1999).

[50] H. C. Scheer, and H. Schulz, "*A contribution to the flow behaviour of thin polymer films during hot embossing lithography*", Microelectronic Engineering **56**, 311-332 (2001).

[51] J. L. Keddie, R. A. L. Jones, and R. A. Cory, "*Size-dependent depression of the glass transition temperature in polymer films*", Europhys. Lett. **27**, 59-64 (1994).

[52] C. J. Ellison, M. K. Mundra and J. M. Torkelson, *"Impacts of Polystyrene Molecular Weight and Modification to the Repeat Unit Structure on the Glass Transition-Nanoconfinement Effect and the Cooperativity Length Scale"*, Macromolecules **38**, 1767-1778 (2005).

[53] G. B. DeMaggio, W. E. Frieze, D. W. Gidley, M. Zhu, H. A. Hristov, and A. F. Yee, *"Interface and Surface Effects on the Glass Transition in Thin Polystyrene Films"*, Phys. Rev. Lett. **78**, 1524-1527 (1994).

[54] J. S. Sharp, and J. A. Forrest, *"Free Surfaces Cause Reductions in the GlassTransition Temperature of Thin Polystyrene Films"*, Phys. Rev. Lett. **91**, 235701 (2003).

[55] J. S. Sharp, and J. A. Forrest, *"Dielectric and ellipsometric studies of the dynamics in thin films of isotactic poly(methylmethacrylate) with one free surface"*, Phys. Rev. E. **67**, 031805 (2003).

[56] J. S. Sharp, and J. A. Forrest, *"Thickness dependence of the dynamics in thin films of isotactic poly(methylmethacrylate)"*, Eur. Phys. J. E. **12**, S97-S101 (2003).

[57] D. S. Fryer, P. F. Nealey, and J. J. de Pablo, *"Thermal Probe Measurements of the Glass Transition Temperature for Ultrathin Polymer Films as a Function of Thickness"*, Macromolecules **33**, 6439-6447 (2000).

[58] Y. Grohens, L. Hamon, G. Reiter, A. Soldera, and Y. Holl, *"Some relevant parameters affecting the glass transition of supported ultra-thin polymer films"*, Eur. Phys. J. E. **8**, 217-224 (2002).

[59] L. Singh, P. J. Ludovice, and C. L. Henderson, *"Influence of molecular weight and film thickness on the glass transition temperature and coefficient of thermal expansion of supported ultrathin polymer films"*, Thin Solid Films **449**, 231-241 (2004).

[60] Y. C. Jean, R. Zhang, H. Cao, J. Yuan, C. Huang, B. Nielsen, and P. Asoka-Kumar, *"Glass transition of polystyrene near the surface studied by slow-positron-annihilation spectroscopy"*, Phys. Rev. B. **56**, R8459-R8462 (1997).

[61] R. Seemann, K. Jacobs, S. Herminghaus, and K. Landfester, "*Freezing of polymer thin films and surfaces: The small molecular weight puzzle*", Journal of Polymer Science: Part B: Polymer Physics **44**, 2968-2979 (2006).

[62] J. A. Forrest, and K. Dalnoki-Veress, "*The glass transition in thin polymer films*", Advances in Colloid and Interface Science **94**, 167-196 (2001).

[63] H. R. Brown, and T. P. Russell, "*Entanglements at Polymer Surfaces and Interfaces*", Macromolecules **29**, 798-800 (1996).

[64] A. M. Mayes, "*Glass Transition of Amorphous Polymer Surfaces*", Macromolecules **27**, 3114-3115 (1994).

[65] G. Reiter, and P. G. de Gennes, "*Spin-cast, thin, glassy polymer films: Highly metastable forms of matter*", Eur. Phys. J. E. **6**, 25-28 (2001).

[66] W. J. Orts, J. H. van Zanten, and S. K. Satija, "*Observation of temperature dependant thickness in ultrathin polystyrene films on silicon*", Phys. Rev. Lett. **71**, 867-870 (1993).

[67] A. Serghei, H. Huth, M. Schellenberger, C. Schick, and F. Kremer, "*Pattern formation in thin polystyrene films induced by an enhanced mobility in ambient air*", Phys. Rev. E. **71**, 061801 (2005).

[68] P. Bernazzani, S. L. Simon, and K. L. Ngai, "*Effects of entanglement concentration on T_g and local segmental motions*", Eur. Phys. J. E. **8**, 201-207 (2002).

[69] S. L. Simon, P. Bernazzani, and G.B. McKenna, "*Effects of freeze-drying on the glass temperature of cyclic polystyrenes*", Polymer **44**, 8025-8032 (2003).

[70] W. E. Wallace, N. C. Beck Tan, W. L. Wu, and S. Satija, "*Mass density of polystyrene thin films measured by twin neutron reflectivity*", J. Chem. Phys. **108**, 3798-3804 (1998).

[71] J. A. Forrest, K. Dalnoki-Veress, and J. R. Dutcher, "*Brillouin light scattering studies of the mechanical properties of thin freely standing polystyrene films*", Phys. Rev. E. **58**, 6109-6114 (1998).

[72] J. Q. Pham, and P. F. Green, "*The glass transition of thin film polymer-polymer blends: Interfacial interactions and confinement*", J. Chem. Phys. **116**, 5801-5806 (2002).

[73] P. Rittigstein, and J. M. Torkelson, "*Polymer-Nanoparticle Interfacial Interactions in Polymer Nanocomposites: Confinement Effects on Glass Transition Temperature and Suppression of Physical Aging*", Journal of Polymer Science: Part B: Polymer Physics, **44**, 2935-2943 (2006).

[74] Y. P. Koh, G. B. McKenna, and S. L. Simon, "*Calorimetric Glass Transition Temperature and Absolute Heat Capacity of Polystyrene Ultrathin Films*", Journal of Polymer Science: Part B: Polymer Physics **44**, 3518-3527 (2006).

[75] J. A. Forrest, K. Dalnoki-Veress, and J. R. Dutcher, "*Interface and chain confinement effects on the glass transition temperature of thin polymer films*", Phys. Rev. E. **56**, 5705-5716 (1997).

[76] J. A. Forrest, and J. Mattsson, "*Reductions of the glass transition temperature in thin polymer films: Probing the length scale of cooperative dynamics*", Phys. Rev. E. **61**, R53-R56 (2000).

[77] J. Mattsson, J. A. Forrest, and L. Börjesson, "*Quantifying glass transition behavior in ultrathin free-standing polymer films*", Phys. Rev. E. **62**, 5187-5200 (2000).

[78] K. Dalnoli-Veress, J. A. Forrest, C. Murray, C. Gigault, and J. R. Dutcher, "*Moleclar weight dependence of reduction in the glass transition temperature of thin freely standing polymer films*", Phys. Rev. E. **63**, 031801 (2001).

[79] P. G. deGennes, "*Glass transition in thin polymer films*", Eur. Phys. J. E. **2**, 201-205 (2000).

[80] C. J. Ellison, and J. M. Torkelson, "*The distribution of glass-transition temperatures in nanoscopically confined glass formers*", Nature Materials **2**, 695-700 (2003).

[81] R. D. Priestley, L. J. Broadbelt, and J. M. Torkelson, *"Physical Aging of Ultrathin Polymer Films above and below the Bulk Glass Transition Temperature: Effects of Attractive vs Neutral Polymer-Substrate Interactions Measured by Fluorescence"*, Macromolecules **38**, 654-657 (2005).

[82] R. D. Priestley, C. J. Ellison, L. J. Broadbelt, and J. M. Torkelson, *"Structural Relaxation of Polymer Glasses at Surfaces, Interfaces, and In Between"*, Science **309**, 456-459 (2005)

[83] T. Miyazaki, K. Nishida, and T. Kanaya, *"Thermal expansion behavior of ultrathin polymer films supported on silicon substrate"*, Phys. Rev E. **69**, 061803 (2004).

[84] M. Yu. Efremov, E. A. Olson, M. Zhang, Z. Zhang and L. H. Allen, *"Glass Transition in Ultrathin Polymer Films: Calorimetric Study"*,Phys. Rev. Lett. **91**, 085703 (2003).

[85] M. Y. Efremov, E. A. Olson, M. Zhang, Z. Zhang, and L. H. Allen, *"Probing Glass Transition of Ultrathin Polymer Films at a Time Scale of Seconds Using Fast Differential Scanning Calorimetry"*, Macromolecules **37**, 4607-4616 (2004).

[86] H. Huth, A. A. Minakov, and C. Schick, *"Differential AC-Chip Calorimeter for Glass Transition Measurements in Ultrathin Films"*, Journal of Polymer Science: Part B: Polymer Physics **44**, 2996-3005 (2006).

[87] E. Donth, *"Characteristic length of the Glass Transition"*, Journal of Polymer Science: Part B: Polymer Physics **34**, 2881-2892 (1996).

[88] D. Long, and F. Lequeux, *"Heterogeneous dynamics at the glass transition in van der Waals liquids, in the bulk and in thin films"*, Eur. Phys. J. E. **4**, 371-387 (2001).

[89] S. Herminghaus, K. Jacobs, and R. Seemann, *"The glass transition of thin polymer films: some questions, and a possible answer"*, Eur. Phys. J. E. **5**, 531-538 (2001).

[90] S. Herminghaus, "*Polymer thin films and surfaces: Possible effects of capillary waves*", Eur. Phys. J. E. **8**, 237-243 (2002).

[91] S. Herminghaus, K. Jacobs, and R. Seemann, "*Viscoelastic dynamics of polymer thin films and surfaces*", Eur. Phys. J. E. **12**, 101-110 (2003).

[92] S. Herminghaus, R. Seemann, and K. Landfester, "*Polymer Surface Melting Mediated by Capillary Waves*", Phys. Rev. Lett. **93**, 017801 (2004).

[93] K. L. Ngai, "*Mobility in thin polymer films ranging from local segmental motion, Rouse modes to whole chain motion: A coupling model consideration*", Eur. Phys. J. E. **8**, 225-235 (2002).

[94] K. L. Ngai, "*The effects of changes of intermolecular coupling on glass transition dynamics in polymer thin films and glass-formers confined in nanometer pores*", Eur. Phys. J. E. **12**, 93-100 (2003).

[95] K. L. Ngai, "*Interpreting the Dynamics of Nano-Confined Glass- Formers and Thin Polymer Films: Importance of Starting from a Viable Theory for the Bulk*", Journal of Polymer Science: Part B: Polymer Physics **44**, 2980-2995 (2006).

[96] J.D. McCoy, and J. G. Curro, "*Conjectures on the glass transition of polymers in confined geometries*", J. Chem. Phys. **116**, 9154-9157 (2002).

[97] T. M. Truskett, and V. Ganesan, "*Ideal glass transitions in thin films: An energy landscape perspective*", J. Chem. Phys. **119,** 1897-1900 (2003).

[98] J. Jäckle, "*Models of molecular cooperativity in liquids near the glass transition*", Progress of Theoretical Physics supplement **126**, 53-60 (1997).

[99] C. Donati, and J. Jäckle, "*The characteristic length of cooperativity derived from dynamic size effects in a lattice gas*", J. Phys.: Condens. Matter **8**, 2733-2740 (1996).

[100] J. Jäckle, "*Models of cooperative diffusion*", J. Phys.: Condens. Matter **14**, 1423-1436 (2002).

[101] K. Binder, J. Baschnagel, C. Bennemann, and W. Paul, *"Monte Carlo and molecular dynamics simulation of the glass transition of polymers"*, J. Phys.:Condens. Matter **11**, A47-A55 (1999).

[102] F. Varnik, J. Baschnagel, and K. Binder, *"Reduction of the glass transition temperature in polymer films: A molecular-dynamics study"*, Phys. Rev. E. **65**, 021507 (2002).

[103] S. Peter, H. Meyer, and J. Baschnagel, *"Thickness-Dependent Reduction of the Glass-Transition Temperature in Thin Polymer Films with a Free Surface"*, Journal of Polymer Science: Part B: Polymer Physics **44**, 2951-2967 (2006).

[104] J. A. Torres, P. F. Nealey, and J. J. de Pablo, *"Molecular Simulation of Ultrathin Polymeric Films near the Glass Transition"*, Phys. Rev. Lett. **85**, 3221-3224 (2000).

[105] S. Butler, and P. Harrowell, *"Glassy relaxation at surfaces: The correlation length of cooperative motion in the facilitated kinetic lsing model"*, J. Chem. Phys. **95**, 4466-4470 (1991).

[106] J. Baschnagel, and F. Varnik, *"Computer simulations of supercooled polymer melts in the bulk and in confined geometry"*, J. Phys.: Condens. Matter **17**, R851-R953 (2005).

[107] H. Kim, A. Rühm, L. B. Lurio, J. K. Basu, J. Lal, S. G. J. Mochrie, and S. K. Sinha, *"X-ray photon correlation spectroscopy on polymer films with molecular weight dependence"*, Physica B. **336**, 211-215 (2003).

[108] H. Kim, A. Rühm, L. B. Lurio, J. K. Basu, J. Lal, D. Lumma, S. G. J. Mochrie, and S. K. Sinha, *"Surface dynamics of polymer films"*, Phys. Rev. Lett. **90**, 068302 (2003).

[109] H. Kim, A. Rühm, L. B. Lurio, J. K. Basu, J. Lal, S. G. Mochrie, and S. K. Sinha, *"Synchrotron radiation sudies of the dynamics of polymer films"*, J. Phys.:Cond. Matt. **16**, S3491-S3497 (2004).

[110] J. Erichsen, K. Dolgner, V. Zaporojtchenko, and F. Faupel, "*Glass transition temperature in thin polymer films determined by thermal discharge in X-ray photoelectron spectroscopy*", Macromolecules **37**, 8813-8815 (2004).

[111] J. A. Forrest, C. Svanberg, K. Révész, M. Rodahl, L. M. Torell, and B. Kasemo, "*Relaxation dynamics in ultrathin polymer films*", Phys. Rev. E. **58**, R1226-R1229 (1998).

[112] L. Hartmann, W. Gorbatschow, J. Hauwede, and F. Kremer, "*Molecular dynamics in thin films of isotactic poly(methyl methacrylate)*", Eur. Phys. J. E. **8**, 145-154 (2002).

[113] K. Fukao, S. Uno, Y. Miyamoto, A. Hoshino, and H. Miyaji, "*Dynamics of α and β processes in thin polymer films: Poly(vinyl acetate) and poly(methyl methacrylate)*", Phys. Rev. E. **64**, 051807 (2001).

[114] K. Fukao, and Y. Miyamoto, "*Slow dynamics near glass transition in thin polymer films*", Phys. Rev. E. **64**, 011803 (2001).

[115] A. Serghei, L. Hartmann, F. Kremer, "*Molecular dynamics in thin films of isotactic poly(methylmethacrylate) - revisited*", To appear on Journal of Non-Crystalline Solids, (2007).

[116] S. Rivillon, P. Auroy, and B. Deloche, "*Chain Segment Order in Polymer Thin Films on a Nonadsorbing Surface: A NMR Study*", Phys. Rev. Lett. **84**, 499-502 (2000).

[117] R. L. Jones, S. K. Kumar, D. L. Ho, R. M. Briber, and T. P. Russell, "*Chain conformation in ultrathin polymer*", Nature **400**, 146-149 (1999).

[118] R. L. Jones, S. K. Kumar, D. L. Ho, R. M. Briber, and T. P. Russell, "*Chain Conformation in Ultrathin Polymer Films Using Small-Angle Neutron Scattering*", Macromolecules **34**, 559-567 (2001).

[119] K. C. Tseng, N. J. Turro, and C. J. Durning, "*Molecular mobility in polymer thin films*", Phys. Rev. E. **61**, 1800-1810 (2000).

[120] K. Kojio, S. Jeon, and S. Granick, "*Confinement-induced differences between dielectric normal modes and segmental modes of an ion-conducting polymer*", Eur. Phys. J. E. **8**, 167-173 (2002).

[121] D. B. Hall, J. C. Hooker, and J. M. Torkelson, "*Ultrathin Polymer Films near the Glass Transition: Effect on the Distribution of α-Relaxation Times As Measured by Second Harmonic Generation*", Macromolecules **30**, 667-669 (1997).

[122] D. B. Hall, R. D. Miller, and J. M. Torkelson, "*Molecular Probe Techniques for Studying Diffusion and Relaxation in Thin and Ultrathin Polymer Films*", Journal of Polymer Science: Part B: Polymer Physics **35**, 2795-2802 (1997).

[123] X. Zheng, B. B. Sauer, J. G. Van Alsten, S. A. Schwarz, M. H. Rafailovich, J. Sokolov, and M. Rubinstein, "*Reptation dynamics of polymer melt near an attractive solid interface*", Phys. Rev. Lett. **74**, 407-410 (1995).

[124] X. Zheng, M. H. Rafailovich, J. Sokolov, Y. Strzhemechny, S. A. Schwarz, B. B. Sauer, and M. Rubinstein, "*Long-Range effects of polymer diffusion induced by a bounding interface*", Phys. Rev. Lett. **79**, 241-244 (1997).

[125] P. A. O'Connell, and G. B. McKenna, "*Dramatic stiffening of ultrathin polymer films in the rubbery regime*", Eur. Phys. J. E. **20**, 143-150 (2006).

[126] P. A. O'Connell, and G. B. McKenna, "*Rheological measurements of the thermoviscoelastic response of ultrathin polymer films*", Science **307**, 1760-1763 (2005).

[127] G. F. Meyers, B. M. DeKoven, and J. T. Seitz, "*Is the Molecular Surface of Polystyrene Really Glassy?*", Langmuir **8**, 2330-2335 (1992).

[128] S. Ge, Y. Pu, W. Zhang, M. Rafailovich, J. Sokolov, C. Buenviaje, R. Buckmster, and R. M. Overney, "*Shear Modulation Force Microscopy study of near surface glass transition temperature*", Phys. Rev. Lett. **85**, 2340-2343 (2000).

[129] Y. Pu, S. Ge, M. Rafailovich, J. Sokolov, Y. Duan, E. Pearce, V.Zaitsev, and S. Schwarz, "*Surface Transitions by shear modulation force microscopy*", Langmuir **17**, 5865-5871 (2001).

[130] T. Kajiyama, K. Tanaka, N. Satomi, and A. Takahara, "*Surface glass transition temperatures of monodisperse polystyrene films by scanning force microscopy*", Sci. and Tech. of Adv. Materials **1**, 31-35 (2000).

[131] K. Tanaka, A. Takahara, and T. Kajiyama, "*Rheological Analysis of Surface Relaxation Process of Monodisperse Polystyrene Films*", Macromolecules **33**, 7588-7593 (2000).

[132] H. Morita, K. Tanaka, T. Kajiyama, T. Nishi, and M. Doi, "*Study of the Glass Transition Temperature of Polymer Surface by Coarse-Grained Molecular Dynamics Simulation*", Macromolecules **39**, 6233-6237 (2006).

[133] J. A. Hammerschmidt, W. L. Gladfelter, and G. Haugstad, "*Probing Polymer Viscoelastic Relaxations with Temperature-Controlled Friction Force Microscopy*", Macromolecules **32**, 3360-3367 (1999).

[134] H. Fischer, "*Thermal probe surface treatment of a bulk polymer: Does a surface layer with a lower glass transition than the bulk exist?*", Macromolecules **35**, 3592-3595 (2002).

[135] M. G. Samant, J. Stöhr, H. R. Brown, T. P. Russell, J. M. Sands, and S. K. Kumar, "*NEXAFS Studies on the Surface Orientation of Buffed Polyimides*", Macromolecules **29**, 8334-8342 (1996).

[136] Y. Liu, T. P. Russell, M. G. Smant, J. Stöhr, H. R. Brown, A. Cossy-Favre, and J. Diaz, "*Surface relaxation in polymers*", Macromolecules **30**, 7768-7771 (1997).

[137] D. M. G. Agra, A. D. Schwab, J.-H. Kim, S. Kumar, and A. Dhinojwala, "*Relaxation dynamics of rubbed polystyrene thin films*", Europhys. Lett. **51**, 655-660 (2000).

[138] A. D. Schwab, and A. Dhinojwala, "*Relaxation of a rubbed polystyrene surface*", Phys. Rev. E. **67**, 021802 (2003).

[139] T. Kerle, Z. Lin, H. C. Kim, and T. P. Russell, "*Mobility of polymers at the air/polymer interface*", Macromolecules **34**, 3484-3492 (2001).

[140] E. Buck, K. Petersen, M. Hund, G. Krausch, and D. Johannsmann, "*Decay kinetics of nanoscale corrugation gratings on polymer surface: Evidence for polymer flow below the glass temperature*", Macromolecules **37**, 8647-8652 (2004).

[141] P. Gasemjit, and D. Johannsmann, "*Thickness of the Soft Layer on Glassy Polystyrene Surfaces*", Journal of Polymer Science: Part B: Polymer Physics **44**, 3031-3036 (2006).

[142] E. H. Lee, and J. R. M. Radok, "*The Contact Problem for Viscoelastic Bodies*", J. Appl. Mech. T. ASME **27**, 438-444 (1960).

[143] B. Du, O. K. C. Tsui, Q. Zhang, and T. He, "*Study of Elastic Modulus and Yield Strength of Polymer Thin Films Using Atomic Force Microscopy*", Langmuir **17**, 3286-3291 (2001).

[144] R. Weber, K. M. Zimmermann, M. Tolan, J. Stettner, W. Press, O. H. Seeck, J. Erichsen, V. Zaporojtchenko, T. Strunskus, and F. Faupel, "*X-ray reflectivity study on the surface and bulk glass transition of polystyrene*", Phys. Rev. E. **64**, 061508 (2001).

[145] V. M. Rudoy, O. V. Dementeva, I. V. Yaminskii, V. M. Sukhov, M. E. Kartseva, and V. A. Ogarev, "*Metal Nanoparticles on Polymer Surfaces: 1. A New Method of Determining Glass Transition Temperature of the Surface Layer*", Colloid Journal **64**, 746-754 (2002).

[146] J. H. Teichroeb, and J. A. Forrest, "*Direct Imaging of Nanoparticle Embedding to Probe Viscoelasticity of Polymer Surfaces*", Phys. Rev. Lett. **91**, 016104 (2003).

[147] S. A. Hutcheson, and G. B. McKenna, *"Nanosphere embedding into polymer surface: A viscoelastic contact mechanics analysis"*, Phys. Rev. Lett. **94**, 076103 (2005).

[148] J. S. Sharp, J. H. Teichroeb, and J. A. Forrest, *"The properties of free polymer surfaces and their influence on the glass transition temperature of thin polystyrene films"*, Eur. Phys. J. E. **15**, 473-487 (2004).

[149] J. S. Sharp, J. A. Forrest, Z. Fakhraai, M. Khomenko, J. H. Teichroeb, and K. Dalnoki-Veress, *"Reply to comment on 'the properties of free polymer surfaces and their effect upon the glass transition temperature of thin polystyrene films' by S. A. Hutchesn, and G. B. McKenna"*, To appear on Eur. Phys. J. E. (2007).

[150] R. M. Papaléo, L. D. de Oliveira, L. S. Farenzena, M. A. de Araújo, and R. P. Livi, *"Probing thermomechnical behavior of polymers at the nanometer scale with single-ion bomardment and scanning force microscopy"*, Phys. Rev. B. **62**, 11273-11276 (2000).

[151] L. S. Farenzena, R. P. Livi, M. A. de Araújo, G. G. Bermudez, and R. M. Papaléo, *"Cratering and plastic deformation in polystyrene induced by MeV heavy ions: Dependence on the molecular weight"*, Phys. Rev. B. **63**, 104108 (2001).

[152] R. M. Papaléo, R. Leal, W. H. Carreira, L. G. Barbosa, L. Bello, and A. Bulla, *"Relaxation times of nanoscale deformations on the surface of a polymer thin film near and below the glass transition"*, Phys. Rev. B. **74**, 094203 (2006).

[153] Z. Jiang, M. Mudkhopadhyay, S. Sinha, S. Song, H. Kim, and L. Lurio, *"Anomalous surfce dynamics near T_g in supported polystyrene films by XPCS"*, Apstract of papers submitted to the MAR07 Meeting of the American Physical Society, (2007).

[154] http://www.tennoji-h.oku.ed.jp/tennoji/oka/2004/polystyrene-iso-b.gif

[155] http://www.polymersource.com/

[156] J. Brandrup, E. H. Immergut, and E. A. Grulke, "*Polyer Handbook*", 4th edition, John Wiley & Sons Inc. (1999).

[157] http://mrsec.wisc.edu/Edetc/nanolab/gold/index.html

[158] The amalgamation of gold was described by Agricola in "*De Re Metallica*", published in 1556.

[159] J. J. Caron, R. B. Haskell, P. Benoit, and J. F. Vetelino, "*A Surface Acoustic Wave Mercury Vapor Sensor*", IEEE Transactions on Ultrasonics, Ferroelectrics, and Frequency control **45**, 1393 (1998).

[160] The manual book of EXACTA 2000 ellipsometer, Waterloo digital electronics, (1999).

[161] D. J. De Smet, "*A Child's Garden of Ellipsometry*", not published.

[162] E. Hecht, "*Optics*", Addison-Wesley Pub. Co. (1974).

[163] E. D. Palik, "*Handbook of Optical Constants of Solids*", Academic Press; 1st edition (1997).

[164] Z. Fakhraai, S. Valadkhan, and J. A. Forrest, *Qualitative discrepancy between diferent measures of dynamics in thin polymer films*, Eur. Phys. J. E. **18**, 143-148 (2005).

[165] D. P. Bertsekas, "*Nonlinear Programming*", Athena Scientific, Belmont, Mass. (1999).

[166] http://www.polymer-physics.uwaterloo.ca/equipment/afm.htm

[167] F. Varnik, J. Baschnagel, and K. Binder, "*Molecular dynamics of supercooled polymer films*", J. Phys. IV. **10**, 239-242 (2000).

[168] R. D. Priestley, L. J. Broadbelt, and J. M. Torkelson, "*Confinement and interfacial effects on the alpha relaxation dynamics of thin polymer films*", Apstract of papers submitted to MAR07 Meeting of the American Physical Society, (2007).

[169] S. F. Swallen, K. L. Kearns, M. K. Mapes, Y. Seol Kim, R. J. McMahon, M. D. Ediger, T. Wu, L. Yu, and S. Satija, *"Organic Glasses with Exceptional Thermodynamic and Kinetic Stability"*, Science **315**, 353-356 (2007).

Paper I

Effect of Sample Preparation on the Glass-Transition of Thin Polystyrene Films [1]

From: BJohns@wiley.com
Date: Wed, 2 May 2007 07:59:27 -0400
Dear Zahra Fakhraai:
Please be advise permission is granted to
Journal of Polymer Science: Part B: 42(24)
Thesis
which will be published by University of
on
every copy using the material and must include
(s);
and/or editor (s); Copyright (year and owner);
"Reprinted
with permission of John Wiley & Sons, Inc."
are
granted to use content that appears in the
source.
Good luck with your thesis
Sincerely,
Brad Johnson, Permissions Assistant

Effect of Sample Preparation on the Glass-Transition of Thin Polystyrene Films

Z. FAKHRAAI,[1] J. S. SHARP,[2] J. A. FORREST[1]

[1]Department of Physics and Guelph–Waterloo Physics Institute, University of Waterloo, 200 University Ave. W., Waterloo, Ontario, Canada, N2L 3G1

[2]School of Physics and Astronomy, University of Nottingham, University Park, Nottingham, NG7 2RD, U.K.

ABSTRACT We have investigated the effect of sample preparation on the glass-transition temperature (T_g) of thin films of polystyrene (PS). By preparing and measuring the glass-transition temperature T_g of multilayered polymer films, we are able to assess the contribution of the spincoating process to the reduced T_g values often reported for thin PS films. We find that it is possible to determine a T_g even on the first heating cycle, and that by the third heating cycle (a total annealing time of 15 min at $T = 393$ K) the T_g value has reached a steady state. By comparing multilayered versus single layered films we find that the whole T_g depends only on the total film thickness, and not on the thickness of the individual layers. These results strongly suggest that the spincasting process does not contribute significantly to T_g reductions in thin polymer films. © 2004 Wiley Periodicals, Inc. J Polym Sci Part B: Polym Phys 42: 4503–4507, 2004

INTRODUCTION

There has been a significant amount of interest in recent years in the physical properties of very thin polymer films.[1–3] In particular, in a number of cases the properties of thin films display significant deviations from that of the bulk material, or even that of much thicker films. Of particular interest is the glass transition temperature (T_g). For many different polymers, measurements of the T_g in thin films have revealed large differences from the bulk value. Of these polymers, the most well studied material is atactic polystyrene (PS). Since the original study by Keddie et al.[4] showing thin film T_g values lower than that of the bulk, there have been many studies aimed at quantifying this behavior.[5] A recurring concern about these and other studies of thin polymer films involves the effect of sample preparation.[6, 7] Such films are typically spin cast from dilute solutions of polymer in a good solvent (such as toluene in the case of PS) and then annealed above the bulk T_g value for a time usually ranging from a few hours to a few tens of hours. During the process of spincasting, the chains may be in configurations not typical of those in equilibrium melts. In addition, even though the films are annealed, in many cases (depending on the substrate on which they are prepared) they are very different from the equilibrium state of a fully dewetted film. This concern is often dismissed, although there is not yet any proof that it is valid to do so. Although a definitive explanation to the observed T_g reductions has not yet emerged, there is compelling evidence that it is related to the presence of the free surface.[8] One way to distinguish between an effect due to the free surface

and one due to sample preparation is to make films with the same thickness (and hence the same relative contribution of the free surface) but different sample preparation history (i.e., solvent concentration and spin speed). The most effective way to implement such a comparison is the use of layered samples. The T_g values of layered samples also have relevance in supporting the conclusion of recent studies by Ellison and Torkelson where layered samples with one labeled layer were used as a way to quantify the depth-dependent T_g value in thin films.[9] In this study, we investigate the relative effect of sample preparation and the free surface by preparing and measuring the T_g value of a series of layered polymer films with up to four constituent layers. We show that it is possible to identify a T_g in all cases, and that after a single heating cycle (393 K for 15 min), the measured T_g of a multilayered sample depends only on the *total* film thickness rather than the thickness of the constituent layers.

EXPERIMENTAL

PS solutions of weight-average molecular weight (M_w) = 641 K, M_w/[number average molecular weight (M_n)]M_N = 1.11, polymer source) were spincast onto either Si (100) substrate (for the first layer) or on single crystal sodium chloride (NaCl) optical windows (Crystaltechno) for the second, third, and fourth layer of each film. The individual layer thicknesses were between 3 nm ≤ h ≤ 150 nm for the one and two layer films and 5 nm ≤ h ≤ 10 nm for three and four layer films. All layers in each sample were made using the same solution, and with the same spin speed. The layers were then separately annealed at 393 K [T_g(bulk) = 370 ± 1K] for 9 h under nitrogen to remove the solvent and relax the polymer chains. This is similar to the annealing conditions used for thin film T_g studies and assures that each layer has the same thermal history and, as a consequence, a similar chain conformation. These layers were then used to make samples in the following manner: a layer supported on NaCl was placed upside down on top of the layer supported on a Si substrate. A drop of deionized water placed on the edge of the salt substrate partially dissolved the salt and placed the second layer on top of the first layer. Once the second layer is placed on top of the first layer, the layers are pulled into contact by surface forces. The two layer film was then washed with deionized water

to make sure there is no salt left on the film and then annealed again for at least 12 h at 343 K to make sure that there is no water left on the film or between the layers. This annealing temperature is well below the bulk T_g and other possible reduced T_gs and therefore no chain relaxation will occur during the final annealing stage. If desired, a third or fourth layer was placed on the film using the above method. This procedure provides samples that are well annealed, in that all of the solvent should have been removed, but the chain conformations will be characteristic of the layer thickness rather than the total film thickness.

The multilayer films made by this method were then placed on a Linkam hot-stage and mounted on the sample stage of an Exacta 2000 fast-nulling ellipsometer (Waterloo Digital Electronics). The films were heated rapidly (90 K/min) to 403 K and held at that temperature for 5 min. The films were then cooled to 313 K with a cooling rate of 1 K/min to measure the T_g. This annealing time at 403 K is much less than a typical annealing time in this study and other studies, and less than that expected to result in significant interface formation at this temperature.[3] The T_g of each film was measured three times during three different heating cycles to examine the effect of annealing time on the T_g. Ellipsometric measurements were performed using a wavelength of 633 nm and an angle of incidence of 60 ± 0.1°. The ellipsometric angles P and A were measured during cooling. Because the values of P and A depend linearly on the film thickness before and after the transition, the inversion of P and A to actual thickness was not necessary and the P and A values and their temperature derivatives were enough to determine the T_g. The T_g can be determined by the constructions of two straight lines, fitted to the high and low temperature ranges (Figure 1) or by calculating their numerical derivatives, and finding the midpoint between the low temperature limit (T_-) and the high temperature limit (T_+).[10] Figure 1 shows the plots of P and A and their temperature derivatives versus temperature for a one-layer film with a thickness of 40 nm. This set of plots shows how the T_g can be defined and that any of the quantities can be used to determine the same value of T_g within the experimental error. This is an important point because in some cases for the multilayer films, the T_g is not discernible in all data types.
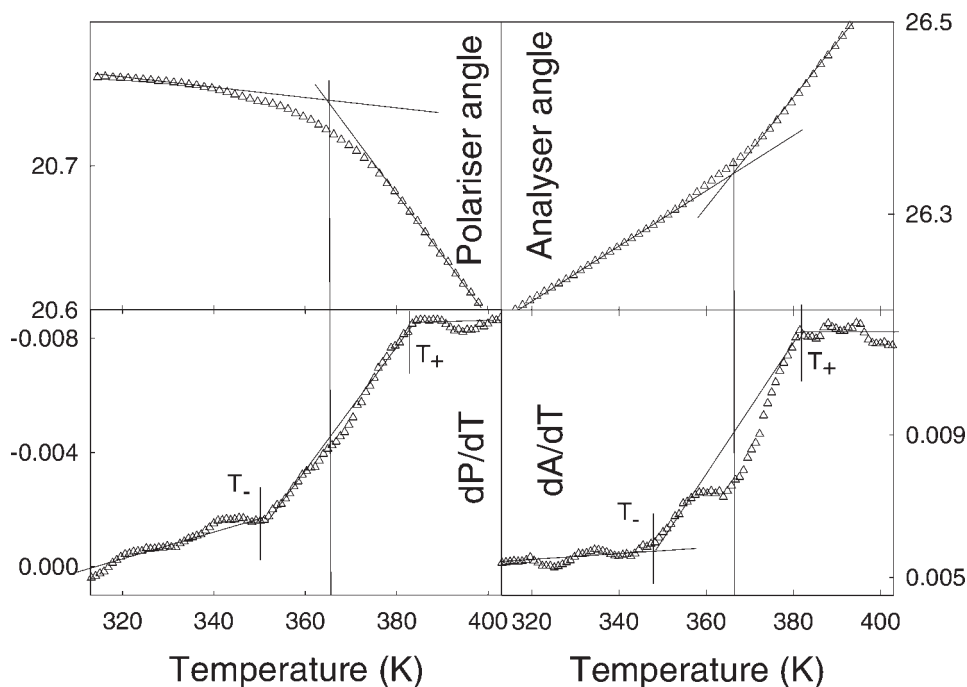
Figure 1 *P, A, dA/dT,* and *dP/dT* versus temperature of a 40 nm one-layer film. Solid lines show the T_g value. The T_g values are the same regardless of what data is used in the determination of the T_g.

RESULTS AND DISCUSSION

Figure 2 shows plots of *P* and *A* values versus temperature for a three-layer film made of 10 nm layers in the first (open symbols) and third (filled symbols) cooling cycle. There are a number of noteworthy points about these plots. In the first case, one can see that the value of the polarizer angle *P* during the third cooling is larger than that in the first cooling cycle. The most likely reason for this difference is that the film thickness decreases slightly during the successive heating and cooling cycles. Once the sample is heated above the T_g for the first time, the layers start to anneal into each other and the interface starts to disappear. This causes the difference between *P* and *A* values in different cooling cycles. The other notable aspect of the plots is the significant curvature in the high temperature region of the *P(A)* versus the temperature plot. This curvature is a result of the convolution of the temperature dependence of *P* and *A* as the sample is cooled with the time dependence of *P* and *A* as the interface in the multilayered samples heal with time. It is easiest to make a quantitative analysis by looking at the temperature derivatives, and we use *dA/dT* in this case. Figure 3
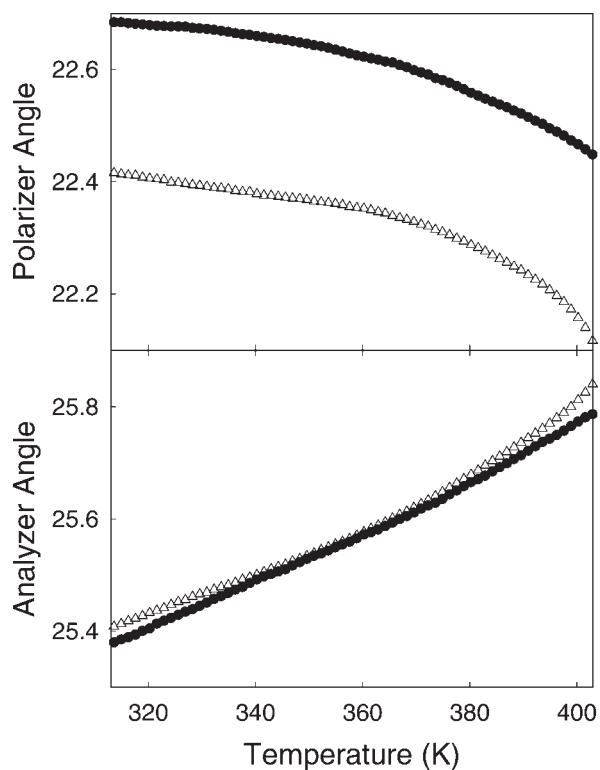

Figure 2 *P* and *A* versus temperature of a three-layer film made of 10 nm layers in the first (△) and third (●) cooling cycles.
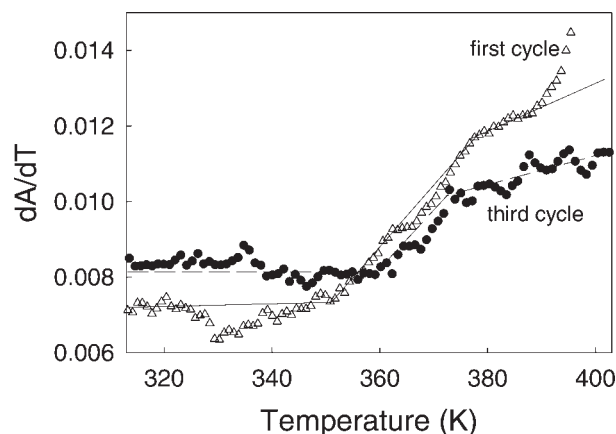
4506 FAKHRAAI, SHARP, AND FORREST

Figure 3 dA/dT versus Temperature of a three-layer film made of 10 nm layers in the first ($\triangle$) and third ($\bullet$) cooling cycles.

shows the dA/dT data that are derived from the data in Figure 2. The high temperature range (temperatures greater than 380 K) shows the extent of the high temperature annealing effect, and as we anneal the film for a longer cumulative time, this high temperature effect diminishes. This dynamical effect is investigated more carefully using two-layer films and will be published separately. The results of simulation and experiments on those films confirm that the changes in the P and A values at high temperatures are due to interface annealing. Although this dynamical process exists at high temperatures, we are still able to define the T_g because of the existence of a plateau at temperatures low enough so the dynamical effect is not observed on the time scale of the experiment, and yet high enough to be above the T_g value. This plateau is clearly seen in Figure 3. A careful analysis of the data in Figure 3 reveals that the T_g values in the third cycle are slightly higher than the T_g values in the first cycle. This effect exists in the measurements of all multilayer films, and does not exist in the measurements of one layer films. The most likely reason for this is the healing of the PS–PS interfaces in the multilayer films. Since the individual layers have an initial surface roughness; the interfacial regions of the multilayer films will not start out with a density the same as the bulk polymer. Although this dynamical process exists, the measurements of the thickness before and after annealing the films shows that the changes in the film thickness are always less than 10% of the total thickness of the film. Since the effect of this dynamical process almost disappears at the end

of the third cooling cycle, the results of T_g measurements at this cooling cycle is used in the analysis. Further annealing of the samples was avoided to ensure that the total annealing time is still negligible in comparison with the total chain disentanglement time, which is of the order of 1000 min for PS at 390 K.[3]

Figure 4 shows the plot of all T_g values at the third cooling cycle versus the total film thickness measured at the end of the cycle. In this figure, the final film thickness is determined from the final values of the P and A angles, and will be less than the sum of the thicknesses of the constituent layers. It can be seen from the plot that the T_g reduction of two, three, and four layer films are the same as the T_g reduction of one layer films with the same total thickness, within the experimental uncertainty. Although there is a noticeable scatter in the T_g values of Figure 4, it is not dissimilar from any other study of film thickness-dependent T_g values in PS films.[5] As a particular example, we can consider the case of the single layer film of 9.5 nm. The measured T_g of this film is 363 K. The T_g of a 28 nm film made of three 9.5 nm layers is 369 K. This value is similar to the T_g of a one layer 34 nm film (370 K) within the experimental error, and is very different from that of the original 9.5 nm layer. The main conclusion to draw from Figure 4 is that after only 15 min of annealing at 403 K, the multilayered films all take on a T_g value typical of a single film with the *same total thickness*. These films have not had enough annealing to relax the polymer chains from the conformations they adopted in the single layers, and so it is reasonable to say that the T_g
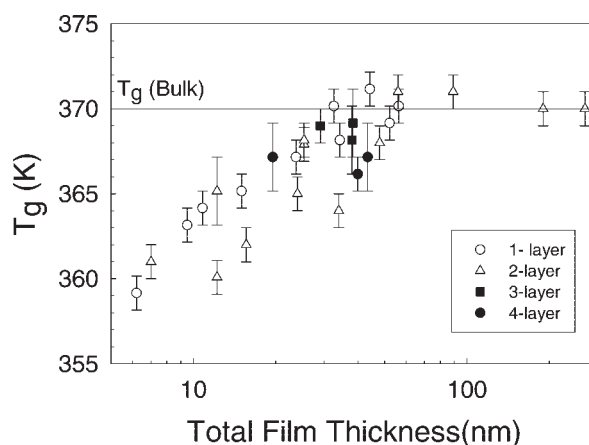

Figure 4 T_g versus film thickness at the end of the third cooling cycle, of one (o), two ($\triangle$), three ($\blacksquare$), and four ($\bullet$) layer films.

reductions of PS films supported on Si wafers are *not* related to chain conformation in the confined geometry of the thin film. Instead, the T_g values depend only on the total thickness of the film. Certainly the films in Figure 4 have had much less annealing than those in typical thin film T_g studies, and thus those studies are not strongly affected by chain conformations. Another way to look at this is to consider the T_g value of a single layer when it is incorporated into a particular sample type. Figure 5 shows the T_g value of 6 and 10 nm layers when they are part of a film of n layers ($1 \leq n \leq 4$) This clearly shows that the T_g values are monotonically increasing with n. This supports the above assertion that it is only the total sample thickness that determines the T_g value.

The high temperature behavior shown in Figure 3 was attributed to interface growth. If this is the case, then the initial multilayer film does have some excess free volume at the interface and one might reasonably expect a slightly lower T_g value. This is similar to what is observed in the interfaces of highly immiscible polymers.[11] To see if this is the case, we can look at the case of a 3 layer film (with 9.5 nm layers) as it is thermally cycled (Fig. 6). The first measurements of T_g has a value of 365 K. This T_g value increases with
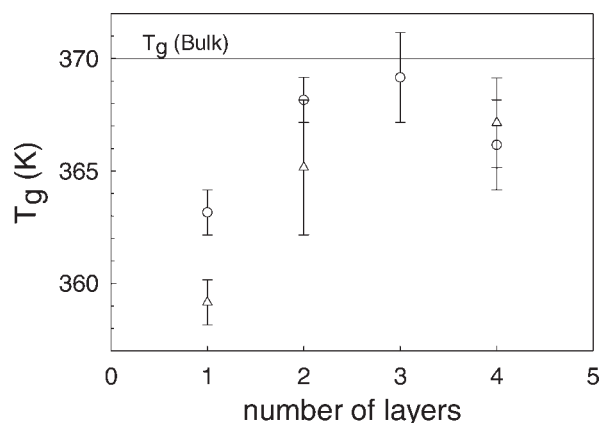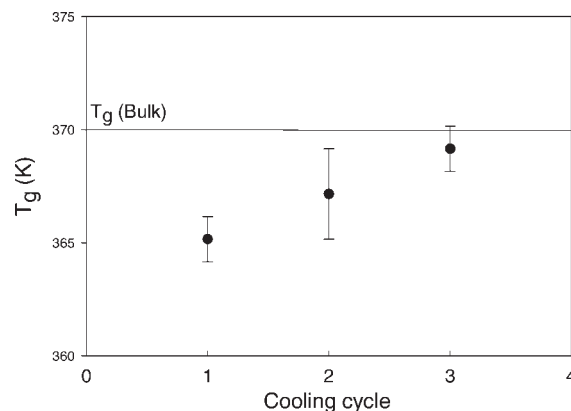

Figure 6 T_g values of a three-layer film made of 9.5 nm layers in different cooling cycles.

each annealing cycle, and by the third cycle has a T_g characteristic of a single film of thickness of 3 $\times$ 9.5 = 28.5 nm.

In summary, we have considered the effect of sample preparation history on the T_g of thin PS films by making multilayer films of thin PS, and show that the only important parameter in defining the T_g reduction is the total film thickness, not the thickness of sublayers.

REFERENCES AND NOTES

1. Reiter, G.; Forrest, J. A. (Eds.) Eur Phys J E 2002, 8.
2. Forrest, J. A. Eur Phys J E 2002, 8, 261.
3. Jones, R. A. L.; Richards, R. W. Polymers at Surfaces and Interfaces; Cambridge University Press: Cambridge, 1999.
4. Keddie, J. L.; Jones, R. A. L.; Cory, R. A. Europhys Lett 1994, 27, 59.
5. Forrest, J. A.; Dalnoki-Veress, K. Adv Colloid Interface Sci 2001, 94, 167–195.
6. Frick, B.; Zorn, R.; Buttner, H. (eds.) J Phys 2000, 10, 7.
7. McKenna, G. B. Eur Phys J E 2003, 12, 191.
8. Sharp, J. S.; Forrest, J. A. Phys Rev Lett 2003, 91, 235701.
9. Ellison, C. J.; Torkelson, J. M. Nature Mater 2003, 2, 695.
10. Kawana, S.; Jones, R. A. L. Phys Rev E 2001, 63, 021501.
11. Forrest, J. A.; Dalnoki-Veress J Polym Sci Part B: Polym Phys 2001, 39, 2664.

Figure 5 T_g versus number of layers for films made of 6 nm ($\triangle$) and 10 nm (o) layers.

Paper II

**Qualitative discrepancy between different measures
of dynamics in thin polymer films** [2]

Dear Sir,
In answer to your request, we are pleased to inform you
that we grant
the
permission to reproduce:
Article "Quantitative discrepancy...”from Eur Phys
Journal E, vol 18
N°2 ,
(2005) p 143-148.
We thank you by advance to cite the primary published
source in your
new
publication. (title, year, issue).
Yours sincerely,
C. GRIFFON
Copyright Dept
EDP Sciences
17 av du Hoggar
PA de Courtaboeuf
91944 Les Ulis cedex A
Phone: +33 (0)1 69 18 75 75
Fax: +33 (0)1 69 28 84 91

Qualitative discrepancy between different measures of dynamics in thin polymer films[★]

Z. Fakhraai[1], S. Valadkhan[2], and J.A. Forrest[1,a]

[1] Department of Physics and Guelph-Waterloo Physics Institute, University of Waterloo, 200 University Ave. W., Waterloo, Ontario, Canada, N2L 3G1

[2] Department of Mechanical Engineering, University of Waterloo, Waterloo, Ontario, Canada, N2L 3G1

Abstract. We have used ellipsometry to measure the initial stages of interface healing in bilayer polystyrene films. We also used ellipsometry to measure the glass transition temperature T_g of the same or identically prepared samples. The results indicate that as the film thickness is decreased, the time constant for the interface healing process increases, while at the same time the measured glass transition temperature *in the same samples* decreases as the film thickness is decreased. This qualitative difference in the behavior indicates that it is not always possible to make inferences about one probe of polymer dynamics from measurements of another. We propose a reason for this discrepancy based on a previously discussed origin for reduction in the T_g value of thin films.

PACS. 68.35.Fx Diffusion; interface formation – 68.35.Ja Surface and interface dynamics and vibrations – 82.35.Gh Polymers on surfaces; adhesion

1 Introduction

The drive toward nanotechnology is accompanied by a need and desire to understand the physical properties of materials whose sample size is in the nanometer regime. It is certainly not clear that such samples, due to effects such as the large surface area to volume ratio for instance, will have properties the same as or even predictable from those of bulk materials. For the case of polymeric materials, the situation is especially interesting. The long-chain nature of polymers introduces an additional length scale that can potentially influence a size scale where a material can exhibit anomalous behavior. The dynamical properties of materials are of particular interest, and for the case of polymers, the dynamic properties of nanoconfined samples have become the subject of significant discussion [1]. The most prominent geometry for the samples studied are thin films.

The first indication of anomalous dynamics in very thin films was from the dewetting studies of Reiter [2] for PS films. That study showed that very thin films dewetted at a faster rate than thicker films. A possible cause of this observation is that the glass transition temperature (T_g), a temperature closely tied to the viscosity in bulk

glass-forming materials, was lower for thin films than for thick films. The first direct measurements of the T_g value for PS films on Si (with an HF etched surface) was made by Keddie, Jones and Cory using ellipsometry [3]. These studies revealed that the T_g value for films with thickness $h \leq 40$ nm was reduced below the bulk value by an amount that increased as the film thickness decreased. This first study has prompted a number of additional studies, and there is an emerging consensus that for the case of PS, thin films have T_g values reduced below the bulk value.

The reasonable consensus of T_g values in thin films does not mean that the dynamics in thin films is well understood. Perhaps one of the most important issues that has surfaced in comparisons with different experiments on thin PS films is that not all measures of dynamics are directly comparable. In bulk materials, this is rarely an issue, and measurements of the T_g value can be compared with measurements of viscosity or dynamical mechanical measurements. In thin films the validity of such comparisons is not obvious. For instance, free-standing films well above their measured T_g values appear to be stable with respect to hole formation: a fact that is not consistent with the idea of a lower viscosity above T_g. In fact such films do not exhibit hole formation until the temperature is raised very near the bulk T_g value. Two possibilities have emerged in the literature as possible explanations for this effect. One possibility is that the dynamics in a thin
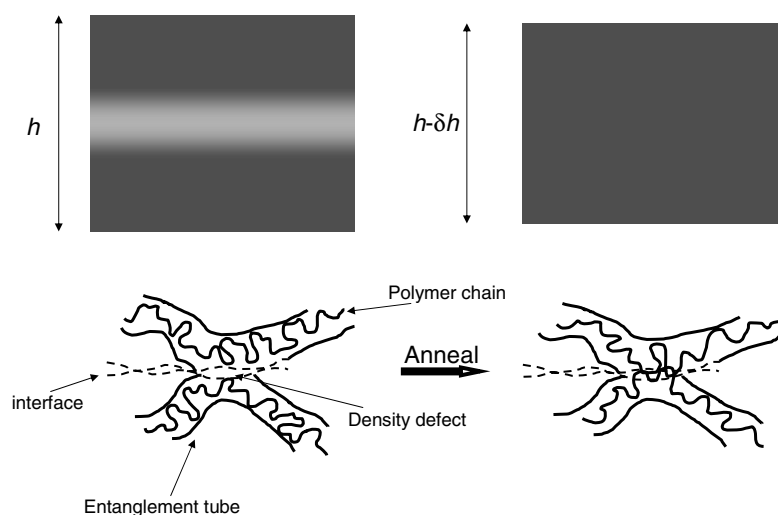

Fig. 1. Schematic diagram of the process that heals interfacial density defect in thin bilayer films.

polymer film are not homogeneous throughout the film and the surface regions have a lower T_g value than the middle part of the film, that perhaps remains bulk-like. Recent experiments have supported the idea that the free surface is a strong contributing factor to T_g reductions [4], and that the T_g in a thin film is not homogeneous [5]. Additionally, in thin films, it is not obvious that the segmental motion associated with the glass transition remains strongly coupled to that of chain motion [6]. While it is obviously necessary to have segmental motion before having any possibility of chain mobility, it may not be sufficient. As an illustration, if a few segments were tethered to the substrate, whole chain motion beyond R_{EE} could not occur even if all segments were very mobile. There has been experimental evidence that polymer chain diffusion in thin films ($h \leq 100$ nm) is slower than in bulk (or thicker films) [7,8]. Unfortunately, these measurements of chain diffusion have also been cited as being due to a thin-film T_g value *greater* than that of bulk PS. It is important to resolve whether the measurements of slower chain diffusion in thin films represent a true contradiction in measures of the glass transition temperature, or whether it is possible to have both a lower T_g and slower chain motion in the same system. One of the difficulties with this comparison is that chain motion is a hierarchial process, and segmental motion and chain motions are at the two extremes of the motion.

We have developed an experiment aimed at making a more direct comparison between the glass transition temperature and chain dynamics on a fairly small length scale. We use ellipsometry to measure the time dependence of incompletely annealed bilayer samples. In such samples the interface region between the two previously annealed layers will have a density less than the bulk value. As the sample is heated above the bulk T_g, the interface heals. Since the interface region is determined by the surface roughness of each film, and this quantity is ~ 1 nm, the interface region should be a few nm. This is much less than the tube diameter of the entangled polystyrene, and so the

density defect can be relaxed by motion out of the plane of the film, but inside the tube, *i.e.* Rouse modes, rather than center-of-mass motion (as depicted schematically in Fig. 1). This is a fundamental difference between these experiments and those described in reference [7]. Since the Rouse modes give rise to the $t^{-1/2}$-dependence of the shear modulus in the glass-rubber transition region, comparison of this interface healing to glass transition temperatures could be considered as a comparison of very similar motions. There are however, reasons to believe that these dynamics in thin films may differ from those of the bulk. Simulations of small polymer chains above T_g have shown that the motion perpendicular to the plane of the film becomes slower for smaller film thicknesses, as does the asymmetry between in-plane and out-of-plane motion. In contrast, Ngai has predicted that the Rouse modes will be unaffected even in films where T_g reductions are observed [9]. This experiment provides a way to test, using the same samples and same technique for measurements of the glass transition temperature, and measures of the Rouse dynamics out of the plane of the film. Once the sample has been sufficiently annealed we can cool the sample and directly measure the dilatometric T_g through the change in thermal expansion. The results show that as the film thickness decreases, both a lower T_g *and* slower chain dynamics out of the plane of the film are measured. This fascinating and apparently self-inconsistent result suggests that great care must be taken when comparing different measures of dynamics in thin polymer films. We provide a tentative explantation based on our previously discussed influence of the free surface on the T_g value in thin PS films [10].

2 Experiment

Solutions of polystyrene ($M_W = 641$ K, $M_W/M_N = 1.11$, Polymer Source Inc.) in toluene were spincast onto either Si(100) substrate (for the first layer) or onto single-crystal

sodium chloride (NaCl) optical windows (Crystaltechno) for the second layer of each film. The individual layer thicknesses were between $4\,\text{nm} \leq h \leq 200\,\text{nm}$. Both layers of each sample were made of the same solution, and with the same spin speed. The layers were then separately annealed at 393 K ($T_g(bulk) = 370 \pm 1$) for at least 9 hours under dry nitrogen gas to remove solvent and relax any strong perturbation introduced by the sample preparation procedure. While this should be sufficient for measurements of T_g, we do not claim that this relaxes the polymer chains. These layers were then used to make two-layer films in the following manner: The layer supported on NaCl was placed upside down on top of the layer supported on Si substrate. A drop of deionized water placed on the edge of salt substrate partially dissolved the salt, and allowed the salt crystal to be removed. Once the second layer is placed on top of the first layer the layers are pulled into contact by surface forces. The two-layer film was then washed thoroughly with deionized water to make sure there is no salt left on the film and then annealed again for at least 12 hours at 343 K to make sure that there is no water left on the film or between the layers. This annealing temperature is well below any possible reduced T_g's and so no chain relaxation should occur during the final annealing stage. This procedure provides samples that are well annealed in that each layer is as well annealed as the samples in majority of T_g studies, but the interfacial region will still have a density value lower than that of bulk PS.

The films were then placed on a Linkam hot stage and mounted on the sample stage of an Exacta 2000 fast-nulling ellipsometer (Waterloo Digital Electronics), with an angular resolution of 6×10^{-4} degrees. The films were heated at 90 K/min to a temperature of 393 K where they were held for 1000 seconds to study the isothermal interface annealing. The films were then cooled after being annealed for several hours to 303 K with a cooling rate of 1 K/min to measure the T_g. Ellipsometric measurements were performed using a wavelength of 633 nm and an angle of incidence of $60 \pm 0.1°$.

The samples are well described by a multilayer polymer system. Each sample consists of 5 different layers; the silicon substrate, a 2 nm silicon oxide layer, the first PS layer, an interfacial layer with an average density less than that of polystyrene, and the top PS layer. Each PS layer was treated as a PS film with the refractive index of 1.595 (a value we consistently measure for PS films). The interface region was treated as a PS layer with an initial density $\rho_0 < \rho_{bulk}$. The interfacial layer will have a lower density than that of bulk PS because the initial surfaces that are brought together have both asperities that need to be annealed out, as well as possibly a slightly lower density near the surfaces. The thickness of this layer, and its initial density are not independent parameters, and allowing both parameters to vary leads to difficulties with the fitting procedure. A number of different measurements lead to the suggestion that the initial density of the interfacial region on a bilayer film can be described by ($\rho_0 = 0.4\rho_{bulk}$). Fixing this initial condition and having the thickness of

the interfacial region as a fit parameter allows for consistently good fits for all data sets. For all experiments the interface region from the curve fitting procedure was from 3 to 5 nm. Before each experiment, the surface roughness of the layers was measured separately using AFM, showing a roughness of $0.9\,\text{nm} < \Delta h < 1.5\,\text{nm}$ for individual layers. This indicates that the roughness of each layer is similar to the chosen interface thickness. The refractive index in the interfacial region was related to the density by the Lorentz-Lorenz relation

$$\frac{n^2 - 1}{n^2 + 1} \simeq \alpha\rho. \tag{1}$$

The thickness of the interface was set to be equal to the initial thickness and its density was described by $\rho(t) = \rho_{bulk}(1 - ae^{-(\frac{t}{\tau_0})^{\beta}})$, where a is a constant determined by the condition $\rho(0) = \rho_0$. A stretched exponential relation with a β value of 0.3 was found to provide the best fit to the kinetic data. Allowing this parameter to vary did not lead to consistently better fits, so for more robust determination of the remaining parameters, we fixed $\beta = 0.3$. We note that in order to have a physically meaningful model, it is crucial to conserve mass. The result of this is that as the density in the interfacial region increases, the thickness of each of the PS layers must decrease with a similar stretched exponential relation. We note that failing to invoke mass conservation leads to a complete inability to fit the data. The ellipsometric angles P and A are then calculated for this multi-layer film at each time as followed; The total reflection coefficient from layer i for each polarization direction (s or p) is equal to [11]

$$R_{i,i-1} = \frac{r_{i,i-1} + R_{i-1,i-2}e^{-2i\delta}}{1 + r_{i,i-1}R_{i-1,i-2}e^{-2i\delta}}, \tag{2}$$

where $\delta = 2\pi n_i \frac{h_i \cos\theta_i}{\lambda}$ is a function of the layer thickness and the index of refraction $r_{i,i-1}$ is the corresponding Fresnel reflection coefficient for s or p polarized light and $R_{i-1,i-2}$ it the total reflection coefficient for the same polarization calculated for the previous layer. The reflection coefficients are calculated one by one from the first layer (silicon) to the last layer (air).

For a null the reflected light should be linearly polarized, which means that the imaginary part of $\frac{E_{p,r}}{E_{s,r}}$ should be equal to zero. This equation gives the P and A angles at each time. The results are then fit to the data using Nelder-Mead [12] simplex direct search method to minimize the sum of the magnitudes of differences between calculated and measured values. This algorithm does not need minimized function derivatives and is among the best and fastest algorithms for numeric optimization when the minimized function is well behaved, and does not have many adjacent local minima.

In the final fitting of the time-dependent data, the only free parameters were the initial thickness of PS layers, the initial thickness of the interfacial layer, and the time constant of interface healing. We note that the alternative technique of floating a PS layer on top of another PS film
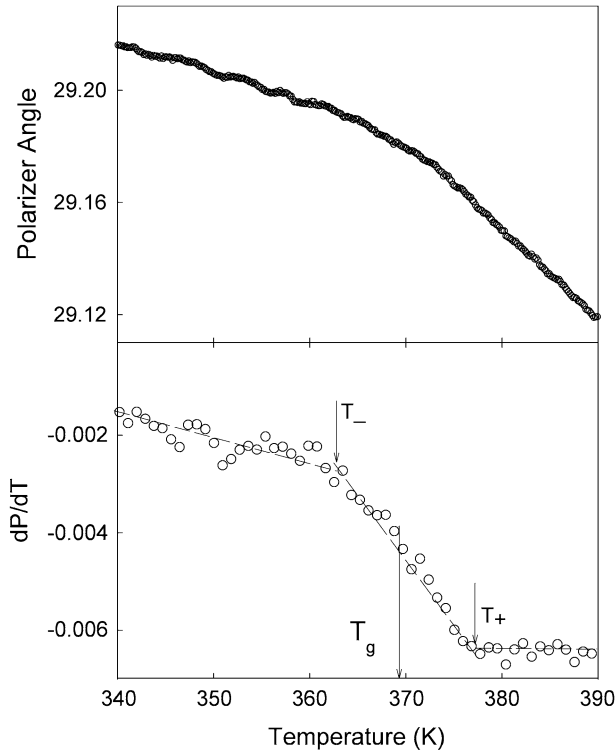
Fig. 2. Polarizer angle *vs.* temperature for a film with total thickness of 20 nm. The T_g is defined as the midpoint of T_+ and T_- values.

Fig. 3. Polarizer *vs.* time for films with total thickness of 32 nm ($\circ$) and 11 nm ($\triangle$). The solid curve shows the results of the simulation. The inset shows the density *vs.* the time values used to obtain the solid curves.

does not provide the same measured interface healing dynamics, and as such are not well described by the process described above. We expect the reason for this is that the floating procedure introduces a significant in-plane stress, and the magnitude of effects due to this stress is similar to that of the interface healing.

After annealing the films for several hours at 393 K, the films were brought to ambient temperature at a cooling rate of 1 K/min to measure their T_g. Since in all T_g measurements the P and A values depend linearly on the thickness before and after transition, the values of P and A and their temperature derivatives were enough to determine the T_g and their inversion to actual thickness was not necessary in this part of the measurement. The glass transition temperature (T_g) can be determined by calculating the numerical derivatives of P and A angle and finding the midpoint between the low-temperature limit (T_-) and the high-temperature limit (T_+) [13]. Figure 2 shows the plots of P and its temperature derivative *versus* the temperature for a film made of two 10 nm layers. The T_g's measured using the A or P values are typically the same within the experimental uncertainty.

3 Results and discussion

Figure 3 shows raw data from a typical interface healing measurement for two different film thicknesses. While the process is obviously slower for the thinner film, the potential for a strongly film-thickness-dependent non-linear
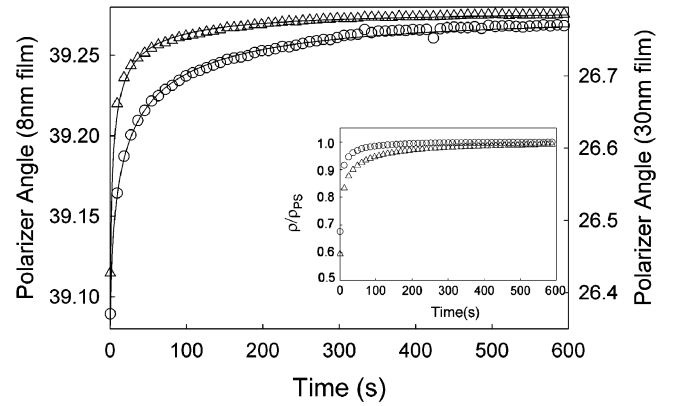
relation between the density of the interphase region and the final measured polarizer angle means that the raw data cannot reliably be used to extract the time constant for interface healing. The inset of the figure shows the time-dependent density of the interfacial layer resulting from obtaining the fits in the figure (solid lines). The density of the interfacial layer reaches its maximum value more rapidly in the thicker film. The average lifetime of the interface healing is calculated to be

$$\tau = \frac{\tau_0}{\beta} \times \Gamma\left(\frac{1}{\beta}\right), \tag{3}$$

where τ_0 is the time constant of the stretched exponential and β is its exponent. A plot of all lifetimes as a function of the total film thickness is shown by the solid circles in Figure 4. The dashed line in the plot indicates the Rouse relaxation time in the entanglements tubes [14] at 393 K obtained from neutron reflectivity experiments of interfacial growth in PS films. The lifetime of the interface healing for thick films ($h > 50$ nm) is very similar to the Rouse relaxation time, confirming that we are probing more local Rouse motions rather than whole chain motion. This is expected as we can only probe the changes until the density of the interfacial region is of the order of the bulk density of PS, and since the density defect at the interface can be almost entirely relaxed with Rouse modes (see Fig. 1), whole chain diffusion cannot possibly be probed. A key point of Figure 4 is that as the film thickness decreases the lifetime of interface healing increases. Our experiment should be relatively insensitive to motion in the plane of the film, and so the results in Figure 4 are at least qualitatively consistent with those of computer simulations that suggest a slowing-down of motion out of the plane of the film [15]. In order to investigate whether the slow-down of the dynamics is a characteristic of the total film thickness or the thickness of the individual layers, we prepared and measured asymmetric samples where the individual layers of the bilayer film had different thicknesses. Unfortunately, the scatter in the lifetime data is sufficiently large that we were not able to draw a definitive conclusion. In Figure 4
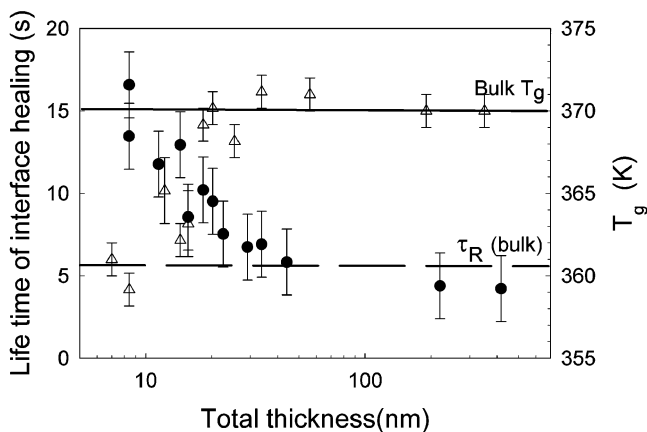
Fig. 4. Time constant for the interface healing (●) of PS bilayer films and the T_g (△) value for the *same* film as a function of the total film thickness.

case we present the lifetime of the interface healing as a function of the total film thickness.

Figure 4 compares the two measures of dynamics measured in our ellipsometric experiments. The triangles are the T_g values measured at a cooling rate of 1 K/min, and the circles are the average lifetimes for the initial stage of interface healing. For many film thicknesses, these two quantities are measured using the *same* film. The difference between these two different measures of the polymer dynamics is striking. The T_g values *decrease* below the bulk value as the film thickness is lowered. This suggests that thin films have a higher mobility than bulk samples. In contrast, the time constant for interfacial healing increases as the film thickness is lowered. This indicates that thin films have a reduced mobility compared to bulk polymer. The most obvious practical consequence of this behavior is the inability of either measurements to make inferences about the other. In thin films it would seem that measurements of T_g cannot be used to predict chain dynamics, and measures of chain dynamics cannot be used to predict T_g. In bulk systems, such comparisons are done routinely [16]. The results of our experiments indicate that these same comparisons are not necessarily valid in thin films.

The physical implications of these results are intriguing. At temperatures just above the glass transition temperature, relaxation in long-chain polymers occurs through the Rouse modes [17]. In a thin film where the T_g value is less than that of the bulk, one might reasonably expect enhanced Rouse dynamics. Clearly, this is not the case in Figure 4. One suggested approach to the problem involves the coupling model of Ngai as applied to thin films [9]. Ngai suggests that the friction factor used in the Rouse derivation of polymer dynamics is fundamentally different from the segmental interactions responsible for the glass transition in that the Rouse modes are not affected by the same intermolecular constraints. This model then leads to a natural separation of Rouse and segmental motions that could be used to rationalize the results of Figure 4. Certainly, the glass transition exists in many

materials other than polymers, and thus must have an origin that is not exclusively polymeric in nature.

An additional explanation is provided by noting that interface healing experiments (or *any* experiment probing chain motion) are all performed at a temperature significantly greater than the bulk T_g value. It seems often overlooked that there are *no* experiments that indicate an enhanced mobility (of any kind) in thin films held above the bulk T_g value. It is only at temperatures below the bulk T_g where thin films provide evidence for relaxation not observed in bulk or thick-film samples. This is not unexpected when considered in the context of the prominent role played by the free surface on the glass transition temperature in thin films [4] and the temperature dependence of the viscoelastic properties of the free surface [18]. We have previously reported evidence that the compliance of the near-surface region in PS is described by the same temperature as the bulk for $T > T_g$, but for $T < T_g$, there is a 4 nm surface layer that has a compliance characterized by $T \simeq T_g(bulk)$ even when the sample temperature is 10 K below the bulk T_g value. This can be compared to recent studies of variable cooling rate measurement of thin-film T_g values that demonstrate no T_g reduction at high cooling rates [19]. This threshold cooling rate corresponds to a temperature, $T^* \sim 377$ K beyond which no anomalies in dynamics can be observed. Taken as a whole, these three studies strongly suggest that there is an upper temperature, near the bulk T_g, where the effects that cause T_g reductions do not exist. At such temperatures, there will be no evidence of these effects and as a result there will be no possibility of even qualitative comparison between any measurements at $T < T^*$ and any measurements at $T > T^*$. We note that within this constraint, there remain very few contradictions in reports of dynamics in thin PS films.

In summary, we have used ellipsometry to measure the T_g values and interface healing times in PS bilayers. The measured T_g values display the now familiar behavior of decreasing as the film thickness is lowered. The interface healing times show the opposite behavior of *increasing* as the film thickness is lowered. The results show that there is no universal answer to the question "what happens to the dynamics in thin polymer films", and suggests that comparisons between different measures of dynamics and at different temperatures may not be valid.

References

1. B. Frick, R. Zorn, H. Buttner (Editors), *International Workshop on Dynamics in Confinement*, J. Phys. IV **10**, Pr7 (2000).
2. G. Reiter, Europhys. Lett. **23**, 579 (1993).
3. J.L. Keddie, R.A.L. Jones, R.A. Cory, Europhys. Lett. **27**, 59 (1994).
4. J. S. Sharp, J.A. Forrest, Phys. Rev. Lett. **91**, 235701 (2003).

5. C.J. Ellison, J.M. Torkelson, Nature Mater. **2**, 695 (2003).
6. A.N. Semenov, Phys. Rev. Lett. **80**, 1908 (1998).
7. X. Zheng *et. al.* Phys. Rev. Lett. **79**, 241 (1997).
8. B. Frank, A.P. Gast, T.P. Russell, H.R. Brown, C. Hawker, Macromolecules **29**, 6531 (1996).
9. K.L. Ngai, Eur. Phys. J. E, **8** 225 (2002).
10. J.A. Forrest, Eur. Phys. J. E, **8**, 261 (2002).
11. R.M.A. Azzam, N.M. Bashara, *Ellipsometry and Polarized Light* (North Holland, Amsterdam, 1987).
12. D.P. Bertsekas, *Nonlinear Programming* (Athena Scientific, Belmont, Mass., 1999).
13. S. Kawana, R.A.L. Jones, Phys. Rev. E, **63**, 021501 (2001).
14. A. Karim, A. Mansour, G.P. Felcher, Phys. Rev. B, **42** 6846 (1990).
15. F. Varnik, J. Baschnagel, K. Binder, J. Phys IV **10**, 239 (2000).
16. P.G. Bruce (Editor), *Solid State Electrochemistry* (Cambridge University Press, 1995).
17. G. Strobl, *The Physics of Polymers* (Springer Verlag, New York, 1997).
18. J.S. Sharp, J.H. Teichroeb, J.A. Forrest, Eur. Phys. J. E **15**, 473 (2004).
19. Z. Fakhraai, J.A. Forrest, Phys. Rev. Lett. **95**, 025701 (2005).

Paper III

Probing Slow Dynamics in Supported Thin Polymer Films [3,4]

AMERICAN PHYSICAL SOCIETY

One Physics Ellipse, College Park, MD 20740 · http://www.aps.org

April 26, 2007

Zahra Fakhraai
fakhraai@yahoo.com

Ref # 4864

Thank you for your permission request dated April 3, 2007. We are pleased to grant you a non-exclusive, non-transferable permission, English rights, limited to **print and World Wide Web format only**, provided you meet the criteria outlined below. Permission is for a one-time use and does not include permission for future editions, updates, additional electronic forms, databases, translations, or any other matters. Permission must be sought for each additional use. This permission does not include the right to modify APS material.

Please print the required copyright credit line on the first page that the material appears: "Reprinted (abstract/excerpt/figure) with permission from [FULL REFERENCE CITATION] as follows: authors names, journal title, volume number, page number and year of publication. Copyright (YEAR) by the American Physical Society.

The following language must appear somewhere on the website: "Readers may view, browse, and/or download material for temporary copying purposes only, provided these uses are for noncommercial personal purposes. Except as provided by law, this material may not be further reproduced, distributed, transmitted, modified, adapted, performed, displayed, published, or sold in whole or part, without prior written permission from the American Physical Society."

Provide a hyperlink from the reprinted APS material (the hyperlink may be embedded in the copyright credit line). APS's link manager technology makes it convenient and easy to provide links to individual articles in APS journals. For information, see: http://publish.aps.org/linkfaq.html

You must also obtain permission from at least one of the authors for each separate work, if you haven't done so already. The author's name and address can be found on the first page of the published Article.

Use of the APS material must not imply any endorsement by the American Physical Society.

Permission is granted for use of the following APS material only:
- Entire paper, Phys. Rev. Lett., Vol. 95, 025701 (2005)

Permission is limited to the single title specified or single edition of the publication as follows:
- Thesis paper to be published by the University of Waterloo.

If you have any questions, please refer to the Copyright FAQ at: http://forms.aps.org/author/copyfaq.html or contact me at assocpub@aps.org.

Sincerely,

Eileen LaManca
Marketing Assistant

P H Y S I C A L   R E V I E W   L E T T E R S

Probing Slow Dynamics in Supported Thin Polymer Films

Zahra Fakhraai and James A. Forrest*

*Department of Physics and Guelph-Waterloo Physics Institute, University of Waterloo, 200 University Avenue W.,
Waterloo, Ontario, Canada N2L 3G1*
(Received 3 September 2004; published 7 July 2005)

We have used variable cooling rate ellipsometric measurements to probe the slow dynamics in thin supported polystyrene films. For the slowest cooling rates (~ 1 K/min) the measured T_g values are reduced below the bulk value with the measured T_g of 341 K for a 6 nm film. As the cooling rate is increased the T_g reductions become smaller until at cooling rates >90 K/min there is only slight evidence for a film-thickness-dependent T_g value. By relating the cooling rate to a relaxation time, we show that the relaxation dynamics of the thin films appears to become Arrhenius with an activation energy that decreases with decreasing film thickness. We discuss this in terms of a possible connection to a length scale for cooperative motion. Finally, the results can be used to resolve a number of outstanding contradictory reports in the literature.

The nature of the glass transition remains an unsolved problem despite decades of study. Many different theoretical approaches have been applied to glass formation, but as yet none have been able to provide a description to encompass the known behavior. For this reason the glass transition is often noted to be the "deepest and most interesting unsolved problem in solid-state theory" [1]. One persisting theme in the literature is the existence of a characteristic length scale for the dynamics in glass forming materials [2–4]. This length scale has been studied in computer simulations at temperatures much above the calorimetric glass transition, and some experimental evidence for such a length scale has been presented [3]. The glass transition in highly confined geometries is among the most promising approaches to learn about the existence of a temperature dependent length scale in glass forming materials [5–7].

One particular sample configuration that has attracted a great deal of attention is that of thin polymer films. For such samples the dynamics are often inferred through measurements of the glass transition temperature T_g. This is a convenient, though obviously indirect measure of the dynamics in the sample. Since the original report by Keddie, Jones, and Cory [8] of the T_g value of thin films of polystyrene (PS) being reduced below the bulk value for films with thickness $h < 40$ nm, many researchers have performed similar studies, mainly using what can be termed as dilatometric techniques [9–11]. There is a growing consensus that for the particular case of PS, the T_g value decreases below the bulk value for sufficiently thin films. In addition there is growing evidence that the free surface plays a key role in these effects [12,13]. Despite this significant agreement between many groups, there are outstanding contradictory reports. Foremost among these reports is the recent observation that T_g values measured using nanocalorimetric techniques do not display a film-thickness-dependent T_g value. This conclusion seems to apply equally well to T_g values measured directly at cool-

ing rates of 1000 K/s [14] to those inferring the T_g through the fictive temperature T_f at rates of 2 K/s [15]. The qualitative difference between the dilatometric and calorimetric measured T_g values is striking and indicates an unsettling lack of understanding of the glass transition in nanoconfined geometries. In turn, the resolution of such a paradox is sure to add significantly to our understanding of dynamics in highly confined geometries and to the glass transition in general. A more serious concern is the fact that despite many measurements of T_g there are almost no measurements of dynamics for supported polymer films: the sample configuration for most of the T_g data. Since it has recently been demonstrated that the glass transition can be strongly affected by the presence or absence of the free surface [12,13] it is not clear that previous dielectric and thermal expansion spectroscopy studies of PS films have sufficient relevance to the systems they are being compared to [16]. The only dielectric relaxation studies on films with a free surface have used isotactic poly(methyl methacrylate) (*i*-PMMA) [17]. In this Letter we present the results of ellipsometric measurements of the T_g value of thin PS films supported by Pt coated SiN substrates at cooling rates ranging from 1 to 130 K/min. Such studies allow the use of T_g measurements as a measure of the dynamics in supported polymer films over 2 orders of magnitude. For the 1 K/min studies we observe large reductions in the measured T_g value of thin films. As the cooling rate is increased, the film thickness dependence of the T_g value becomes less pronounced until at a rate of 130 K/min there are only slight indications of any dependence of the T_g on the film thickness. The particularly striking aspect of the results is the very narrow range of cooling rate that results in reduced T_g values. The findings show that only the very slow dynamics are affected by nanoconfinement and that the effects persist for a relatively short time window of 2 orders of magnitude in relaxation time. The significance of this work is threefold. Most importantly, it

provides a quantification of the dynamics in thin supported films; second, it leads to a reasonable resolution of existing contradictory reports. Finally, it may lead to significant advances in our understanding of the glass transition.

PS films were produced by spin coating solutions of PS ($M_w = 641$ K, $M_w/M_n = 1.11$, Polymer Source Inc.) in toluene. The substrates used were the same ones employed for the nanocalorimetry studies of [14], Pt(50 nm)/Ti/SiN(50 nm)/Si, in order to be able to address the possibility of a strong substrate sensitivity being a cause for the aforementioned discrepancy. The samples were annealed under dry N_2 at a temperature of 393 K for 15 h and cooled to room temperature at <1 K/min. The samples were placed on the block of a Linkham temperature controlled stage. The T_g values were measured using an EXACTA 2000 fast nulling ellipsometer. The sampling time of the ellipsometer could be set to values as low as 0.3 s and still have sufficient resolution in the measured ellipsometric angles (P, A) for reliable T_g determination. We believe that such measurements are at the limit of those feasible with ellipsometry. For ellipsometric measurements, the sample is heated to 403–423 K, and then cooled to 293 K at rates of 1, 3, 6, 10, 20, 30, 40, 50, 70, 90, and 130 K/min. The heating rate is 130 K/min for all measurements. Since the thermal properties are dominated by the substrate, we can make quantitative comparisons between thin films and thick films. Since the analyzer angle (A) of the Pt coated substrates changes linearly in the high and low temperature ranges (and the polarizer angle changes very little), unlike some other polymer-substrate combinations (such as *i*-PMMA on Al) [17], the ellipsometric data do not need to be numerically inverted to determine T_g. The ellipsometric data are analyzed by taking the numerical derivative of the A data, and the T_g is defined as the midpoint of the high (T_+) and low (T_-) temperature limits. Figure 1 shows an example of raw

data, as well as how the data are used to determine T_g for a 6 nm film measured at a cooling rate of 30 K/min. Although the contrast between the low temperature range and the high temperature range is very small in very thin films, the technique allows us to determine the T_g with an accuracy of ±2 K.

Measured T_g values as a function of film thickness are shown in Fig. 2 for cooling rates of 1 or 3 K/min, 50 K/min, and 130 K/min. The most striking aspect of these data is that the film thickness dependence of the T_g values depends strongly on the cooling rate. The 1 K/min data show a strong T_g dependence to the film thickness. As the cooling rate is increased the thickness dependence of the T_g values decreases, so that at the cooling rate of 130 K/min the film thickness dependence of the T_g values are only slightly more than the experimental error. More quantitatively, the largest T_g reductions occurs for the 6 nm film and is 32 K below that of the 90 nm film for 1 K/min and is only 10 K below that of the 90 nm film for 130 K/min. The fact that the 1 K/min and 3 K/min data do exhibit large T_g reductions allows us to rule out the substrate as a cause of the discrepancies between previous T_g studies and those of Ref. [14]. By making comparisons between thin films and a thick film (rather than bulk PS) we can eliminate any possible effects due to different temperature gradients at different cooling rates.

Other studies of T_g in thin films have suggested that for the case of supported PS films (though not for freestanding films [11]) the apparent T_g reductions are due to a broadening of the transition [18]. This observation also holds true in the present work, and, in particular, the diminishing of T_g reductions at high cooling rates is a reflection of a narrowing of the transition as compared to lower cooling rates. In our experiments, we observe that the difference
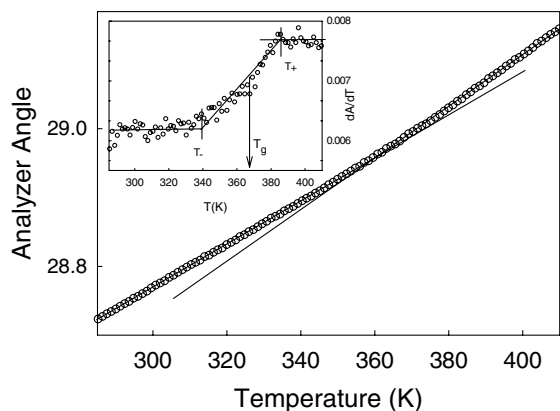

FIG. 1. The analyzer data and their temperature derivative (inset) for a 6 nm PS film as a function of temperature. The T_g is defined as the midpoint of T_+ and T_- values. The cooling rate is 30 K/min.

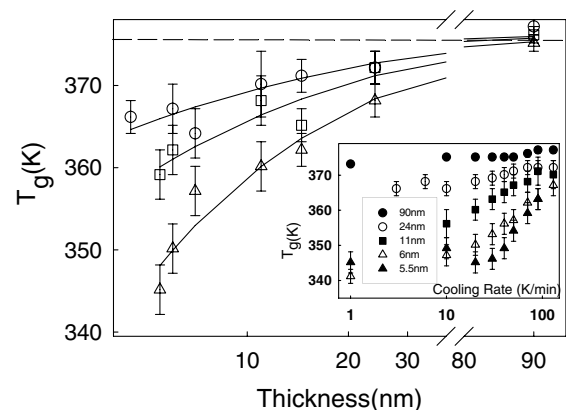
FIG. 2. Measured T_g values as a function of film thickness at 1 or 3 K/min (△), 50 K/min (□) and 130 K/min (○) cooling rates. The T_g values of 90 nm film are used as an indication of bulk T_g values. The solid lines are to guide the eye. The inset shows T_g as a function of cooling rate for 90 nm (●), 24 nm (○), 11 nm (■), 6 nm (△), and 5.5 nm (▲) films.

between T_+ and T_- (which defines the width of the transition) remains almost independent of film thickness at a cooling rate of 130 K/min, while the difference is increasing as the thickness is decreasing in the cooling rates of 1 or 3 K/min. It is interesting to note that the value of T_+ is also decreasing, but T_- decreases more rapidly, so that the width of transition increases in thinner films.

The T_g values for all cooling rates and films of thickness 5.5, 6, 11, 24, and 90 nm are shown in the inset of Fig. 2. We can see that the T_g of 5.5 and 6 nm film show the strongest cooling rate dependence. As we increase the thickness the T_g value depends less strongly on the temperature, so that the T_g of 90 nm film displays a cooling rate dependence one would expect from a bulk material. The cooling rates used to measure a T_g value can be considered as an inverse of some relaxation time probed by that experiment. The data for the 90 nm film can be used as a measure of the dynamics of "bulk" PS over the range of relaxation times of 7 to 1000 s, using the relation that a cooling rate of 10 K/min corresponds to a relaxation time of 100 s [16,19]. As expected there is only a slight rate dependence due to the fact that the relaxation time is such a strongly varying function of temperature.

In order to make a sensible comparison between the T_g values presented in the present work, and other studies of relaxation time (τ) in confined systems, it is useful to cast it in the form as a plot of $-\log(\tau)$ versus $1/T$ [6,7,20]. Figure 3 shows such a plot where the relaxation time is written in terms of the experimental cooling rate. The results cast in this form are quite remarkable and are
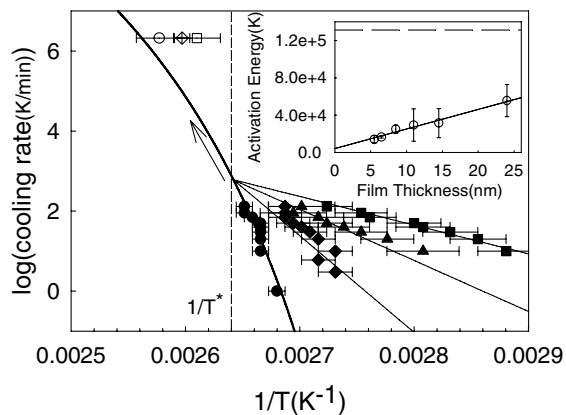

FIG. 3.   The log(cooling rate) vs $1/T$ for 90 (●), 24 (◆), 11 (▲), and 6 nm (■) films. The curved line is the bulk Vogel-Fulcher-Tamman (VFT) curve for PS and other lines are Arrhenius fit, passing through a single incidence point on the VFT curve. The data points at high cooling rates are the data from Ref. [14] for three different film thicknesses. The dashed line indicates T^* above which no confinement effect is seen. The inset shows the plot of activation energy vs film thickness and the linear fit to the data. The dashed line indicates the slope of the VFT curve at the incidence point which corresponds to a film thickness of 61 nm.

similar to effects reported in dielectric studies of liquids in pore glass [20], polymethylphenylsiloxane (PMPS) intercalated into galleys of silicates [7], and i-PMMA confined between Al surfaces [6]. Before commenting specifically on the results, it is worth reiterating that these measurements correspond to relaxation in supported PS films (with no capping layer) and as such are unique in their comparison to a broad and extensive literature on the T_g value of such samples. The thick solid curved line is obtained using the parameters of the Vogel-Fulcher-Tamman (VFT) equation

$$\tau = \tau_0 \exp\left(\frac{B}{T - T_0}\right) \qquad (1)$$

obtained by fitting relaxation time data for bulk polystyrene [19] in the same temperature range as the present experiments ($B = 1169$ K, $T_0 = 342.8$ K). Since the molecular weight used in the current study is between the two high molecular weight polymers used in Ref. [19], the parameter values of those fits are averaged to obtain the curve in Fig. 3. We employ the relation between the cooling rate and the relaxation time as that obtained for bulk PS [19] (10 K/min ~100 s). It is encouraging to note that although these values are derived from bulk measurements and do not come from a fit to our data (which we do not believe to be meaningful given the small range of cooling rates), they agree with our data within the experimental error. This comparison demonstrates that the 90 nm film behaves like a bulk polystyrene sample. The most prominent feature of the data for thin films is the strong deviation from the bulk (and thick film) VFT-like behavior. For all of the thin film data, the relaxation times exhibit Arrhenius behavior (rather than VFT), with a film-thickness-dependent activation energy. Equally remarkable is that if we fit the data to a simple Arrhenius form and then extrapolate each line to where it intercepts the bulk VFT line, we find that all films intersect at essentially the same temperature of $T = 378.5 \pm 1.4$ K. This corresponds to a cooling rate between 158 and 2068 K/min. For any cooling rates above this critical value, all films will have a T_g the same as the bulk polymer. It is interesting to note that this temperature is very similar to the value of where the surface of PS films seems to show viscoelastic properties that differ from the bulk [21]. This provides a further link between T_g reductions in thin films and surface properties of the polymer.

The slope of each of the straight line fits provides an activation energy E_a. The inset shows how these E_a values vary with the film thickness, if we fit each curve so that it passes through the intersection point shown in the graph. The decreasing value of E_a with film thickness is certainly indicative of a smaller total barrier for relaxation. The fact that this effect occurs only for fairly thin films can be discussed in terms of the idea of a length scale for the dynamics in glass forming materials. In the bulk material,

as the temperature is lowered, more segments have to be involved in any rearrangement, and the apparent activation energy increases. As the film thickness is decreased, once the length scale for cooperative dynamics approaches the film thickness, all rearrangements can be affected by the different constraints at the free surface. Once this condition is reached, the process would be a simple activated process with an activation energy that depended on film thickness. The onset of such a confinement effect could occur only when the value of E_a is tangent to the bulk VFT behavior. This limit is given by the dashed line on the figure inset and the intercept of the E_a versus h plot with this value occurs at a film thickness of 61 ± 6 nm. It is remarkable that this is so similar to the *maximum* value of h where T_g reductions are first observed in supported PS films [11]. It is also interesting to consider the limit of $h \to 0$. That corresponds to the case where all segments are at the free surface. Such a system would be expect to be Arrhenius with a value of E_a similar to the high temperature limit of the bulk VFT (i.e., $E_a \sim B$). If we do that extrapolation we find $E_a = 4180 \pm 2099$ K. This is the same order of magnitude as that for the high temperature limit of the bulk value $B = 1169$ K. Aside from the possible connection to an intrinsic length scale for the dynamics, the data and analysis above can be used as a stringent test of *any* theories used to describe the glass transition in thin films.

An interesting consequence of the data presented above is the resolution of the contradiction between the body of literature measuring T_g reductions for thin PS films and those studies reporting no change in T_g or even increases in T_g for thin films. Figure 3 shows the existence of a very well defined region (simplified to a single point $1/T^*$, (rate)*, the dashed line in Fig. 3) that serves as a boundary for anomalous dynamics. We have explicitly shown that experiments probing relaxation times shorter than those corresponding to (rate)* show bulk behavior, and it also follows that measurements at temperatures higher than $T^* \simeq 378$ K must similarly fail to reveal anomalies. This is a fascinating suggestion. For instance, in the calorimetric measurement of Ref. [14], even in the measurements of the fictive temperature, the smallest cooling rate was 2 K/s (120 K/ min) [15]. This is very close to the largest cooling rate used in the present experiment, and the results from the two studies are similar. These cooling rates can be compared with an oscillatory technique employing a frequency of $\simeq 0.6$ Hz. Indeed, it seems that almost all reports in the literature that contradict reports of anomalous T_g values are taken in the region beyond $1/T^*$, (rate)*, and thus are entirely consistent with the behavior shown in Fig. 3.

We have demonstrated that the reduced T_g values often reported in thin PS films display a striking cooling rate dependence, which is qualitatively different from that of the bulk polymer. This effect is so pronounced that for cooling rates only as high as a few K/s, we would not expect to see any film-thickness-dependent reductions in

T_g. The cooling rates are related to relaxation times, and when plotted in this way, we see that thin films display a clear Arrhenius behavior. The film-thickness-dependent activation energies can be used to suggest an onset of confinement effects of 61 ± 6 nm, in excellent agreement with experiment. A possible explanation of the effect is given in terms of a temperature dependent correlation length for the dynamics in glass forming materials. Finally, the results provide a natural explanation for most of the remaining apparently contradictory experiments in the literature.

*Corresponding author.
 Electonic address: jforrest@uwaterloo.ca
 [1] P. W. Anderson, Science **267**, 1609 (1995).
 [2] G. Adam and J. H. Gibbs, J. Chem. Phys. **43**, 139 (1965).
 [3] *International Workshop on Dynamics in Confinement*, edited by B. Frick, R. Zorn, and H. Buttner [J. Phys. IV (France) 10 (2000)].
 [4] G. B. McKenna, Eur. Phys. J. E **12**, 191 (2003).
 [5] K. Jackson and G. B. McKenna, J. Non-Cryst. Solids **131**, 221 (1991).
 [6] L. Hartmann, J. Gorbatschow, J. Hauwede, and F. Kremer, Eur. Phys. J. E **8**, 145 (2002).
 [7] S. H. Anastasiadis, K. Karatasos, G. Vlachos, E. Manias, and E. P. Giannelis, Phys. Rev. Lett. **84**, 915 (2000).
 [8] J. L. Keddie, R. A. L. Jones, and R. A. Cory, Europhys. Lett. **27**, 59 (1994).
 [9] Special issue on "Properties of thin polymer films," edited by G. Reiter and J. A. Forrest [Eur. Phys. J. E **8** (2002)].
 [10] J. A. Forrest, Eur. Phys. J. E **8**, 261 (2002).
 [11] J. A. Forrest and K. Dalnoki-Veress, in Adv. Colloid Interface Sci. **94**, Nos. 1–3, 167 (2001).
 [12] J. S. Sharp and J. A. Forrest, Phys. Rev. Lett. **91**, 235701 (2003).
 [13] C. J. Ellison and J. M. Torkelson, Nat. Mater. **2**, 695 (2003).
 [14] M. Y. Efremov *et al.*, Phys. Rev. Lett. **91**, 085703 (2003).
 [15] M. Yu. Efremov, E. A. Olsen, M. Zhang, Z. Zhang, and L. H. Allen, Macromolecules **37**, 4607 (2004).
 [16] K. Fukao and Y. Miyamoto, Phys. Rev. E **64**, 011803 (2001).
 [17] J. S. Sharp and J. A. Forrest, Phys. Rev. E **67**, 031805 (2003).
 [18] S. Kawana and R. A. L. Jones, Phys. Rev. E **63**, 021501 (2001).
 [19] C. M. Roland and R. Casalini, J. Chem. Phys. **119**, 1838 (2003).
 [20] M. Arndt, R. Stannarius, H. Groutheus, E. Hempel, and F. Kremer, Phys. Rev. Lett. **79**, 2077 (1997).
 [21] J. S. Sharp, J. H. Teichroeb, and J. A. Forrest, Eur. Phys. J. E **15**, 473 (2004).

Paper IV

Measuring the surface dynamics of glassy poly-mers[5]

Measuring the surface dynamics of glassy polymers

Z. Fakhraai and J.A. Forrest[*]

Department of Physics and Astronomy and Guelph-Waterloo Physics Institute,

University of Waterloo, 200 University Ave. W.,

Waterloo, Ontario, Canada, N2L 3G1.

Abstract

We have carried out a simple, direct experiment to measure the time dependent relaxation function of the first few nm of a polymer surface. We measure this relaxation for polystyrene (PS) as a function of temperature in the range $293K < T < 369K$. Relaxation can be observed at all temperatures, and provides the strongest evidence to date for enhanced surface mobility relative to the bulk. The temperature dependence of the relaxation time is much weaker than in bulk PS, and appears to be Arrhenius at temperatures below $\sim 350K$. Comparing to thin film relaxation reveals a notable self-consistency and allows us to estimate the glass transition temperature of the surface to be 282K.

It is almost 15 years ago that the question was asked "Is the molecular surface of polystyrene really glassy "[1]. The answer to this question and the more general problem of developing an understanding of the properties of polymer surfaces is of tremendous current interest. Such understanding will have important implications for friction, lubrication, adhesion and any applications involving polymer modification by way of coatings. At a more fundamental level, polymer surfaces, and in particular the surfaces of polymers such as atactic polystyrene that have no tendency to crystallize, represent an excellent model system for amorphous material surfaces. While the ideas of surface melting in crystals are well understood, the surface properties of amorphous solids are not. Of equal impact is the growing evidence that the properties of the free polymer surface play a crucial role in observed anomalies in the glass transition temperature of thin polymer films[2]. Understanding the properties of the polymer surface may lead to the development of an understanding of dramatic reductions in the glass transition that have been observed in polymer films[3]. This in turn may provide crucial clues to develop our understanding of glass formation in general-a problem noted to be the deepest and most important unsolved problem in solid-state physics[4]. Despite over a decade of study, experiments have yet to determine conclusively whether or not there is enhanced mobility at polymer surfaces.

A key reason for this lack of consensus in the literature is that most experiments have ambiguities that do not allow them to lead to definitive conclusions. There are a significant number of experiments that use AFM based rheology to infer surface properties. Many of these studies conclude that the surface properties of polymer films show no difference from that of the ˜bulk polymer[5] while others suggest enhanced mobility[6]. Such experiments have a number of fundamental difficulties. For example, AFM based measurements involve imprecisely known interactions between the AFM tip and the polymer surface, interaction with an unknown surface depth, may involve stresses near the yield stress, and usually employ oscillatory probe motion at a frequency large enough that anomalous dynamics may not be expected[7]. Experiments involving nanoparticle interaction with the polymer surface suffer from a similar problem in that the detailed interaction between the nanoparticle and the polymer surface is not well charcterised[8–10], and this leads to a disparity in conclusions. A class of experiments that has shown particular promise in determining the surface properties is that involving surface relaxation of an applied surface perturbation. In some experiments, the surface is perturbed by a rubbing process that applies stress and

aligns the polymer chains [11, 12]. A difficulty with these experiments is that the alignment is done at temperatures well below T_g and so the stresses involved must exceed the yield stress. In a related, but less extreme, class of experiments a topological perturbation is introduced to the surface, and the relaxation of the surface (driven by surface tension) can be measured directly using AFM.The perturbation in such cases should be small enough that the relaxation can be considered to be a linear response[13, 14]. A limited number of these experiments have been performed and suggest some enhanced surface mobility. The experiments of Kerle *et al.* used relaxation of a roughened polymer surface over many length scales. The experiments by Johansmann *et al*[14, 15] used single length scales as small as 100nm and a single temperature of 363K, and saw evidence for enhanced surface mobility at this temperature. Relaxation of nanoscale surface deformation caused by heavy ion bombardment of PMMA shows evidence for enhanced surface mobility, but the extent of damage by the ion irradiation makes the stress, degree of radiation damage and even the chemical composition of the polymer near the damage track unclear[16]. Also notable are measurements of the glass transition temperature of a near surface layer. These experiments are indirect measures of the surface dynamics. Positron annihilation lifetime experiments of the near surface have shown no evidence for a surface T_g differing from the bulk[17]. In contrast, the recent fluorescence measurements by Ellison *et al*[18] provide evidence for a lower T_g value in the 14 nm layer near the polymer free surface. In order to obtain a definitive result. There are a number of experimental constraints that should be satisfied:

- The measurement should not be a measurement of the glass transition temperature, as this has shown to not always be a direct reflection of the dynamics. Instead the experiments should measure either equilibrium fluctuations or the isothermal response to a well characterized perturbation.

- The experiment should interact with a small and well defined surface region. There is some experimental evidence to suggest that this region [8, 19, 20] should be of the order of 4 nm.

- In experiments involving relaxation of a surface perturbation, the mechanism of the driving force for relaxing the perturbation should be clearly defined. The driving forces should be small enough that observations correspond to a linear response.

- The surface dynamics should be measured over a wide temperature range, especially below the bulk T_g so that we may hope to determine when the surface itself vitrifies.

Despite the large amount of experimental effort that has gone into this problem, there are no reports of experiments that satisfy all of the above constraints. Here, we describe a simple experiment that *does* satisfy the constraints and allows us to not only *definitively* address the long-standing question concerning the mobility of polymer surfaces, but also to provide a near complete quantification of the polymer surface mobility. We show conclusively that the free surface of polystyrene has an observable mobility even at temperatures as low as 80K below the bulk T_g value. The temperature dependence of the relaxation time reveals a transition to an Arrhenius behavior with a relatively small activation barrier for T $\lesssim$ 350K. By combining this data with a key finding of a previous study[7] we provide the first robust estimate for the surface glass transition temperature of amorphous polystyrene. The technique described is applicable to essentially any polymer surface.

A novel aspect of the experiment is the production of large numbers of non-overlapping nanometer sized indentations (nanoholes) on the polymer surface. These nanoholes are produced in a way such that they are very regular and well characterized (inverted spherical cap) with an average depth of 2-4 nm. This is 1-2 orders of magnitude less than the depth used for bulk studies performed at $T > T_g$(bulk)[21] and the depth probed in the studies of grating decay at $T < T_g$[15]. The production of such surface defects is a crucial aspect of being able to measure the near surface properties with a high resolution. We produce these nanoholes by first coating a solution of 23 ± 3 nm gold spheres onto the surface of a spincast and annealed (413K for 12hours under dry nitrogen) polystyrene film (100nm thickness, M_w= 641K, M_w/M_n=1.11 Polymer Source). We then heat the samples at 378K for 10-15 minutes to allow the spheres to partially embed into the polymer surface [8]. We choose embedding times and temperatures that produce average values of $\simeq$ 2nm-4 nm embedding. After we have embedded the gold nanoparticles into the PS surface, it is necessary to remove them without applying a large stress to the PS surface. This is done by placing a drop of Mercury on the polystyrene surface. The mercury forms an amalgam with the gold, which essentially dissolves the gold into the mercury droplet. The use of mercury to dissolve small amounts of gold is the same procedure used in the mining of gold[22]. We then turn the sample on an angle and the mercury droplet slides off. Mercury has a high surface tension which minimizes its interaction with the PS film. After this process what

is left in the place of the nanoparticles are small holes that can be measured with Atomic Force Microscopy (AFM). Imaging the sample after removal of the gold nanospheres in this way does not show evidence for surface damage (such as that observed if water is used to remove the nanoparticles). The T_g of samples made using this procedure is the same as the bulk value, and EDX (Energy Dispersive X-ray Analysis) did not give evidence for excess mercury left on the polymer surface. Figure 1 illustrates the sample preparation technique and analysis: Figure 1(a) shows the sample with the embedded gold nanoparticles, Figure 1(b) shows the same sample (but not the same location on the sample) after exposure to mercury to remove the nanospheres. It is clear that in the place of nanospheres there are holes surrounded by a rim of PS. Figure 1(c) then shows the histogram of hole depth data (from a 5 $\mu m \times 5\mu m$ image) that is used to find the average hole depth. A trace used to find the depth of a single hole is shown in Figure 1(d). Each sample is measured after nanohole formation to ensure there are enough holes on the surface to get adequate statistics., and that the hole size distribution is reasonable. A noteworthy aspect of these experiments is that there is an inherent sensitivity to the sharpness of the AFM tip. If the tips radius of curvature were much larger than that of the nanohole, we would have significantly reduced ability to measure the depth of the hole. This problem is minimized by using sharp tips, and frequent changing of the tip.

The nanohole covered samples are ideally perturbed samples for surface relaxation studies. We measure each sample only once after annealing has begun to avoid stress caused by repeated heating and cooling of the samples. This means that we need at least one sample per annealing time and to determine the relaxation curve for any sample temperature requires 10-15 samples with identical thermal history and similar initial hole depth distributions. For a given sample temperature, all of the prepared samples are placed in the sample oven in dry nitrogen. After some time interval, one of the samples is removed, allowed to cool to room temperature and then measured using AFM. Each AFM image contains many holes ($\sim$ 50) and it is the average over all holes that is used. This procedure is repeated at a number of elapsed annealing times until holes are no longer observed. Even when the holes have relaxed to the point where the depth is too small to be measured, there is a persistent rim that allows one to know that a hole did formerly exist there. If such holes simply disappeared, then we would only observe the largest holes at long times and the resulting analysis would provide average values that are too large. The measured hole depths

are used to determine the time dependence of the average indentation depth at constant annealing temperature-the relaxation function. The entire experiment is then repeated at different annealing temperatures. This allows us to find a relaxation time as a function of the annealing temperature over a range of 70K. Even though we do not explicitly determine the time dependent compliance of the near surface region. The temperature dependence of any relaxation function (diffusion, dielectric relaxation, compliance) contains the same information.

Figure 2 shows the time evolution of nanoholes at a sample temperature of 293K. It is clear from the figures that the holes relax even at this temperature which is almost 80K below the bulk T_g value. The driving force for this relaxation is the PS surface tension and for a spherical hole provides a stress of $\frac{2\gamma}{r} = 1.3 \times 10^6 Pa$. This is a factor of ~ 50 less than the yield stress of PS and provides confidence that what we observe is a linear response. The images of Figure 2 provide definitive evidence that the surface of PS is *not* glassy at temperatures where the bulk of the sample certainly is. Images such as these shown in Figure 2, but over a larger distance (typically $5\mu m \times 5\mu m$) are used to provide the hole depth values for each time and annealing temperature.

The time evolution of the hole depth can be used to obtain a relaxation function for each temperature studied. If the shape of the relaxation function is not temperature dependant then it is possible to find a scale factor in time such that if the data is multiplied by that factor (a shift in the log (time) axis) then the relaxation curves at different temperatures can be superimposed. This is a commonly used technique to describe the temperature dependence of relaxation times in glass forming materials. Figure 3 shows the superposition plot as well as the shift factors used to arrive at the cumulative plot. Note that each data point on this plot is obtained from a different sample, and the resulting scatter is mainly a result of the fact that each sample has a slightly different distribution of hole sizes (all with average values between 2-4 nm). The data in Figure 3 are scaled to a reference temperature of 369K, which is the highest temperature for which we were able to get reliable relaxation measurements. It is interesting to note that the relaxation function appears to be a single, rather than stretched, exponential. This is in contrast to the relaxation function of bulk PS which exhibits significant stretching with a β value of 0.4. Also displaying large deviations from the bulk are the shift factors used to collapse the relaxation functions. For bulk PS, the shift factors for PS have the form $log(a_T) = \frac{C_1(T-T_{ref})}{C_2+T-T_{ref}}$, where C_1=12.7-13.7, T_{ref}=373K,

and C_2=49.9 [23]. An obvious consequence of this form is the divergence of shift factors at a temperature $T^* = T_{ref} - C_2$=322.9K. In the inset, this would correspond to a continuously increasing slope as the temperature is lowered, and diverging at T^* (denoted by the dashed line). The surface relaxation data clearly does not obey this behavior, but instead the slope decreases with decreasing temperature. The difference between bulk and surface shift factors is made obvious by comparison of the surface data to the solid line in the inset which corresponds to the WLF shift factors for bulk PS. Figure 3 represents a reasonably complete quantification of the dynamics of the top 2-4 nm surface layer of polystyrene.

While it is not always reasonable to directly compare different relaxation processes, we can certainly compare the temperature dependence of such relaxations. We have recently reported measurements of the slow dynamics of thin PS films[7] obtained using cooling rate dependent measurements of the glass transition temperature T_g. Those studies also revealed an Arrhenius temperature dependence for thin film relaxation at temperature below the bulk T_g (reproduced in Figure 4 along with our data for the surface relaxation). The inset of the figure shows the slope of log(relaxation time) (expressed in terms of cooling rate) versus 1/T (the activation energy) for the thin films as a line, and the slope of the surface relaxation for $T < 350K$ as the solid symbol. The agreement between the extrapolation of the thin films activation barrier to zero thickness, and that for the surface layer is remarkable and suggests that the thin film relaxation is a direct result of surface relaxation. This is strong evidence that the reduced values of T_g measured in thin PS films are determined by the properties of the free surface. In order to more directly compare the temperature dependence of the two relaxation features (thin film versus surface relaxation), it is necessary to find the scaling factor between relaxation times of the two different processes. This corresponds to a shift along the log (cooling rate) axis. In order to find the shift factor we use the fact that for the thin film relaxations, the linear fits to the relaxation data seemed to intersect at or near a single point[7]. If we shift the linear portion of the surface relaxation data to also meet at the same point, we obtain the line shown in Figure 4. This procedure allows us to address the question of the T_g value of the polymer surface. If we extrapolate the Arrhenius fit to the data to the cooling rate of 1K/min (common rate for measuring T_g values), we can estimate the temperature at which the surface region would vitrify. The dashed line in the plot of figure 4 shows this point, which corresponds to a surface glass transition temperature of $T_g^{surf} = 282K \pm 3$. It is interesting to compare this number to other proposed estimates

of the surface glass transition. A layer model of thin film dynamics was used to estimate a surface T_g of 305 ± 21K [24]. Ellison *et al*[18] used fluorescence measurements to show a T_g value of the first 14 nm of the surface layer to be $\sim 337K$. We should also reiterate here that the surface relaxation has a much weaker temperature dependence than bulk PS. This means that even at temperatures below the T_g^{surf} there will still be observable surface relaxation. It is important to emphasize that the observation of relaxation at temperatures as low as 80K below the bulk T_g does *not* mean the surface always behaves as if it has a T_g 80K or more below the bulk value. Instead, the surface should be viewed as having the following behavior. At temperatures above the bulk T_g the surface and bulk behave in a similar manner[9]. As the temperature is lowered below T_g, the relaxation time of the bulk of the material increases very rapidly, while that of the surface does not. This is evident in comparing the bulk VFT behavior (the solid line in figure 4) with the measured relaxation time of the surface. The apparent difference in surface and bulk T_g then increases as the temperature is lowered below T_g.

In conclusion, we have devised and carried out a simple experiment that enables us to unambiguously measure the temperature dependent relaxation time for the very near (2-4 nm) surface region of polystyrene films. The surface region shows relaxation at all temperatures measured (down to 293K), and the resulting relaxation times display a surprisingly weak temperature dependence below the bulk T_g value. The surface relaxation shows a remarkable consistency to recently reported thin film relaxation data and this comparison allows us to provide an estimate for the surface glass transition temperature of $T_g^{surf} = 282K$. This data provides a framework upon which a successful theory of reduced glass transitions in thin films can be based.

———————

* corresponding author. email: jforrest@uwaterloo.ca

[1] G. F. Meyers, B. M. DeKoven, and J. T. Seitz, Langmuir, **8**, 2330 (1992).

[2] J.S. Sharp, J.A. Forrest, Phys. Rev. Lett. **91**, 235701, (2003).

[3] J.A. Forrest, Eur. Phys. J. E **8**, 261 (2002).

[4] P. W. Anderson, Science **267**, 1615 (1995).

[5] S. Ge, Y. Pu, W. Zhang, M. Rafailovich, J. Sokolov C. Buenviaje, R. Buckmaster, and R. M.

Overney, Phys. Rev. Lett., **85**, 2340 (2000).

[6] J. Hammerschmidt, W. Gladfelter, G. Haugstad, Macromolecules **32** 3360 (1999).

[7] Z. Fakhraai, J.A. Forrest, Phys. Rev. Lett. **95**, 025701 (2005).

[8] J. H. Teichroeb, J. A. Forrest, Phys. Rev. Lett, **91**, 016104-1 (2003).

[9] J.S. Sharp, J.H. Teichroeb, J.A. Forrest, Eur. Phys. J. E, **15**, 473 (2004).

[10] S. A. Hutcheson and G. B. McKenna, Phys. Rev. Lett., **94**, 076103 (2005).

[11] Y. Liu, T. P. Russell, M. G. Samant, J. Stöhr, H. R. Brown,A. Cossy-Favre, J. Diaz, Macromolecules, **30**, 7768 (1997).

[12] A. D. Schwab and A. Dhinojwala, Phys. Rev. E **67**, 021802(2003).

[13] T. Kerle, Z. Lin, H. Kim, and T. P. Russell, Macromolecules **34**, 3484 (2001).

[14] E. Buck, K. Petersen, M. Hund, G. Krausch, and D. Johannsmann, Macromolecules **37**, 8647 (2004).

[15] P. Gasemjit, D. Johannsmann, J. Poly. Sci. B: Poly. Phys **44** 3031 (2006).

[16] R. M. Papalo, R. Leal, W. H. Carreira, L. G. Barbosa, I. Bello, A. Bulla, Phys. Rev. B **74**, 094203 (2006)

[17] L. Xie, G. B. DeMaggio, W. E. Frieze, J. DeVries, D. W. Gidley, H. A. Hristov, and A. F. Yee, Phys. Rev. Lett., **74**, 4947 (1995).

[18] C. J. Ellison, J. M. Torkelson, Nature Materials, **2**, 695 (2003).

[19] T. Sasaki, A. Shimizu, T. H. Mourey, C. T. Thurau, and M. D. Ediger, J. Chem. Phys. **119**, 8730 (2003).

[20] V. M. Rudoy, O. V. Dement́eva, I. V. Yaminskii, V. M. Sukhov, M. E. Kartseva, and V. A. OgarevÔ, Colloid J. **64**, 746 (2002).

[21] I. Karapanagiotis, W.W. Gerberich, Macromolecules, **38**, 3420 (2005).

[22] This was first published in 1556 by Georgius Agricola in De Re Metallica, but the technique may have been used even in Roman times.

[23] J. D. Ferry, "Viscoelastic Properties of Polymers", 3rd edition, Wiley, New York (1980).

[24] J. A. Forrest, J. Mattsson, Phys. Rev. E, **61** R53 (2000).

figure captions

figure 1. Illustration of the process used to create nanoholes in the PS surface. (a) PS surface covered by Au nanospheres that have been partially embedded. (b) The surface of the same PS sample after Au nanospheres have been removed by exposure to liquid Hg. (c) histogram showing hole depth and (d) The line scan of the indicated line in bart (b) used to measure the depth of a single hole. Note the existence of the rim around the holes.

figure 2. Evolution of nanoholes at a sample temperature of 293K. the annealing times are (a) 0 minutes (b) 4420 minutes (c) 29700 minutes (d) 96420 minutes. The inset of each figure shows the line scan of the indicated holes which are used to find their depth.

figure 3. Time dependence of the relaxation of nanoholes for all temperatures. The time data are shifted by a factor a_T so that they agree with the data at the reference temperature of 369K. The solid line is a single exponential fit. The logarithm of the shift factors used to produce superposition are shown in the inset. The solid curve in the inset corresponds to the bulk WLF shift factors.

figure 4. Comparison of surface dynamics (▲) and thin film data. The solid lines are fits to the thin film and bulk data of reference [7]. The inset is the activation Energy for this films (solid lines) and the boundary of error (dashed lines) as well as the activation energy of the surface (●). The dashed line in the main graph is the extrapolation of the surface relaxation data to a cooling rate of 1 K/min. This is used to extract a surface glass transition temperature of 282K (indicated by the arrow).